RAQUEL HÚNGARO COSTA

RECUPERAÇÃO DE SULFATO DE MAGNÉSIO POR ROTA HIDROMETALÚRGICA A PARTIR DE UM REJEITO DA FLOTAÇÃO DO MINÉRIO DE ZINCO

SÃO PAULO

2021

RAQUEL HÚNGARO COSTA

RECUPERAÇÃO DE SULFATO DE MAGNÉSIO A PARTIR DE UM REJEITO DA FLOTAÇÃO DO MINÉRIO DE ZINCO POR ROTA HIDROMETALÚRGICA

Dissertação apresentada à Escola Politécnica da Universidade de São Paulo como requisito para obtenção do título de Mestre em ciências.

SÃO PAULO

2021

RAQUEL HÚNGARO COSTA

RECUPERAÇÃO DE SULFATO DE MAGNÉSIO A PARTIR DE UM REJEITO DA FLOTAÇÃO DO MINÉRIO DE ZINCO POR ROTA HIDROMETALÚRGICA

VERSÃO CORRIGIDA

Dissertação apresentada à Escola Politécnica da Universidade de São Paulo como requisito para obtenção do título de Mestre em ciências.

Área de concentração: Engenharia Química

Orientadora: Profa. Dra. Denise Crocce Romano Espinosa

Coorientadora: Dra. Tatiana Scarazzato

SÃO PAULO

2021

RAQUEL HÚNGARO COSTA

RECOVERY OF MAGNESIUM SULFATE FROM A ZINC ORE FLOTATION TAILING USING HYDROMETALLURGICAL ROUTE

São Paulo

2021

RAQUEL HÚNGARO COSTA

RECOVERY OF MAGNESIUM SULFATE FROM A ZINC ORE FLOTATION TAILING USING HYDROMETALLURGICAL ROUTE

Master Thesis presented to University of Sao Paulo, Polytechnic School as a requirement to obtain the title of Master of Science.

São Paulo

2021

RAQUEL HÚNGARO COSTA

RECOVERY OF MAGNESIUM SULFATE USING HYDROMETALLURGICAL ROUTE FROM A ZINC ORE FLOTATION TAILING

Master Thesis presented to University of Sao Paulo, Polytechnic School as a requirement to obtain the title of Master of Science.

Concentration area: Chemical Engineering

Advisor: Prof. Dr. Denise Crocce Romano Espinosa

Co-advisor: Dra. Tatiana Scarazzato

São Paulo

2021

Este exemplar foi revisado e alterado em relação à versão original, sob responsabilidade única do autor e com a anuência de seu orientador.

São Paulo, 13 de janeiro de 20

Assinatura do autor Raquel Húngaro Costa

Assinatura do orientador

Catalogação-na-publicação

Húngaro Costa, Raquel
RECOVERY OF MAGNESIUM SULFATE FROM A ZINC ORE FLOTATION TAILING USING HYDROMETALLURGICAL ROUTE / R. Húngaro Costa, D. Crocce Romano Espinosa, T. Scarazzato -- São Paulo, 2020.
126 p.

Dissertação (Mestrado) - Escola Politécnica da Universidade de São Paulo. Departamento de Engenharia Química.

1.Zinc tailing 2.Leaching 3.Magnesium sulfate 4.Toxic metals 5.Cementation I.Universidade de São Paulo. Escola Politécnica. Departamento de Engenharia Química II.t. III.Crocce Romano Espinosa, Denise IV.Scarazzato, Tatiana

For you who always encouraged me, believed me, and gave me the best love,

Nicholas Braun Rodrigues.

AGRADECIMENTOS

Ao Ser Supremo que nos guia.

À Profa. Dra. Denise Crocce Romano Espinosa, por aceitar ser minha orientadora, pela compreensão em momentos atípicos, e pelas contribuições e acompanhamento do trabalho.

À Dra. Tatiana Scarazzato, pelas dicas como pesquisadora durante toda sua jornada de coorientação, pela paciência e amizade durante esse tempo, deixando o trabalho mais leve durante essa fase tão importante.

Ao Prof. Dr. Jorge Alberto Soares Tenório, por disponibilizar o laboratório para o desenvolvimento deste trabalho, pelos ensinamentos e questionamentos que me fez crescer como pesquisadora e pessoa.

À empresa Votorantim Metais/Nexa Resources pela disponibilização do material a ser estudado e pela confiança.

À técnica do laboratório da Escola Politécnica da USP Ana Carolina, que sempre se dispôs a ajudar e ensinar química para um trabalho melhor. Assim como, a amizade durante todo esse tempo de aprendizado.

Ao meu noivo, Nicholas Braun Rodrigues, que nunca mediu esforços para me incentivar, me fazendo acreditar sempre no melhor. Por todos os momentos de descontração e apoio.

À Paula Aliprandini pelas discussões a cada dia sobre etapas do trabalho, conversas que me fizeram crescer no mestrado e, pelas conversas que deixaram esse tempo de pesquisa mais leves acompanhados de um bom café.

Ao Caio e a Yara pelas conversas e momentos extrovertidos. Pela motivação e apoio a cada etapa turbulenta, assim como as boas risadas em momentos de descontração. À Jaqueline que se fez presente assim que chegou ao laboratório disposta a ajudar.

À toda equipe do Laboratório de Reciclagem, Tratamento de Resíduos e Metalurgia Extrativa (LAREX), que se tornaram amigos durante um momento cheio de desafios como o mestrado, aprimorando, portanto, o conhecimento nesta etapa.

Ao apoio do Laboratório de Tratamento de Minérios e Resíduos Industriais do Departamento de Engenharia de Minas e de Petróleo da Escola Politécnica da USP.

Aos meus pais e irmãos, Valéria Húngaro Costa e Luiz Carlos Costa pelos ensinamentos da vida que sempre estarão guardados comigo, à minha irmã Vívian, pelo carinho mesmo à distância e ao seu marido, Cristiano, pelos bons momentos juntos, ao meu irmão Leandro pelo exemplo de dedicação, vocês cinco são meus eternos amores.

À Sonia Olsen Braun, por acreditar na pesquisa e pelo bom humor como forma de incentivo.

Aos meus amigos e primas, Izabele Zarpelão, Aline Prieto, Tiago Silva, Veronica Baruque, Elise Húngaro e Ane Húngaro, que sempre estiveram próximos comigo mesmo à distância, me incentivando e apoiando em decisões como esta.

Para todos os demais amigos que contribuíram de alguma maneira para a realização deste trabalho de forma direta ou indireta.

Ao Departamento de Engenharia Química da Escola Politécnica da Universidade de São Paulo, pela oportunidade de realização do mestrado.

À Empresa Brasileira de Pesquisa e Inovação Industrial (EMBRAPII-FUSP), pelo suporte financeiro do projeto de pesquisa n° 600032.

“The Universe is the all, and you are the one. All’s existence and ability to move forward is dependent on this law (…) The Universe always moves forward, a constant cycle. It is one thing that binds all together (…) One is all, all is one.”

(Fullmetal Alchemist)

RESUMO

O reaproveitamento de minerais a partir de rejeitos é fundamental para gerar menos impactos ao meio ambiente. A investigação de métodos que visam recuperar elementos que possam gerar subprodutos a partir de rejeitos de mineração vêm sendo estudada, como por exemplo, o rejeito do beneficiamento do zinco. O rejeito da etapa de flotação do beneficiamento do zinco foi caracterizado, inicialmente, para investigar novas rotas para obtenção de subprodutos a partir de gangas. A ganga do rejeito do zinco contém dolomita, hematita e impurezas, que são consideradas elementos tóxicos, ex.: chumbo e cádmio. O trabalho teve como objetivo a obtenção de sulfato de magnésio e sulfato de cálcio a partir do rejeito utilizando processamento físico, simulação termodinâmica (software *FactSage*) e rota hidrometalúrgica a partir da dolomita. Identificou-se na caracterização do rejeito de zinco, por espectrometria de emissão óptica por plasma acoplado indutivamente (ICP-OES) a seguinte composição: 7,96% Fe, 10,3% Mg, 17,4% Ca, 1,47% Si, 1,74% Zn, 0,2% Pb, 0,33% Al, 0,02% Cd, e 0,07% Mn. A difratometria de raios-X (DRX) identificou as fases de dolomita, hematita e quartzo. Nas análises realizadas no MEV-EDS foi possível visualizar as partículas desagregadas de hematita, dolomita e quartzo o que permitiu uma separação física dessas fases. Portanto, a concentração de dolomita foi investigada na separação magnética e gravítica para eliminar principalmente o ferro do material em estudo. A separação magnética *rougher cleaner* apresentou uma melhor concentração da dolomita encontrada na fração não-magnética a qual foi caracterizada por ICP-OES e apresentou uma composição de 0,34% Al; 21,6% Ca; 0,04% Cd; 2,7% Fe; 11,9% Mg; 0,08% Mn; 0,2% Pb; 1,37% Si; e 1,73% Zn. Posteriormente, realizou-se uma simulação com o software *FactSage* para avaliar as melhores condições de lixiviação referente a relação S:L, variação da concentração de ácido sulfúrico e da temperatura. Inicialmente, utilizou-se na simulação, como referência, a dolomita pura e, em seguida, considerou-se a composição obtida na fração não-magnética (90,3%) e os demais elementos encontrados. As condições da dolomita pura foram selecionadas em 1,2mol.L^{-1}, em uma relação S:L igual a 1:10, e temperatura a 25°C, obtendo-se uma extração de 100% do Mg na simulação. Em seguida, a simulação com 90,3% de dolomita obteve uma extração do Mg de 100% utilizando 1,0mol.L^{-1} de H_2SO_4 na relação S:L igual 1:10 a 25°C. Os ensaios de lixiviação foram realizados utilizando essas condições, variando-se a temperatura em 25 – 50 – 75 e 90°C e o tempo de 5 a 180min. Obteve-se um rendimento da extração de Mg de 72%± 5% a 50°C em 35min. Na etapa de purificação, utilizando o método de cementação, houve uma remoção do cádmio de 90,2% no licor da lixiviação com o pó de zinco numa relação de 100:1 em 5min a 25°C. Os subprodutos obtidos a partir da rota hidrometalúrgica foram $MgSO_4$ e $CaSO_4$, com o intuito de serem utilizados na agricultura, sendo o sulfato de magnésio (40% de $MgSO_4 \cdot 7H_2O$ para cada 1kg) como fertilizante (macronutriente secundário) e o sulfato de cálcio como condicionador do solo (7,5% para cada 1kg).

Palavras-chave: Rejeito de zinco; Lixiviação; Sulfato de magnésio; Metais tóxicos; Cementação.

ABSTRACT

The reuse of minerals from tailings is essential to generate less impact on the environment. The investigation of methods that aim to recover elements that can generate by-products from mining tailing has been studied, such as, for example, the zinc beneficiation tailing. The tailing acquired in the flotation step of the zinc beneficiation was initially characterized to investigate alternatives routes to obtain by-products from the gangues found in this tailing. The gangue of zinc tailing may contain dolomite, hematite, and impurities that are considered toxic elements, e.g. lead and cadmium. This work aimed to obtain $MgSO_4$ and $CaSO_4$ from real flotation tailing generated in zinc beneficiation. Thus, using physical processing, thermodynamic simulation (*FactSage* software), and hydrometallurgical route from dolomite. The following composition was identified in the characterization of zinc tailing by inductively coupled plasma optical emission spectrometry (ICP-OES): 7.96% Fe, 10.3% Mg, 17.4% Ca, 1.47% Si, 1.74% Zn, 0.2% Pb, 0.33% Al, 0.02% Cd, and 0.07% Mn. X-ray diffractometry (XRD) identified the phases of dolomite, hematite, and quartz. In the SEM-EDS analyses, it was possible to observe the disintegrated hematite, dolomite, and quartz particles, which allow the physical processing of these phases. Therefore, a dolomite concentration was investigated in the magnetic and gravity separation to eliminate mainly iron from the material understudy. The magnetic separation with the *rougher cleaner* route showed a better concentration of dolomite (90.3%) found in the non-magnetic fraction. The non-magnetic fraction was characterized by ICP-OES and presented a composition of 0.34% Al; 21.6% Ca; 0.04% Cd; 2.7% Fe; 11.9% Mg; 0.08% Mn; 0.2% Pb; 1.37% Si; and 1.73% Zn. Subsequently, a simulation was performed with the *FactSage* software to evaluate the leaching conditions varying the S:L ratio, the sulfuric acid concentration, and temperature were studied. Initially, pure dolomite was used in the simulation as a reference. Afterward, the composition was provided in the non-magnetic fraction of 90.3% and the other phases found in the zinc tailing were considered. The conditions for the pure dolomite were selected in 1.2mol.L^{-1} in a S:L ratio equal to 1:10, at room temperature showed 100% Mg extraction. Then, the simulation with 90.3% dolomite had 100% Mg extraction in 1.0mol.L^{-1} H_2SO_4 in a S:L ratio equal to 1:10 at room temperature. The leaching tests were performed using these conditions, varying the temperature in 25 – 50 – 75 and 90°C and the time from 5 to 180min, which a Mg and Ca extraction yield of 72% ± 5% and 2%, respectively, were obtained at 50°C in 35min. Using the cementation step, the purification method resulted in a 92.3% cadmium removal in the liquor from leaching with zinc powder in a 100:1 ratio in 5min at 25°C. The by-products obtained were $MgSO_4$ and $CaSO_4$, to be used in agriculture, magnesium sulfate (40% of $MgSO_4 \cdot 7H_2O$ for each 1kg) as a fertilizer (secondary macronutrient), and calcium sulfate as a soil conditioner (7.5% for each 1kg).

Keywords: Zinc tailing; Leaching; Magnesium sulfate; Toxic metals; Cementation.

LIST OF FIGURES

LIST OF TABLES

SUMMARY

1 INTRODUCTION

The main objective of zinc extraction is galvanization, which avoids the corrosion of metals. Its production can be carried out through a hydro or a pyrometallurgical route. The most well-known zinc utilization ores are sulfides, oxides, and silicates. This metal is the third most common in the non-ferrous group – aluminum and copper are above it (Xu et al., 2012).

In the beneficiation of zinc, one of the steps to obtain its concentrate is flotation. A possibility of gangue minerals of a zinc ore includes noble silver, pyrite, hematite, limonite, dolomite, calcite, and quartz (Önal et al., 2005). The gangue composition may vary due to the environment and ores found in the local geology. In the case of zinc, the sulfide or oxides ores are the most common. For each type of zinc ore, there is a specific beneficiation, which results in different types of wastes, e.g. zinc silicates can generate tailings with different compositions comparing with the zinc sulfides (Edraki et al., 2014). The presence of some toxic elements, such as lead and cadmium, can be found in zinc tailing. Therefore, the importance of studying strategies to eliminate toxic metals for the acquisition of by-products from the gangue material (Abkhoshk et al., 2014a; Chen et al., 2020; Xu et al., 2010).

Investigating methods that contribute to the sustainability of natural resources is essential within the research. Studies have shown the possibilities of reusing or recycling the tailings from the beneficiation of metal mining. One way to recover such metals or compounds is through the hydrometallurgical route, which can be evaluated conditions for the combination in interest extraction. For example, some possibilities are to use tailing containing magnesium, aluminum, iron, and calcium silicates, even with the presence of metals considered to be toxic (e.g. Pb and Cd). Zinc itself can be recovered through leaching methods in waste generated in mining. Copper is another metal that is studied for recovery from tailing – around 20% copper is found as sulfides. Therefore, depending on the sulfide found smaller particles in the tailings can be extracted using the leaching technique. Another well-known method that collaborates to recover ores of interest is the gravity and magnetic separation, in which it aims to recover iron present in hematite and magnetite, reaching in some cases an iron concentration up to 60% (Dubiński, 2013; Edraki et al., 2014; Hansen et al., 2005; Marabini et al., 1998).

Dolomite may be found in flotation tailing from zinc beneficiation and plays a vital role in refractories, in which two of the basic refractories are MgO and CaO acquired

from dolomitic minerals. However, one of the focuses of the industries is magnesite for the manufacture of magnesia [$Mg(OH)_2$] and magnesium sulfate [$MgSO_4$] (Sadik et al., 2016).

Considering the importance and role of sustainability-related to mining and its tailings, which are usually destined for dams and landfills, it is essential to know the elements of interest and strategize ways to recover them from tailings. The innovation and developing projects that aim to reuse resources, especially those arising from mining, are tools for sustainability. Critical and precious metals are acquired from exhausting natural sources. They are characterized, for example, by their difficulty with substitution and their concentration in ores. Magnesium is considered a critical element due to its economic importance and its supply risk (Perez et al., 2019). Hence, tailings that were deemed to be non-explorable may be an outlet, and the use of hydrometallurgical routes, as well as purification techniques, may be feasible alternatives to recover such elements. The removal of toxic metals from mining tailing also contributes to sustainability concepts and contributes to reducing the exploitation of new resources (Ayres, 1997; European Comission, 2017; Jha et al., 2001; Monteiro et al., 2019; Perez et al., 2019; Schulze et al., 2020).

Studies that aim the reuse of materials that are disposed of in landfills seek the return of secondary materials with some purpose. For example, Chojnacka et al., (2019) reported the reuse of biomass after specific treatments (thermo-chemical treatment/incineration/wet extraction) to use N, P, K, and Mg as fertilizers, as they are considered macronutrients (Chojnacka et al., 2019). Thus, purification techniques are essential for the reuse of tailings with the intention to obtain by-products. Examples of purifications are cementation and precipitation by sulfides (Gupta, 2003; Havlik, 2001).

It is known that magnesium sulfate is used in agriculture as a fertilizer and it is considered a secondary macronutrient along with C, H, O, N, P, K, Ca, and S. Dolomitic limestone is one of the natural sources of such essential elements (Mg and Ca) (Jones, 2012). Therefore, the recovery of magnesium sulfate from dolomite evaluated in this work aimed to produce a potential raw material for fertilizers.

2 LITERATURE REVIEW

2.1 MINING AND ZINC

The term mining refers to the extraction of a mineral from a soil; a mineral that contains viable economic value is known as ore; the set of new minerals of ore is denominated gangue or secondary mineral (Gupta, 2003; Inácio et al., 2010).

The influence of minerals is evident in the development of the countries and society in general because of the demands of a growing population and a superior quantity of raw material to supply its needs. The procedures for processing these minerals to obtain products (metallic or oxides) are known as extractive metallurgy (Havlik, 2001; Inácio et al., 2010).

The use of metals and the introduction of mining into human life has been known for years, allowing modernity for society and civilization. In the past, known mining techniques (casting and forging of iron), discovered by trial and error, were passed down from generation to generation. Nowadays, the extraction processes involve complex operations, sustained in the methods of the past. The first metals used by man were copper and gold, and around 4000B.C., the copper-tin casting technique was discovered, producing copper and bronze (Rosenqvist, 1974).

The treatment or ore beneficiation refers to operations objectifying to modify the granulometry, relative concentration, and minerals' shape. However, because they are non-renewable resources, the conservation of mineral resources must be considered, taking into account environmental and social problems (Inácio et al., 2010).

According to the United Nations World Commission on Environment and Development Report, " *Sustainable development is supporting the needs of the present without compromising the ability of future generations to meet their own needs (...)*". Thus, the use of methods and techniques that aim to provide a better use of resources, more specifically mineral resources, and reduce impacts from exploitation is an initial and representative step towards achieving sustainable development (Reuter, 2013; UN. General Assembly (42nd sess.: 1987-1988), 1987). Sustainable Development is a constant progression of new techniques to minimize the exploitation of resources, reusing, recycling, reducing environmental, social, and economic impacts.

Zinc is categorized as an element from the group of non-ferrous, and it is the 23rd most abundant element in the crust. In a ranking of the most produced metals globally, it

only appears after iron, aluminum, and copper. The minerals found for the extraction of zinc are zincite [ZnO], sphalerite [ZnFeS], willemite [Zn_2SiO_4], hydrozincite [$2ZnO_3.3Zn(OH)_2$)], calamine or hemimorphite [Zn_4Si_3 $O(OH)_2$)], smithsonite [$ZnCO_3$], gahnite [$ZnAl_2O_4$], wurtzite [(Zn,Fe)S] and franklinite [(Zn,Mn)O.Fe_2O_3]. Table 1 shows the zinc content in its main minerals, with emphasis on willemite and calamine, which are found in Brazil. Commonly, zinc is found in nature in the form of sulfides, which are associated with lead (galena), copper (chalcopyrite), silver (argentita), and iron (pyrite). However, the ones that matter most economically are smithsonite and hydrozincite as carbonates and, hemimorphite and willemite as silicates (Abkhoshk et al., 2014; Boni et al., 2009; Song et al., 1999).

Table 1 shows that due to lower content in willemite, comparing to other zinc ores, such as zincite and sphalerite, it becomes an indicator in the generation of tailings. Then, there are other minerals present (gangues) that are found in these tailings.[1]

Table 1 - Zinc minerals and their percentage content. Adapted from (Sinclair, 2005).

Mineral	Formula	Zinc content (%)
Sphalerite	ZnFeS	67.0
Smithsonite	$ZnCO_3$	52.2
Willemite	$2ZnO.SiO_2$	58.7
Zincite	ZnO	80.4
Calamine	$2ZnO.SiO_2.H_2O$	54.0

2.1.1 History of zinc

In the 14th century a new tin-like metal, later known as zinc, was described by an Indian. It was made by indirect heating of the calamine with the use of coal. From India, the production of zinc went to China, which produced, mainly, brass. Thereby, zinc production expanded, and the metal began to be exported, making Europe familiar with the material through the Arab and Portuguese merchants. In the Holy Roman Empire of the German Nation, the philosopher Alberto Magnos (1200-1280) described that the zinc mineral could be used to color copper as gold. Meanwhile, in Italy, the metallurgist Vannocio Biringuccio (1480-1539) pioneered obtaining the zinc mineral, calamine (Lew,

[1] Theoretically, an inorganic compound found geologically is considered a mineral. It became an ore when it has an economic value (Inácio et al, 2010).

2008).

Primarily zinc is used for galvanizing (the process of coating a metal), in which more than 50% of its production is destined to this technique that serves to protect the iron against corrosion. The British chemist Humphry Davy (1778-1829) proposed the cathodic protection against corrosion, thus introducing the use of zinc to control the corrosion of ship hulls. The scientist Luigi Galvani (1737-1798) was the first to introduce the galvanic current principle. However, in 1741, the proposal of the French chemist Paul-Jacques Malouin (1701-1778) was granted a known hot-dip galvanizing tool. Some of the areas in which the electroplating of materials is used, due to the ease of the combination of zinc and metals, are the automobile, civil construction, and appliance industries (Mineral Resources Program, 2011).

Zinc is well-known for its various applications nowadays, such as brass and zinc alloys, coatings, and zinc oxide (Abkhoshk et al., 2014). Sectors in which chemical compounds are used, e.g. zinc oxides, are the textile and ceramic industries, rubber vulcanization, and the cosmetics industry. Finally, zinc is used in the production of cells and batteries, for application in the soil when there is a deficiency of this element and medicine. The automotive sector accounts for about 40% of the zinc consumption in Brazil (Mineral Resources Program, 2011; Sinclair, 2005).

2.1.2 Zinc extraction

The extraction of zinc is done by pyrometallurgical or hydrometallurgical processing. However, hydrometallurgy with acid leaching processing is the predominant route for obtaining zinc from willemite and hemimorphite, the acid dissolution of zinc from these minerals is presented in Equation 1 and 2 (Xu et al., 2010).

$$Zn_2SiO_4 + 2H_2SO_4 \rightarrow 2ZnSO_4 + Si(OH)_4 \qquad \text{Equation 1}$$

$$Zn_4SiO_2O_7(OH)_2.H_2O + 4H_2SO_4 \rightarrow 4ZnSO_4 + Si_2O(OH)_6 + 3H_2O \qquad \text{Equation 2}$$

Brazil has 6.4Mt of zinc reserves and resources. However, it does not present itself as the top ten countries with the largest reserves in 2018 and 2019, as shown in Table 2, with the leading countries and their reserves. Zinc resources of the world are about

1.9bilion tons (Bechir, 2019; USGS, 2020). [2]

Table 2 - Countries with greater reserves of zinc ore. Adapted from USGS, (2020).

Country	**Reserves**
United States	11,000
Australia	68,000
Bolivia	4,800
Canada	2,200
China	44,000
India	7,500
Kazakhstan	12,000
Mexico	22,000
Peru	19,000
Russia	22,000
Sweden	3,600
Other countries	34,000
World total (rounded)	250,000

Unit: 10^3ton

Although Brazil is not among the largest reserves and resources of total zinc reserves, it is in the non-sulfide zinc. The countries with these resources are Iran (Mehdi Abad), Namibia (Skorption), and United States of America (Franklin) as the first three countries with smithsonite, hemimorphite, sauconite, willemite, franklinite and zincite mines, presented in Table 3. Brazil was listed in the *ranking*, which offers the mineral with the most significant willemite, sphalerite, and franklinite resources. Brazil is also represented with 23.7% and 18% of the non-sulfide Zn in the world (Abkhoshk et al., 2014).

[2] In a simplified form, it is understood as "*reserves* - what could be economically extracted or produced, which do not signify that extraction facilities are in place and operative, and *resources* - economic extraction of a commodity from the concentration that is currently or potentially feasible" (U.S. Geological Survey, 2020).

Table 3 - Countries with the main deposits of non-sulfides zinc ore. Adapted from Abkhoshk et al., (2014).

Country (Name)	Main zinc minerals	Resources
Iran (Mehdi Abad)	Smithsonite, hemimorphite	218Mt Zn: 7.2%, Pb: 2.3%, Ag: 51g.t^{-1}
Namibia (Skorpion)	Smithsonite, hemimorphite, sauconite	24.6Mt Zn: 10.6%
Peru (Accha)	Smithsonite, hemimorphite, sauconite	5.1Mt Zn: 8.15%, Pb: 0.9%
Yemen (Jabali)	Smithsonite	9.4Mt Zn: 10.8%, Pb: 2.3%, Ag: 77g.t^{-1}
Mexico (Sierra Mojada)	Smithsonite, hemimorphite, sauconite	20.4tMt Zn: 10.6%
Brazil (Vazante)	Willemite, Sphalerite, franklinite	18.8Mt Zn: 23.7%
Brazil (Areiense)	Willemite, Sphalerite	9.9Mt Zn: 18%
Iran (Angouran)	Smithsonite	18Mt Zn: 28%, Pb: 2%
United States (Franklin)	Willemite, franklinite, zincite	21.8Mt Zn: 19.5%, Pb: 0.005%

The process to obtain zinc is varied depending on its source mineral, in which they are classified as minerals sulfides - the most common minerals are sulfides of zinc and lead that are sphalerite and galena, or non-sulfide minerals also called of oxidation ores - divided into two types, the hypogenic weathering (formation occurs inside the earth, deeper) and/or supergene (formation of deposits near the surface) - in some cases, the ores mixtures of sulfides and oxides are considered in this classification (Magalhães Baltar, 1980; S Moradi and Monhemius, 2011).

In most Brazil cases, the minerals do not contain sulfides but contain zinc oxides and silicates, so the processes are executed without the roasting step. The roasting is used to eliminate sulfur from the sulfide zinc ore, thus obtaining an oxide which has a soluble characteristic for acid leaching, also reducing the risk of not releasing H_2S in a leaching carried out with sulfide zinc (Santos, 2009).

A simplified flowsheet of the zinc beneficiation is shown in Figure 1. First, the

ore is destined for the comminution step in the mines, following successive crushing, obtaining a ground ore; the next steps are flotation and filtration, with a zinc concentrate acquired that aims to reach a concentration of zinc around 50 to 60.3wt.% - which can be varied depending on the mineralogy. If the ore is characterized as zinc sulfide, there is a roasting stage to remove the sulfide. Subsequently, there is the leaching for zinc extraction and finally, the purification and casting steps. In the hydrometallurgical route, using leaching, later the electrolytic deposition and melting, the zinc content is 99.99%. In the flotation step, a zinc tailing is generated, in which the gangues of the material are found (Bechir, 2019; Sinclair, 2005).

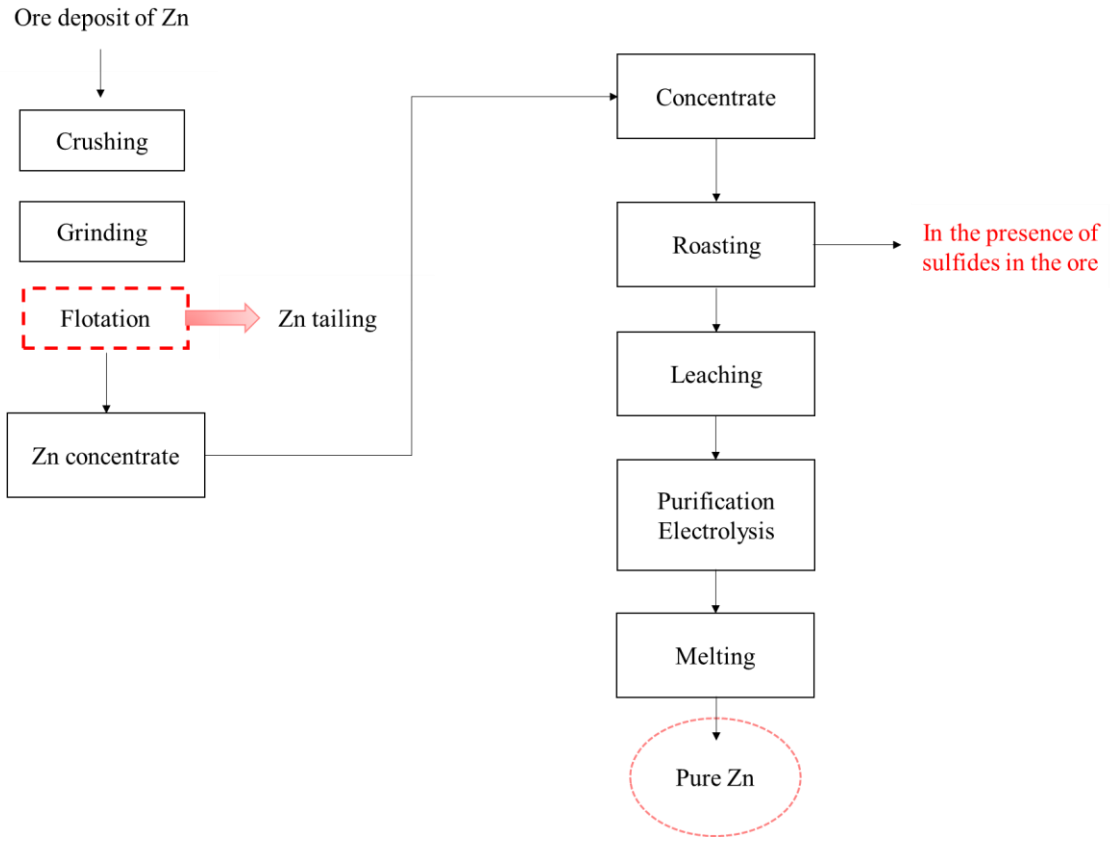

Figure 1 - Flowsheet of the process of obtaining zinc. Adapted from Sinclair, (2005).

2.1.3 Flotation

In extractive metallurgy, the terms known as gangue and concentrate have the following definition. A gangue is known as a set of new minerals of an ore. Therefore, the fraction of interest that is physically released from the gangue is known as the concentrate. In some cases purification is used to treat the concentrate and to remove

impurities (Inácio et al., 2010).

Flotation is a separation process in an aqueous medium that promotes selectivity in the separation of study materials during the ore beneficiation (Inácio et al., 2010). This technique proposes to add chemical products to obtain a concentrate, therefore, the addition of these products induces hydrophobic or hydrophilic characteristics, depending on the nonpolar or polar properties of each material. The hydrophobic substance is one in which the material's surface has a nonpolar characteristic – affinity with air and not water. The hydrophilic substance is one with a polar surface – affinity with water. When air is injected into the suspension, and there is a stable foam, the hydrophobized particles separate in this foam, and the hydrophilized particles sink, causing the separation at the bottom of the equipment (Gupta, 2003; Utimura, 2014).

This technique is classified into two types, one of them is direct flotation (gangue resides in the pulp and the concentrate in the floating fraction), and the other is reverse flotation (gangue floats and the concentrate remains in the pulp). In Figure 2, the direct flotation scheme is presented, which starts from the ground raw material from the ore. The pulp density is adjusted to reach 15-35% solids. There is a formation of foam on the surface, which contains the concentrate ore. The gangue is removed from the bottom of the flotation cell. Being a method used for the mineral processing and pretreatment of oxidized zinc minerals, there are currently studies focused on the flotation of zinc oxide ores for better process selectivity using the reverse flotation (Ejtemaei et al., 2014; Gupta, 2003).

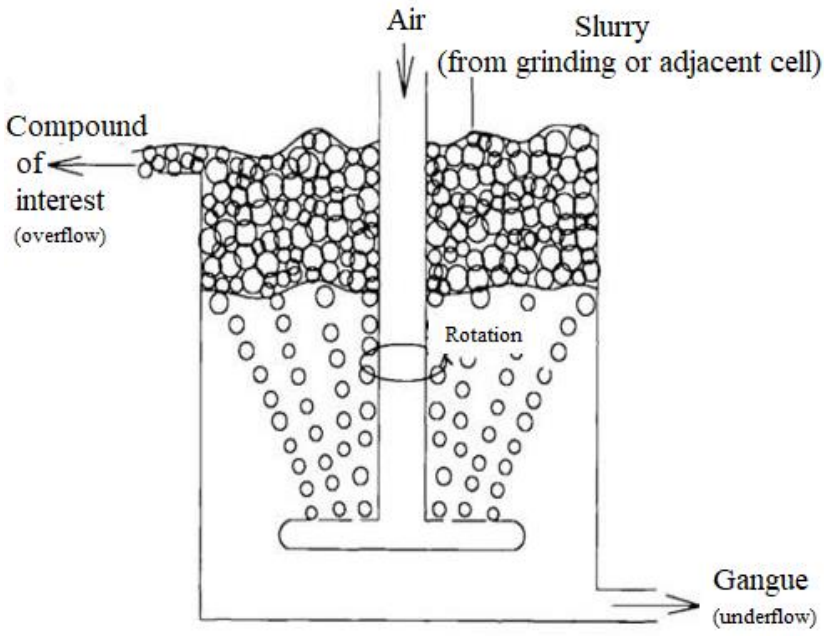

Figure 2 - Basic scheme of the flotation process (Gupta, 2003).

In a flotation process, one of the studied parameters is the granulometry of the material, that allows the process of separation, the size of the particles interferes in this separation of the concentrate and gangue material. Studies show that in the case of sulfide minerals, such as copper (chalcopyrite), zinc (sphalerite), and lead (galena), the optimum particle sizes for flotation are 150 to 20µm (Wills; Finch, 2013; Bechir, 2019). However, a wide granulometric range may be used, depending on the ore. It is assumed that for sulfide minerals, the conditions are up to 5µm (Chaves, 2013; Bechir, 2019). For zinc silicates, studies indicate that the current flotation process, which shows satisfactory results, does not occur with particles less than 20µm (Bechir et al., 2019).

2.1.4 Zinc tailing and reuse

Some of the known gangue of zinc tailing is dolomite, goethite, quartz, kaolinite, calcite, barite, and feldspar (Bulatovic, 2007; Ejtemaei et al., 2014).

The impacts arising from mining occur throughout the entire chain. The main problems are deforestation, road construction giving access to the whole infrastructure of the mine, drilling, and exploration sites. Other issues that are cited are stockpiling of waste and tailings dams, excessive use of water for various purposes, disturbance of natural habitats, cultural heritage (in some cases), noise, accidental or deliberate release of untreated solid, liquid, and/or gaseous contaminants into the ecosystem (Lottermoser, 2007).

The consequence of the mining and mineral processing industry is not only the volume of processed materials but also the volume of waste produced. For example, zinc has a world production estimated at 13million tons, according to United States Geological Survey (USGS, 2020).

Despite achieving around 25-30% of recycling rates (secondary production from zinc scrap), there is still a problem faced by mineral processing companies, which is the final destination and control of the tailings generated in their process of production (U.S. Geological Survey, 2020).

Some alternatives are based on the risks to the environment and aim the reuse for reducing the tailing destined for dams (Edraki et al., 2014; Lei et al., 2015). The destination of this tailing can obtain other options, such as the reuse of the material that is eliminated as gangue during the zinc beneficiation. Table 4 shows some components generally found in zinc ore and some gangues associated (Abkhoshk et al., 2014; Souza

et al., 2009, 2007).

Table 4 - Elemental composition of non-sulfide zinc ores from different parts of Brazil. Adapted from Abkhoshk et al.(2014)

Author	Ore type	Zinc minerals	Gangue minerals	Major elemental composition (wt.%)
Souza et al. (2007)	Zinc silicate calcine	Willimite (major) Franklinite (minor)	Quartz, dolomite, hematite and magnetite	43.5 Zn; 1.25 Pb; 5.9 Fe; 23.3 SiO_2
Souza et al. (2009)	High iron zinc concentrate	Willimite (major) Franklinite (minor)	Quartz, dolomite and hematite	34-39 Zn; 8-11 Fe; 22-25 SiO_2
Souza et al. (2009)	Low iron zinc concentrate	Willimite (major) Franklinite (minor)	Quartz and hematite	46-48 Zn; 3-4 Fe; 26-30 SiO_2

It is observed that, for disposal, the treatment of the tailing is necessary because, depending on its chemical composition, it becomes a risk to the environment. Thus, choosing alternatives to recover metals or other tailings elements may create a purpose and a path for sustainability (Dudka and Adriano, 1997; Erdem and Özverdi, 2011).

The zinc extraction can be associated with the previous extraction of lead to be concentrate first than zinc, considering that both ores are related. Depending on the site's geology, information associated with zinc may also contain silver ore. The lead oxide ore, when found in a dolomitic matrix, has more than one lead ore, being cerussite ($PbCO_3$), anglesite ($PbSO_4$), and pyromorphite ($Pb_5(PO_4)3Cl$). The most common oxides related to dolomite, in these deposits, lead can be found as cerussite ($PbCO_3$) with the presence of galena (PbS). Therefore, toxic elements are found and arise in zinc flotation with each case and ore types (Asadi et al., 2017; Bulatovic, 2007; S. Moradi and Monhemius, 2011).

2.1.4.1 Alternatives for Zn tailing

Studies have investigated possible routes for Zn tailing with the reuse of gangues that are discarded and may have other purposes through physical processing, hydrometallurgical and, pyrometallurgical obtaining a secondary product despite the presence of elements such as Pb and Cd, which according to Xu et al., (2010), using pressure acid leaching of Zn silicate ores reported 0.01% CdO in the Zn ore. Other elements analyzed were Mg, Ca, Al, Pb, Zn, Fe, and K – that can be recovered. Another study also showed impurities during the beneficiation of the Zn oxide in the leaching step.

Such elements were Co, Cd, Ni, Cu, Fe, As, Sn, Se, Ge, and Sb (Abkhoshk et al., 2014). Thus, alternatives are investigated to eliminate toxic elements, such as Cd and Pb of the by-product.

Some routes for Zn tailing to recover elements or even treat ores already found in the tailing are studied, discoursing different alternatives. A study investigated the recovery of Zn from a Pb/Zn flotation tailing, aiming to improve the Zn extraction. Thus, Zn leaching was performed using ferric sulfate and sulfuric acid. The conditions evaluated to recover 94.3% Zn were established with an H_2SO_4 concentration of 1.14mol.L^{-1}, 2.49 acid/ ferric sulfate ratio, S:L ratio equals to 1:1, the temperature at 80°C and 320rpm (Asadi et al., 2017).

In the study of Chen et al., (2020), 36 samples were forwarded to analysis and characterization, and Cd, Cu, Pb and Zn were identified. The concentration of each element varied from 6.99 to 89mg.kg^{-1} of Cd; 75.3 to 602mg.kg^{-1} of Cu; 0.53% to 2.63% of Pb and, 0.30 to 2.54% of Zn. Due to the weathering and acidity process (244kg H_2SO_4/ton), the bioavailability of toxic metals was 37.8% Pb, 12.9% Cd, 12.2% Cr, 5.95% Cu, and 5.46% Zn. One of the alternatives that have been investigated is the addiction of the mining tailing in cement to produce concrete and mortars. For this, there is the immobilization of toxic elements in cement, which follow the specifications of the limits of these toxic metals, such as Pb. Therefore, alternatives that evaluate the leaching method in bricks/mortars/plasters products are made from Pb/Zn tailing and other chemical components; the immobilization of these elements is verified (Li et al., 2017).

Wang et al., (2018) incorporated a Pb/Zn tailing for concrete production, which is a development for a novel sustainable Ultra-High-Performance Concrete (UHPC). Tailings are used to replace cement at 10-20-30-40% by weight. The mechanical properties of concrete decrease with the increase of added tailings. Hence, it is recommended to include less than 30wt.% of Pb/Zn tailings to guarantee the material's resistance. It was also observed that with the increase in the addition of Pb/Zn tailing there was a resistance to the action of the chloride ion with the leaching.

According to Liu et al., (2017), the obtaining of porous ceramic product using a Pb/Zn tailings and fly ash were prepared by sintering, which showed chemical stability of the samples due to the increase in the vitreous phase, so the reaction between the substrate and solid with the acid solution is restricted, using fly ash and Pb/Zn tailings.

After taking into consideration some aspects regarding the alternatives for the mining tailing generated, one of them is the recovery of the secondary material obtained

in the flotation process. One of the minerals present in the gangue is dolomite. Nowadays, the recycling of mining tailings has become an alternative, for example, to use the by-products in agroforestry, building materials, coatings, resin products, glass, ceramics. As they can be used as fertilizers in agriculture and the construction industry, clay-rich waste may improve sandy soils (Lottermoser, 2007).

2.2 PHYSICAL PROCESSING

Some of the techniques used for physical processing are magnetic and gravity or density separation. Gravity separation has been used for centuries aiming the concentration of ores. Magnetic separation is capable of separating materials that contain iron, such as magnetite, and is also known for the concentration or purification of mineral substances (Inácio et al., 2010; Sampaio et al., 2007).

Thus, it is essential to characterize the material (mineralogy) to understand its behavior under the magnetic field's application. Some ores can be attracted to or repelled by it. The mineral substances may be characterized as ferromagnetic (strongly attracted, e.g. magnetite) and paramagnetic (slightly attracted, e.g. hematite); the ones that are repelled are known as diamagnetic. The magnetic separation can be used in wet or dry medium, in which the difference between them is based on the material granulometry. Hence, fractions usually higher than 63µm are submitted to dry low-intensity magnetic separation (LIMS), and fractions lesser than 63µm or between 63 to 125µm are often suitable for wet low-intensity magnetic separation (WLIMS) (Inácio et al., 2010; Kukurugya et al., 2018).

The wet high-intensity magnetic separator (WHIMS) can separate paramagnetic materials, for example, hematite, and aims to concentrate the material of interest, being the magnetic fraction or the non-magnetic fraction. In some cases, the intensity of the magnetic field may vary from 8000 to 13000Gauss. For particles smaller than 63µm, the intensity is higher or equal to 8000Gauss for a satisfactory separation from a paramagnetic material. The intensity may be adjusted by controlling the amperage of the coil input. The material used in the magnetic separation is characterized by 30% wt. of tailings and 70% wt. of water (Junca, 2009; Sierra et al., 2013).

Gravity and density separation are based on the differences of densities, granulometry and medium density. For density separation, some common organic with the density of the medium is tetrabromoethane ($CHBr_2CHBr_2$), bromoform ($CHBr_3$),

methylene iodide (CH_2I_2), clerici's solution ($CH_2(COOTI)_2HCOOTI$), trichloroethane (CCl_3CH_3), trichlorobromine methane (CCl_3Br), methylene bromide (CH_2Br_2), tribromo-fluoromethane (CBr_3F) used to separate minerals in solution (Inácio et al., 2010).

An example of the application of gravity separation is the shaking table, in which the concentration criterion, presented in Equation 3, must be greater than 2. Table 5 shows the meaning of the concentration criterion values. The granulometry must be in a range from 37µm to 2mm. When the fine fraction reaches 5% of the material, it may impair the separation, causing the pulp viscosity to increase and making it difficult to recover the material of interest (Inácio et al., 2010; Sampaio et al., 2007).

$$CC = (\rho_d - 1)/ \rho_l - 1) \qquad \text{Equation 3}$$

In which:

ρ_d = densities of the denser mineral;
ρ_l = densities of the less dense mineral;
and water density equal to 1.

Table 5 - Meaning of the concentration criterion values.

Concentration criterion (CC)	**Meaning**
>2.5	Efficient separation up to 74µm
2.5 – 1.75	Efficient separation up to 147µm
1.75 – 1.50	Separation up to 1.4mm, but difficult
1.70 – 1.20	Separation up to 6mm, but difficult

2.3 HYDROMETALLURGY PROCESSING

Hydrometallurgy intends to produce metals or compounds, in which extraction or recovery derives from minerals. At least one of the reactions during the operation is performed in an aqueous medium (Gupta, 2003).

On the other hand, pyrometallurgy requires blast furnaces on its route for the extraction or purification of metals. The use of temperature and heating allows high reactions and chemical equilibrium, resulting in a molten or gaseous state. The principle of hydrometallurgy the use of a suitable leaching agent to dissolve the metals of interest. Usually, hydrometallurgical processing is followed by a purification step, in which, adsorption, solvent extraction, ion-exchange resins, or electrochemical reduction may be used, which objective is to remove impurities and separation of metals of interest.

Precipitation is the main purification step used. Figure 3 shows a simplified flowsheet of a hydrometallurgical process unit (Gupta, 2003; Havlik, 2001).

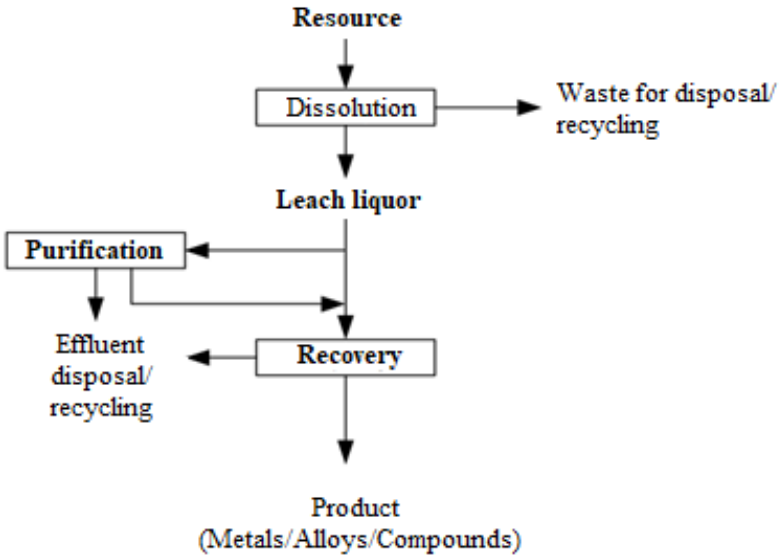

Figure 3 - Basic unit of hydrometallurgical process, (Gupta, 2003).

2.3.1 Leaching

The leaching, being the central unit of the hydrometallurgical route, allows directing the yield of the recovered metal. It is based on the extraction of the selected element e.g. diluted sulfuric acid used in zinc mining tailings under atmospheric or pressurized conditions. The interactions between the factors and effects of the process are generally the temperature, solid-liquid ratio, and acid concentration. The leaching function is to dissolve the metals present in a solid through an aqueous solution containing the leaching agent. It is also defined as the dissolution process of soluble substances in a solid material in a solvent. Therefore, it is important to choose a suitable leaching agent for the required metal to be transferred to the solution. The general conditions for providing the dissolution can be derived from the thermodynamic data presented in the Pourbaix diagram (Gupta, 2003; Havlik, 2001).

2.3.2 Cementation

Cementation is used to extract elements from the solution acquired in processes during the beneficiation of ores, for example, obtained in the leaching step. This technique may be used when other methods, such as precipitation, are not appropriate. In

cementation it is essential to evaluate the reduction potential of each element and the global redox reaction. Cementation aims to reduce the element that must be eliminated and oxidize the added element in a metallic form – as a powder, according to Equation 4. The element that is reduced is more electropositive than the oxidized one. An example of cementation is using Zn to precipitate Cd electrochemically. In this case, Cd is more electropositive than Zn, as shown in Table 6 (Havlik, 2001; Younesi et al., 2006).

$$Me_1 + Me_{2(s)} \rightarrow Me_{1(s)} + Me_2 \qquad \text{Equation 4}$$

Table 6 – Electrode potentials of metal. Adapted from Havlik (2001).

Metal		**E^0[V SHE]**	
Me_2	**Me_1**	**Me_2**	**Me_1**
Zn	Cu	–0.763	+0.34
Fe	Cu	–0.44	+0.34
Ni	Cu	–0.23	+0.34
Zn	Ni	–0.763	–0.23
Cu	Hg	+0.34	+0.798
Zn	Cd	–0.763	–0.402
Zn	Fe	–0.763	–0.44
Co	Ni	–0.27	–0.23

Figure 4 shows cementation as a step in the treatment of a solution acquired during the leaching. According to material composition or the ore beneficiation and elements of interest, precipitation, cementation and/or electrolysis may be feasible to obtain the desired product. Therefore, some factors that contribute to the electrochemical reduction of elements are the contact time, the ratio of metallic and oxidized elements, agitation, particle size and pH of the solution (Havlik, 2001; Ku et al., 2002).

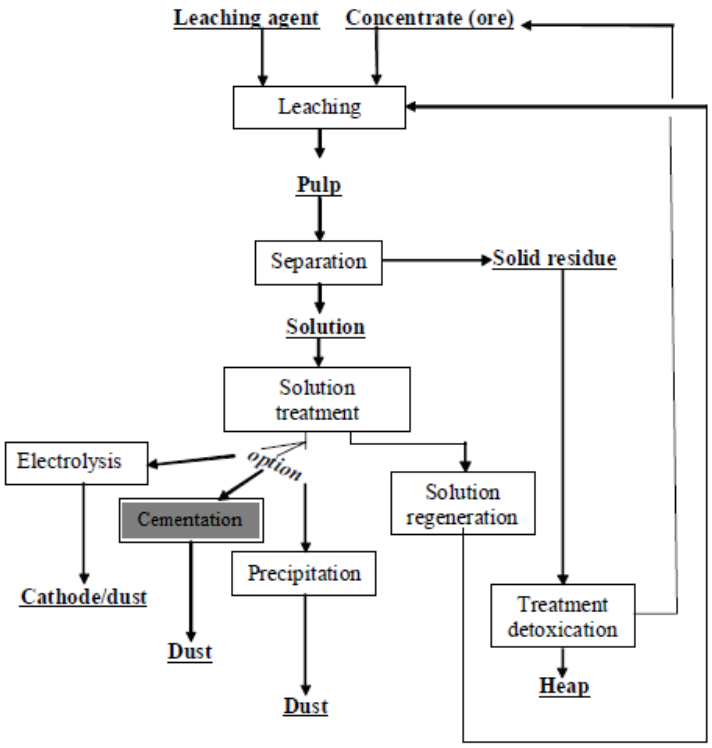

Figure 4 - Hydrometallurgical route and the purification process. Havlik (2001).

According to the literature, cementation is an alternative that has shown satisfactory results to eliminate impurities. The Zn:Cd ratio, the initial concentration of Cd (1050 to 7250mg.L^{-1}) and lower (109 to 474mg.L^{-1}), reaction kinetics, the particle size of Zn powder, and the Zn behavior during the cementation process was evaluated to remove Cd as an impurity using Zn powder (Halikia and Voudouris, 2005; Sadegh Safarzadeh et al., 2007; Sędzimir, 2002; Younesi et al., 2006).

In the studies carried out by Younesi et al., (2006), a temperature of 20°C was used for cementation tests, and the time was evaluated up to 1000s, observing the behavior of Cd concentration from 109 to 474mg.L^{-1} with a Zn:Cd equal to 5:1. 60% Cd removal was obtained in 16min. However, at concentrations from 1050 to 7250mg.L^{-1}, after 3.5min, Cd was removed by 100%. According to Halikia and Voudouris (2005), Zn tends to dissociate during cementation as a function of time depending directly medium's pH, stirring speed, and cadmium concentration. The solubility of Zn can be influenced by increasing the pH, impairing the removal of Cd.

2.3.3 Sulfide precipitation

Precipitation is a reaction that occurs in a solution between one or more soluble species mixed to a precipitating agent to form an insoluble product, known as a precipitate. Equation 5 to 7 demonstrate the reaction and chemical equilibrium in the precipitation of metal sulfide in the presence of metal ions and sulfide (Jackson, 1986; Lewis, 2010).

$$H_2S_{(aq)} \rightleftarrows H^+_{(aq)} + HS^-_{(aq)} \qquad \text{Equation 5}$$

$$HS^-_{(aq)} \rightleftarrows H^+_{(aq)} + S^{2-}_{(aq)} \qquad \text{Equation 6}$$

$$Me^{2+}_{(aq)} + S^{2-}_{(aq)} \rightleftarrows MeS_{(s)} \rightarrow Kp_s \qquad \text{Equation 7}$$

The sulfide ion can form precipitates with metallic cations according to Equation 7. The equilibrium constant of the precipitation reaction is presented by Equation 8 as a function of temperature and ionic strength. (Jackson, 1986; Lewis, 2010).

$$Kp_s = [Me^{2+}][S^{2-}] \qquad \text{Equation 8}$$

Figure 5 shows the sulfide species in a system as a function of the medium's pH found at a constant temperature. The equilibrium concentration of sulfide ions is dependent on the pH of the saturated solution of hydrogen sulfide (Lewis, 2010).

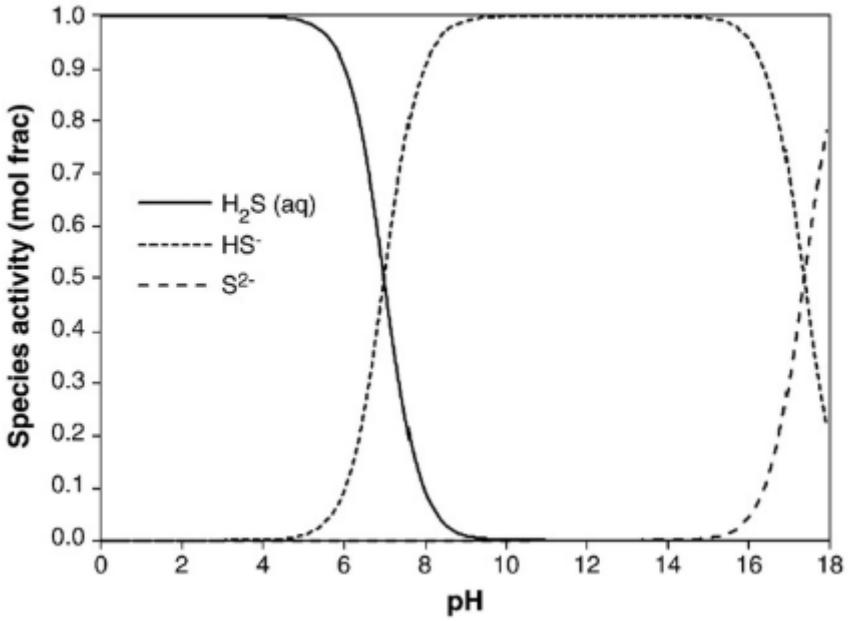

Figure 5 – Sulfide speciation in the function of the pH, Lewis, (2010).

When the solubility product is known, as shown in Equation 9 to 11, and the S^{-2}/pH ratio is applied for more than one metallic sulfide, the trend of precipitation at a constant temperature is known (Jackson, 1986).

$$K_s = a_{M^{2+}}^{m} x\, a_{s^{2-}}^{n} \qquad \text{Equation 9}$$

or

$$a_{M^{2+}}^{m} = \frac{K_s}{a_{s^{2-}}^{n}} \qquad \text{Equation 10}$$

or

$$log\ a_{M^{2+}} = \frac{log\ K_s}{m} - \frac{n\ log\ a_{s^{2-}}}{m} \qquad \text{Equation 11}$$

It is shown in Equation 10, a demonstration of the sulfides precipitation for specific metals including Cd and Pb, as is presented in Figure 6. Sulfide precipitation is given according to the metal's activity log to be precipitated and the log of S^{2-}, which is added into the solution; thus, the pH is varied. As presented in Figure 6, Cd is precipitated as CdS at pH0 and Pb at pH-1 (Jackson, 1986).

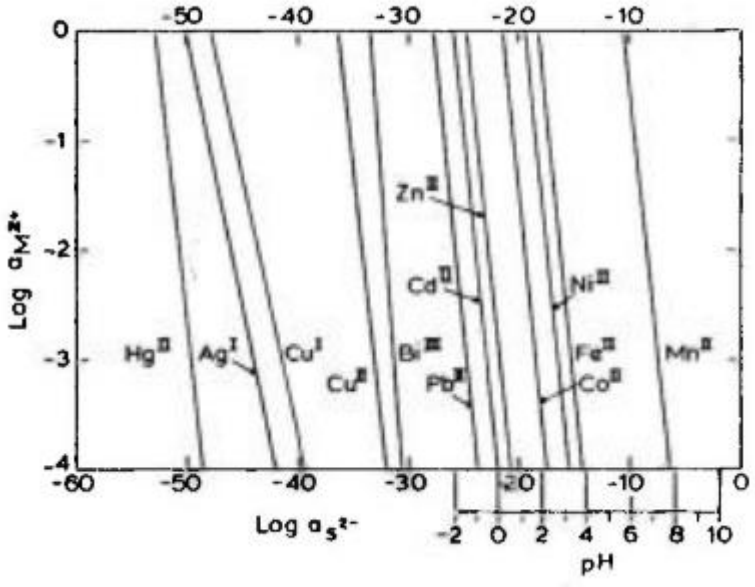

Figure 6 – Sulfide precipitation diagram, at 25 ° C and 1atmosphere pressure of hydrogen sulfide, (Jackson, 1986).

Precipitation by sulfides can be carried out with other sulfides in aqueous media such as Na_2S, NaHS, and NH_4S (Lewis, 2010). Studies for Cd precipitation used sodium sulfide (Na_2S) from 0.1 to 1.0mol.L^{-1}. As the amount of Na_2S increased, the precipitation of CdS in an acidic solution of H_3PO_4 also increased (Ennaassia et al., 2002). The sulfide

precipitation of CdS in supersaturated solutions in an aqueous medium at pH 2 at 25°C was also investigated by Dalas et al., (1991).

In precipitation, difficulties can be found in some elements that are presented. For example, the calculations attributed to the curves represented for the equilibrium solubility compared with a study carried out for precipitation by cadmium sulfides tests are incompatible. This may be justified due to the formation of colloidal CdS particles, which difficulties completing the separation of the solids from the aqueous phase (Ennaassia et al., 2002; Lewis, 2010).

2.4 DOLOMITE AND MAGNESIUM

Dolomite is the main object of this study. The dolomite is composed of double salts of magnesium and calcium carbonate and contains low concentrations of iron and manganese impurities. It is formed from calcite transformations in the presence of magnesium ions. Dolomite rock is useful in the chemical industry for the preparation and serves as building stone and decoration (Czerwinski, 2011; Friedrich and Mordike, 2006; Mordike and Ebert, 2001).

The molecular structure of dolomite is presented in Figure 7, and it is shown its crystalline form as a rhombohedral system (Figure 7a). Layers of Mg^{2+} and Ca^{2+} cations are intercalated and regularly alternated by $(CO3)^{2-}$ anions, allowing it to be a stable structure (Putnis, 1995; Klein and Mizusaki, 2007).

In Figure 7b) there is a two-dimensional chemical structure of dolomite, carbonate ions $(CO_3)^{2-}$ with a single and double valence bond between carbon and oxygen. There are three oxygen atoms bonded to the carbon in covalent bonds. The dolomite molecules are formed due to the ionic bond between the positive charge of Mg and Ca, and the two negative charges of carbonate (Solihin et al., 2018).

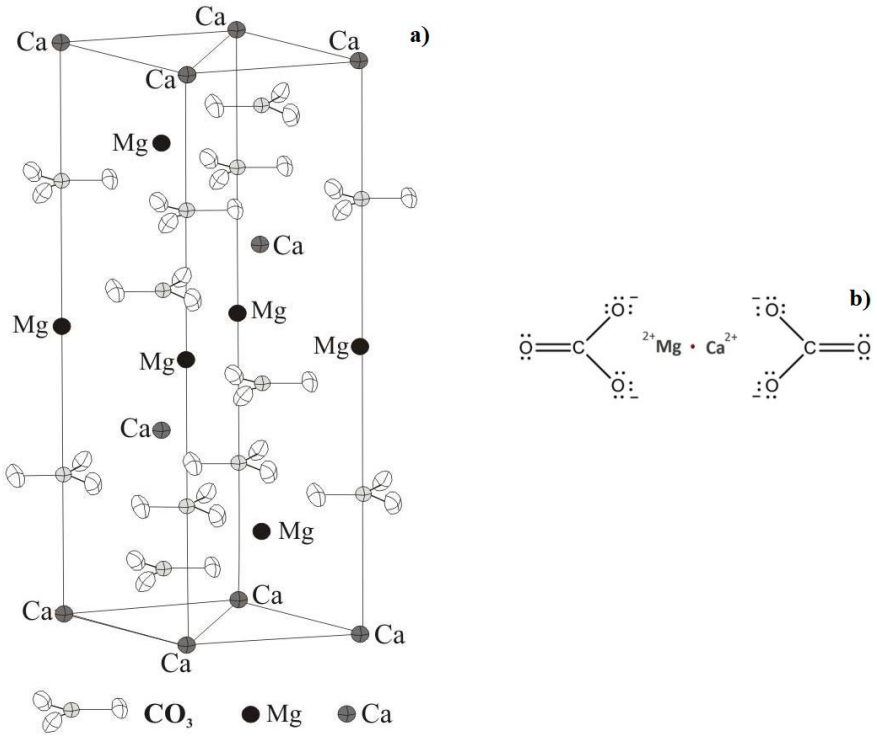

Figure 7 – a) Crystalline structure of dolomite, crystallized in the rhombohedral system (Putnis, 1995); b) Molecular structure of dolomite (Solihin et al., 2018).

When found in nature, dolomite dissociates in water, making magnesium available to the environment. Its dissolution occurs in the presence of an aqueous medium followed by the immediate precipitation of the hydrated magnesium carbonate, thus occurring a dissolution/precipitation process. Dolomite creates some layers during the carbonate dissolution process. These layers, which are created with the carbonate grows over time and do not reach a stabilization thickness, except when the carbonate dissolves faster than the mineral's precipitation. Thus, the reaction on the surface occurs in seconds or minutes at room temperature. During this time, a superficial rearrangement of the carbonates in an aqueous medium occurs (Renard et al., 2019).

The Scottish chemist Joseph Black introduced magnesium in 1755, after discovering that the magnesia contained a new element - magnesium. Magnesia was initially known as "white stone" or "white earth". Magnesium is found in nature as bivalent due to its arrangement of electrons. The low standard reduction potential of magnesium is the reason why no metallic magnesium is found in nature. The main raw materials to produce magnesium are shown in Table 7. They differ in magnesium content and production methods and their origin. Some are mined, some in open-pit mining, others originate from various processes in seawater and salt lakes, and others originate

from the waste of the asbestos production process (Horst, Friedrich E.; Mordike, 2006).

Table 7 - Raw materials of magnesium and their respective chemical formula, (Horst, Friedrich E.; Mordike, 2006).

Material	Chemical formula
Magnesite	$MgCO_3$
Dolomite	$MgCO_3 \cdot CaCO3$
Bischofite	$MgCl_2 \cdot KCl \cdot 6H_2O$
Serpentine	$3MgO \cdot 2SiO_2 \cdot 2H_2O$
Sea water	$Mg^{2+}_{(aq)}$

According to the last update of the European Commission's report, magnesium has been considered a critical raw material. Several 61 materials were evaluated, and 21 were characterized as critical raw materials. They are assessed according to the growth of human population, the increase in the exploitation of resources, their economic importance, and the number of reserves available for exploration. Such materials are defined as essential for industrial activity. However, having limited reserves available that present some difficulty for their exploration. The supply risk associated with magnesium is due to the problematic replacement of the material, to its end-of-life recycling rates, and the disposition or even a commercial dominance of these ores is in China. According to Figure 8, magnesium is the second material with the greatest economic importance and the fifth in supply risk. (Mathieux et al., 2017; Perez et al., 2019).

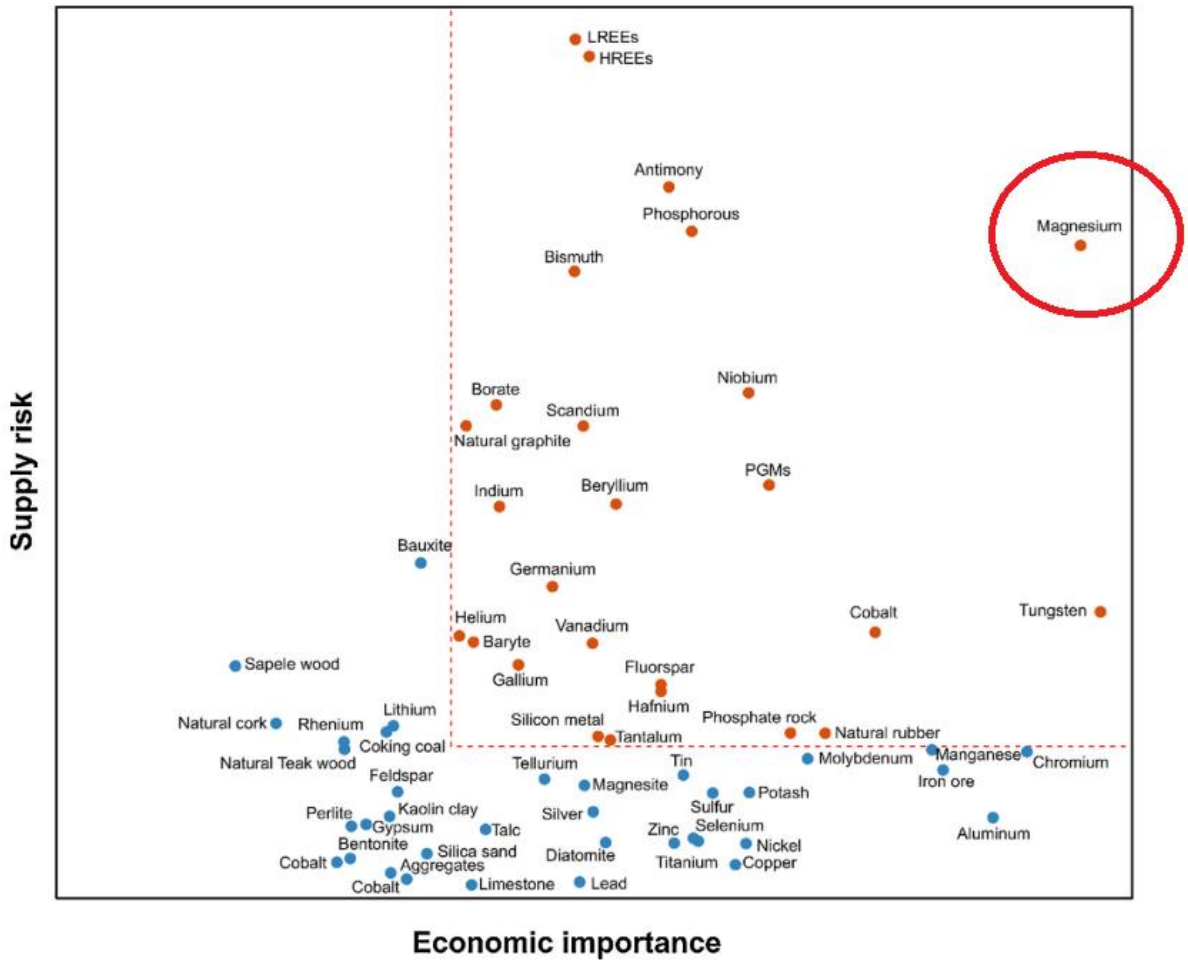

Figure 8 – Critical raw materials in the upright (red) according to their economic importance and supply risk. Adapted from Perez et al., (2019).

Magnesium is used in several areas (fertilizers; construction; refractories; transportation; desulfurization agent; packaging), it is an economically important material, and, as shown in Figure 9, China accounts for 87% of the global magnesium supply. Besides, 14% of the total amount of magnesium is recycled and returns to the economy as secondary material. (Mathieux et al., 2017; Peiró et al., 2018; Perez et al., 2019).

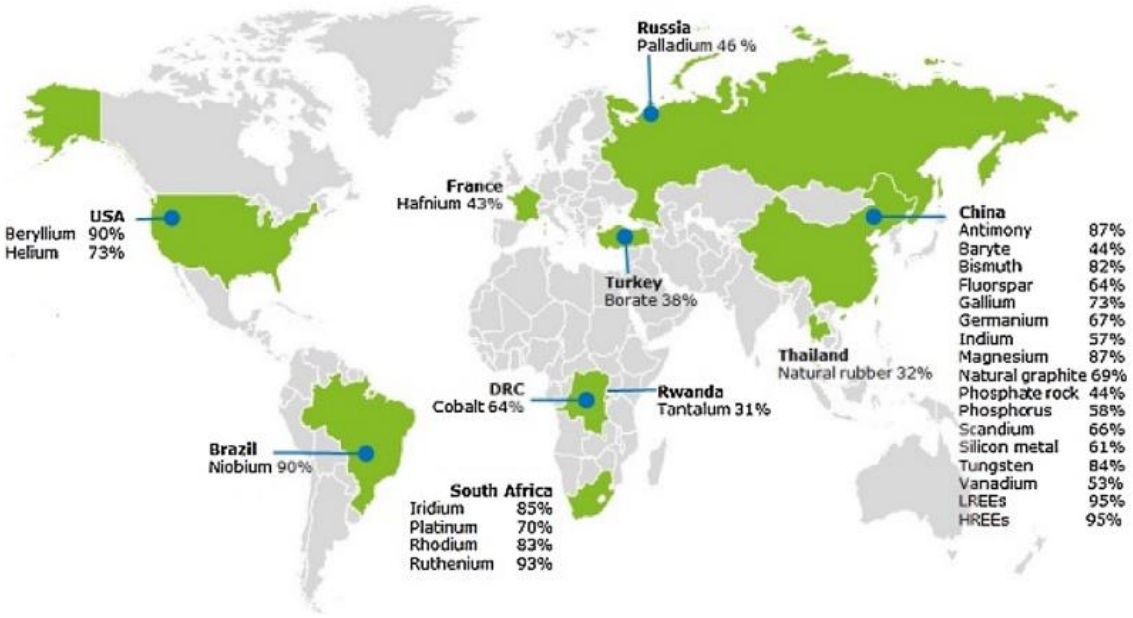

Figure 9 – Scheme of critical raw materials in the upright (red) about their economic importance and supply risk, Perez et al., (2019).

Thus, it is shown the importance of recovering magnesium as a secondary product. Studies show the feasibility of magnesium extraction using hydrometallurgy from dolomite, magnesite, dolomite phosphate rock, nickel laterite, and magnesite tailings (Abali et al., 2006; Karidakis, 2005; Puthiya et al., 2017; Solihin et al., 2018; Xiong et al., 2014).

2.4.1 Magnesium leaching

According to the literature, magnesium leaching varies due to the initial material, which can be dolomite or magnesite associated with other impurities and even acquired in tailing. Therefore, the conditions of the leaching agent and its concentrations may vary. For example, the magnesite ($MgCO_3$) leaching was used to obtain magnesium compounds for an industrial process. Magnesium may also be obtained for some purposes such as refractory manufacturing, used in the cement, glass, lime, paper, pharmaceutical, and chemical industries. In the industrial process, one of the interests is to produce pure $MgSO_4$. Thus, using H_2SO_4 as a leaching agent allowed the formation of soluble $MgSO_4$. Conditions for $MgCO_3$ leaching to obtain $MgSO_4$ were used $2mol.L^{-1}$ of H_2SO_4 an S:L ratio equals to 1:20 at a temperature of 65°C, in 60min of leaching. The dissolution of Mg achieved 96.32% (Abali et al., 2006).

A study reported the leaching of magnesium from a dolomitic phosphate ore using

as a leaching agent a dilute waste containing 3.85wt.% H_2SO_4 obtained from titanium dioxide pigment production. The Mg removal achieved 98.31% being demonstrated that dolomite is dissolved by H^+ using the dilute waste acid. The qualitative analysis by XRD showed the dissolution of dolomite and the gypsum formation (Xiong et al., 2014).

Another study (Solihin et al., 2018) aimed to evaluate the extraction of magnesium and calcium using hydrochloric acid to obtain magnesium oxide. Some industrial uses of MgO are pharmaceutical, slow-release fertilizer, fire retardant materials, and catalysts. In the referred study, the dissolution of magnesium and calcium carbonate using HCl was stabilized in 5-10s. The evaluated acid concentrations were 0.05 - 0.1 - 1.0 - 2.0 - 2.5 and 3.0mol.L^{-1}. The dissolution of carbonate released carbon dioxide. The gas caused the pressure to increase and, consequently, the temperature as well, if considering a closed system. As the pressure increased, the dolomite dissolution reaction occurred in 5 to 300s. Therefore, with an HCl acid concentration of 3mol.L^{-1} and a molar HCl/Dolomite ratio of 3 the extractions achieved 100% Mg, and 80% Ca in 5min.

Özdemir et al., (2009) recovered ($MgCl_2 \cdot 6H_2O$) from a magnesite tailing. The evaluation of the temperature, HCl concentration, S:L ratio, particle size and stirring speed was carried out. The product achieved a purity of 91% after evaporating the leaching solution. The conditions used were: temperature of 40°C, 1.0mol.L^{-1} of HCl, S:L ratio of 1:100, particle size of 100µm, stirring speed of 1250rpm and leaching time of 60min.

2.4.2 Solubility curve of $MgSO_4$

One of the factors for investigating leaching using dolomite is the evaluation of its solubility curve. In this curve, the influence of temperature in g.L^{-1} of $MgSO_4$ in H_2O was studied, as shown in Figure 10. The temperature range in which $MgSO_4$ develops a re-precipitation is observed. The solubility of magnesium sulfate is extremely relevant to know its behavior in hydrometallurgy processing. Magnesium presents a behavior known as inverse solubility, because, as the temperature increases – mainly above 60°C, magnesium sulfate tends to precipitate (Figure 10). This is a support material to investigate the thermodynamic reaction of the product of interest in the leaching process (D'Ans, 1933; Kay, 1969; Podder and Kalkura, 2001; Robson, 1927, Wanderley et al., (2020).

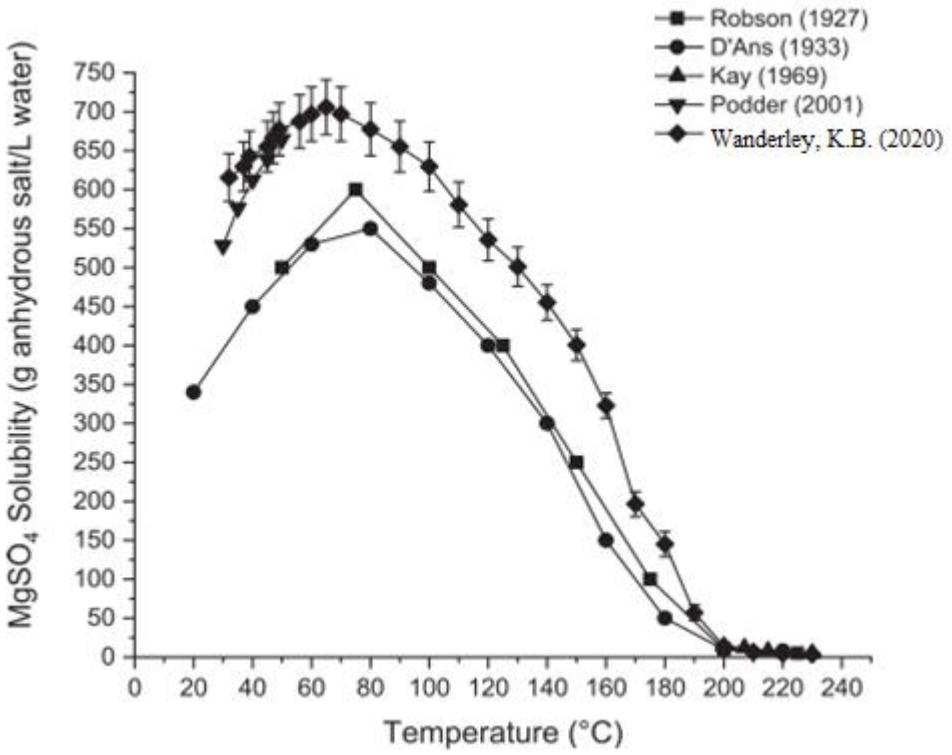

Figure 10 - Solubility curves of magnesium sulfate in $g.L^{-1}$ as obtained by different authors (D'Ans, 1933; Kay, 1969; Podder and Kalkura, 2001; Robson, 1927, Wanderley et al., (2020). Adapted from Wanderley et al., (2020).

Crystallization can be used to form $MgSO_4$ from leaching liquors. Wanderley et al., (2020) performed a study to crystallize $MgSO_4$ without decomposition of the material. The stabilization period was set in 5h. The authors achieved 81% of the crystallization of magnesium sulfate monohydrate salt ($MgSO_4 \cdot 7H_2O$) at 230°C and pH equal to 5.7. According to Figure 10, at about 80°C, a peak in the solubility of $MgSO_4$, is noticeable. At temperatures above 100°C, the solubility decreases from $700g.L^{-1}$ to less than $650g.L^{-1}$ with a tendency to decline. Hence, from 200 to 230°C, the $MgSO_4$ may be precipitated in its crystallized form.

2.4.3 Solubility curve of $CaSO_4$

Considering that one molecule of dolomite contains two calcium carbonates and magnesium, the $CaSO_4$ solubility curve and its phases found in an aqueous medium at temperatures from 0 to 120°C are shown in Figure 11.

Figure 11 shows that calcium sulfate, at temperatures less than 40 to 60°C, has the most stable phase as gypsum. Both gypsum and anhydrite phases present less solubility

when compared with bassanite – which is soluble in temperatures from 10 to 20°C. From 30°C, bassanite has a decreased solubility. Unlike the gypsum and anhydrite phases, there was no increase in the solubility curve regardless of the temperature (Driessche et al., 2019; Freyer and Voigt, 2003).

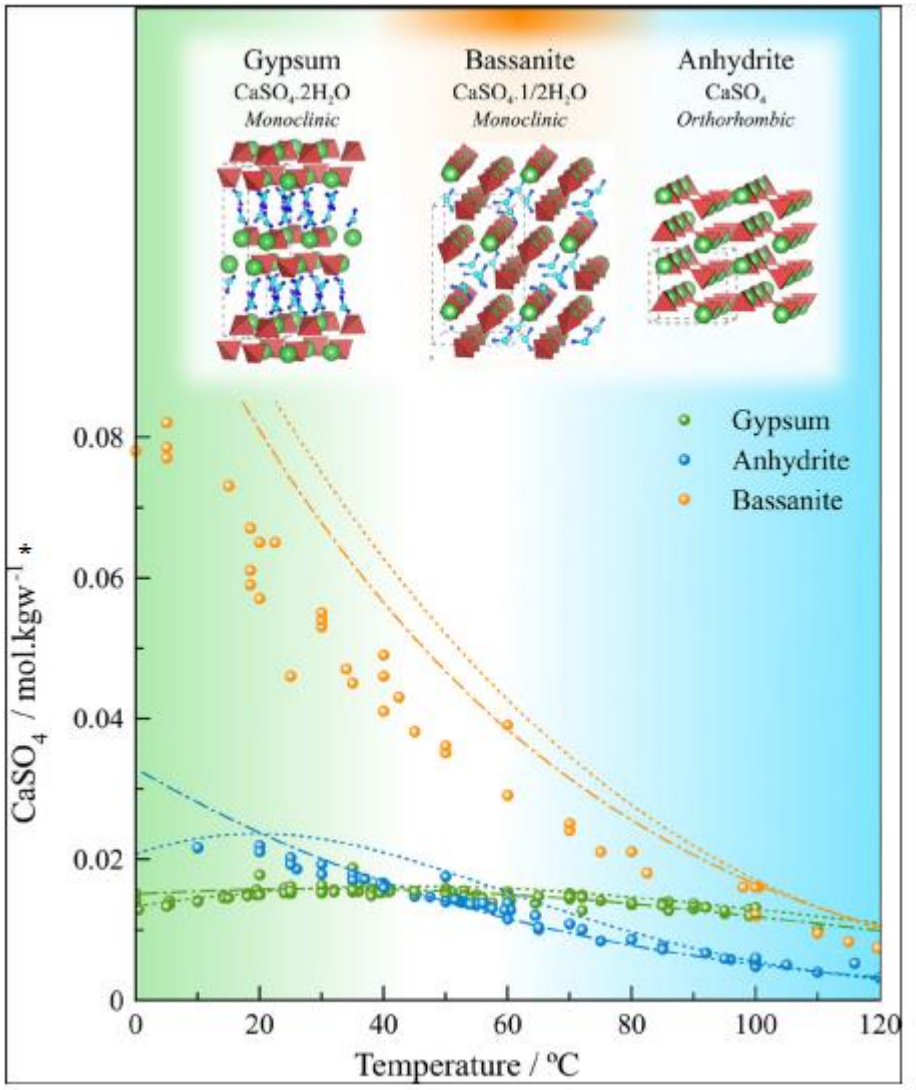

Figure 11 – $CaSO_4$ solubility curve in three phases: gypsum, anhydrite, bassanite, and their respective crystalline structures represented by green dots – Ca; red tetrahedra – SO_4^{-2}; blue structure – water molecules. Adapted from (Driessche et al., 2019). *****mol.kgw^{-1} which *w* represents water.

2.4.4 Fertilizer for soil

Soil is the primary environment for the development of planting and ecosystem interaction. To know the methods and techniques of soil fertility is to understand the basic need for plant production. Soil fertility in modern agriculture is a part of a dynamic system. Therefore, to identify some parameters and indicators such as the law of minimum (crop production is limited by mineral nutrient less available to plants), soil

correction and the cation exchange capacity (CEC) can collaborate to obtain a soil with better planting conditions and even to prevent problems such as erosion. The most common magnesium source is dolomitic limestone - an excellent material containing calcium and magnesium which neutralizes soil acidity (Lopes, 1998). The extension in which a crop can benefit from an applied nutrient depends on the form or the physical and chemical composition in which it is applied. The way in which nutrients are applied to the soil has always been considered a key factor, particularly influencing the availability of magnesium, since there is a variation in the solubility in water between the various forms of magnesium (Härdter et al., 2004).

The macronutrients in the soil and their availability are essential factors for their subsequent absorption by plants. Figure 12 shows a general scheme of how nutrients behave in soils with adsorption of elements such as Ca, Mg, NH, Na, K, which occurs in the presence of clay, facilitating the release of plants with the correct management. It is also presented that there is less interaction with the macronutrients in the sandy soil (Jones, 2012; Lopes, 1998; Whalen, 2012).

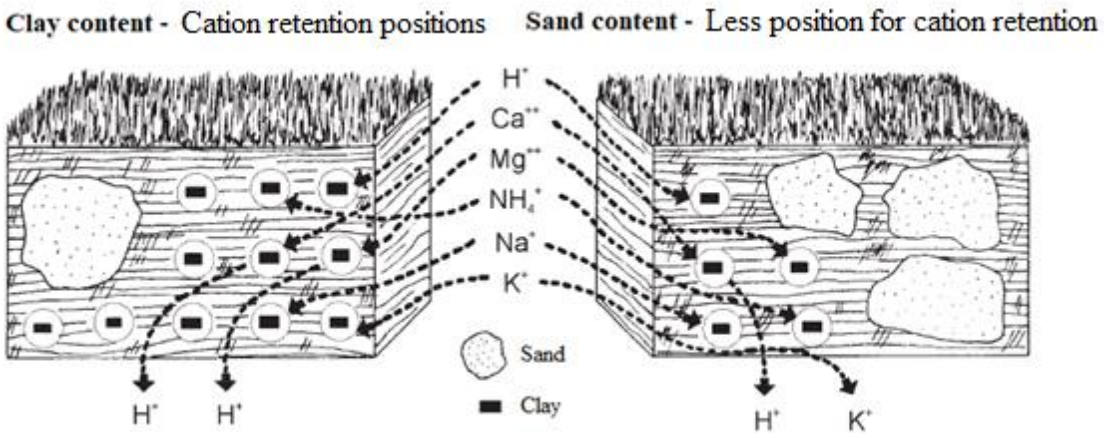

Figure 12 – Adsorption and reserve of nutrients in predominantly sandy and clay soil. Adapted from Lopes (1998).

Some nutrients are considered essential for soil and agriculture. In Figure 13, the primary and secondary macronutrients, as well as micronutrients are shown. Both Ca and Mg is classified as secondary macronutrients. The difference between Ca and Mg is that $MgSO_4$ is considered as a fertilizer for secondary macronutrients, while Ca is also applied as liming or soil conditioner. The soil condition related to Mg and Ca deficiency is soil acidity (pH<5.4) when both elements are leached through the soil by the actions of rain

or irrigation. When Mg deficiency occurs, there is an excess of Ca and K. On the other hand, for Ca deficiency, there is an excess of Al solubility compared to Ca. The excess of Al and lower levels of Mg and Ca concerning Al are responsible for the productivity of crops grown in acidic soils since Al inhibits root development and tends to limit the absorption of other nutrients (Jones, 2012; Lopes, 1998).

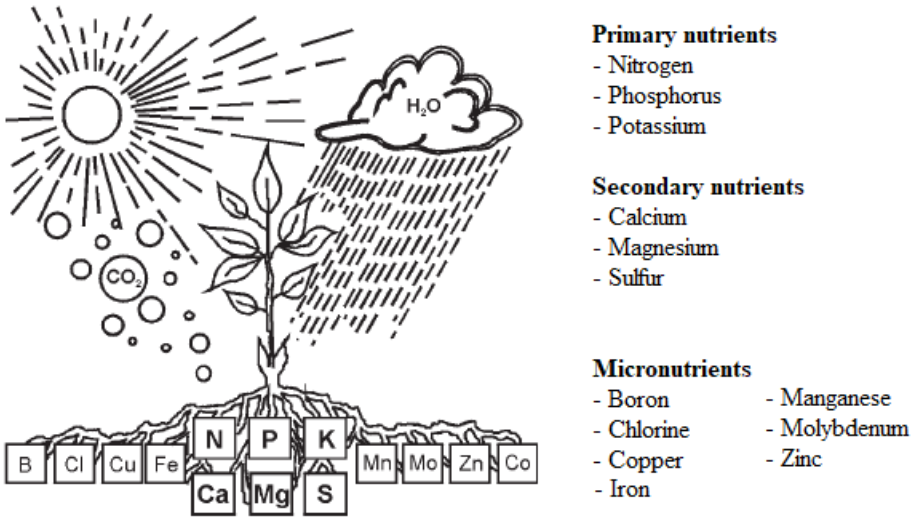

Figure 13 – General scheme of primary and secondary macronutrients also the micronutrients for plants Adapted from Lopes, (1998).

Besides that, added by fertilizers or correctives, magnesium in soil comes from the weathering of rocks that contain minerals such as biotite, dolomite, and chlorite. As a cation, Mg^{2+} is subject to cation exchange, which is why it is found in the soil solution and is adsorbed to the surfaces of clays and organic matter (Lopes, 1998).

Calcium and sulfur found in gypsum are used to correct the soil, mainly as liming or conditioner, which reduces the toxicity of aluminum and are present in soil colloids, and does not directly supply to Ca and S. Both Ca and S are available in their soluble form (ionic), as they are found on a horizon below the surface of the ground - calcium has a Ca^{2+} cation with mobility for plants, meaning that is available. Unlike liming, which acts in the superficial ground, gypsum as a conditioner of soil has a role in reducing the toxicity of Al present in the medium. Due to aid the supply of nutrients to plants, reducing the presence of Al improves the roots system and absorption of water and nutrients in the roots (Whalen, 2012).

As is shown in Figure 14, there is a reservoir of cations available, but these cations in soil may behave in an acidic or basic form. For example, Al^{3+} (exchangeable) and H^{+}

(not exchangeable) are acidic in soil. On the other hand, Ca^{2+}, Mg^{2+}, K^{+} and Na^{+} have a basic behavior. The cation exchange capacity at pH 5.5 is considered effective due to the availability of Ca, Mg, K, and Na cations. At pH 7, the total reservoir of cations in the soil is represented, which covers all available cations. The more acidic a soil is, higher the content of these acidic cations and the lower the content of basic cations (Lopes, 1998).

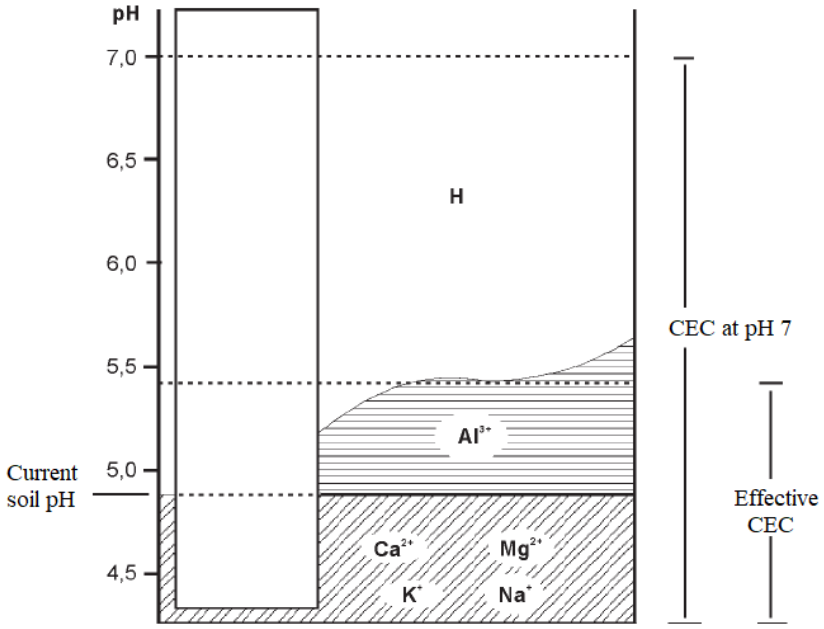

Figure 14 – Availability of cations in the soil in relation to pH and cation exchange capacity (CEC). Adapted from Lopes, (1998).

2.5 CEMENT AND MINING TAILING

The use of the tailing obtained in mining as an aggregate in cement for civil construction material is an option that has been studied. However, some specifications must be followed to classify a cement. According to Law N° 12,305, of august 2, 2010, (Lei n° 12305/10) which instituted the Política Nacional de Resíduos Sólidos (PNRS), the term in *English* is National Solid Waste Policy, in 2010 defines the destination of waste generated, and the concrete by the Associação Brasileira de Normas Técnicas (ABNT), the term in *English* is Brazilian Association of Technical Standards, through NBR 10004 – Waste classification, is defined as an inert material. According to ABNT-NBR 10004 waste is classified into two major classes (ABNT NBR 10004, 2004):

- Waste class I – Hazardous;
- Waste class II – Non-hazardous, which is subdivided into:
    - Class II A – Non-inert;
    - Class II B – Inert.

Thus, Waste class II B is defined according to ABNT NBR 10004, (2004) as:

> Any residues that, when sampled in a representative manner, according to ABNT NBR 10007, and submitted to dynamic and static contact with distilled or deionized water, at room temperature, according to ABNT NBR 10006, have none of their constituents solubilized at higher concentrations water potability standards, with the exception of appearance, color, turbidity, hardness and flavor, as per Annex G. / *Quaisquer resíduos que, quando amostrados de uma forma representativa, segundo a ABNT NBR 10007, e submetidos a um contato dinâmico e estático com água destilada ou desionizada, à temperatura ambiente, conforme ABNT NBR 10006, não tiverem nenhum de seus constituintes solubilizados a concentrações superiores aos padrões de potabilidade de água, excetuando-se aspecto, cor, turbidez, dureza e sabor, conforme anexo G.*

The waste undergoes a sorting process that classifies it among the previously presented classes. In Class II B a solubilization test is performed, which presents the extract maximum limit for the solubilization tests. Cadmium and lead have limits equal to $0.005 mg.L^{-1}$ and $0.01 mg.L^{-1}$, respectively (ABNT NBR 10004, 2004).

Therefore, mining tailing that is studied with the intention of being added to the cement production process must follow the same protocols, that is, behave inertly to the environment. From this, studies that show the immobilization of toxic and harmful elements to the environment as well as to living beings have been investigated (Faure et al., 2019; Gesoglu et al., 2016; Singh et al., 2020; Sun et al., 2020).

The purpose of cement production is to be used as concrete, as well as mortar, in building blocks and to seal gaps. The most well-known cement is Portland Cement which is based on a hydraulic blinder consisting of clinker, gypsum, and inorganic materials (blast furnace slag, compost of silicate or limestone with a total content of inorganic materials from 6 to 35wt.%) (Darmanto and Amalia, 2020).

The gypsum used in the production of cement has been studied and the concentration of gypsum added to the material is currently 5% (Gesoglu et al., 2016). A study performed by Hansen and Sadeghian (2020) investigated the recycling of gypsum waste for concrete. They used an amount above 5% to produce cement and evaluated the mechanical performance of concrete using gypsum powder with fly-ash – fulfilling the

role of complementary material. The different gypsum concentrations ranged from 0-5-10-15-20%, 25% and 50% of fly ash.

Cement with the addition of mining tailing containing toxic elements was immobilized in cement. Li et al., (2017) studied the addition of Pb/Zn tailing containing Zn, Pb, Cd, and Cu in bricks, in accordance with concentrations within the local leaching standards. The analyzes showed that the presence of aluminum and silicon could interact with lead, forming $PbAl_2Si_2O_8$, which facilitates the immobilization of lead. However, an excess of SiO_2 and Al_2O_3 may result in lead leaching due to the difficulty of forming stable structures.

Nouairi et al., (2018) studied the addition of a Pb/Zn tailing in clinker/cement. The inertia of the material was evaluated considering the presence of toxic metals such as Pb. Cement and mortars were submitted to acid attack (with aqua regia) following the accepted standards for waste in landfills in accordance with Article 16 and Annex II of Directive 1999/31 / EC, to simulate the leaching and to compare the clinkers with the addition of the tailings. The immobilization of Pb, Zn, and Cu was 75 to 85% in the products obtained as mortar, presenting no risk to the environment.

2.6 LEGISLATION AND AGRICULTURE PRODUCTS

In Brazil, there are some specifications and maximum limits of some toxic metals for each product used in agriculture, precisely because it considers the quality of the soil and crops which also aims for living beings' safety. Therefore, the CONAMA (Conselho Nacional do Meio Ambiente, the term in E*nglish* is the National Environment Council), has the following RESOLUTION Nº 420, OF DECEMBER 28th, 2009 published in Diário Oficial da União (DOU, 2016). Correlations: Amended by CONAMA Resolution Nº 460/2013 (CONAMA, 2013, 2009):

> It provides for criteria and oriented values of soil quality regarding the presence of chemical substances and establishes guidelines for the environmental management of areas contaminated by these substances because of anthropic activities. / *Dispõe sobre critérios e valores orientados de qualidade do solo quanto à presença de substâncias químicas e estabelece diretrizes para o gerenciamento ambiental de áreas contaminadas por essas substâncias em decorrência de atividades antrópicas.*

From the resolution, normative instructions are also directed to products to be used in agriculture. Normative instructions expose the maximum limits for toxic metals established by the Secretary of Agricultural Defense – (SDA, 2016):

> Art. 1º Fertilizers, correctives, inoculants and biofertilizers, to be produced, imported or commercialized, must satisfy the limits established in Annexes I, II, III, IV and V of this Normative Instruction concerning the maximum concentrations allowed for phytotoxic agents, pathogenic to man, animals and plants, toxic heavy metals, pests and weeds. / Art. 1º Os fertilizantes, corretivos, inoculantes e biofertilizantes, para serem produzidos, importados ou comercializados, deverão atender aos limites estabelecidos nos Anexos I, II, III, IV e V desta Instrução Normativa no que se refere às concentrações máximas admitidas para agentes fitotóxicos, patogênicos ao homem, animais e plantas, metais pesados tóxicos, pragas e ervas daninhas.

The normative instructions (IN) are presented in Annexes according to each specification (Annex II, III and V). Magnesium sulfate is considered a fertilizer as a secondary macronutrient and fits into Annex II. Following Annex II, the limits for mineral fertilizers are presented in Table 8. Thus, for products that are considered fertilizers, such as magnesium sulfate ($MgSO_4$), the limits of toxic metals are determined in Annex II.

Materials such as calcium and magnesium carbonate must comply with the standards designated in Annex III. The soil correctives are mainly known for contributing to the liming of the soil, which tends to decrease or eliminate acidity, and in the supplementation with magnesium and calcium for plants. Some other advantages of liming are in providing nutrients such as phosphorus, which decreases the amount of aluminum and manganese in the medium and helps in fixing nitrogen in plants (Jones, 2012; Lopes, 1998).

Calcium and magnesium carbonate, known as dolomite, may be used as soil correctives. Therefore, the maximum limits for toxic elements are presented in Annex III. Gypsum has a similarity in its applicability in the soil about liming – soil corrective. Annex V shows the maximum limits of contaminants admitted in organic fertilizers and soil conditioners. An example of soil conditioner is calcium sulfate – as gypsum (Lopes, 1998).

Table 8 – Limits of toxic metals according to Annexes II, III and V. Adapted from SDA, 2016.

Metal	Maximum allowed value in the total mass ($mg.kg^{-1}$)
ANNEX II: Maximum toxic elements allowed for secondary macronutrient fertilizers.	
Arsenic	10.0
Cadmium	20.0
Lead	100.0
Chromium	200.0
Mercury	0.20
ANNEX III: Maximum limit of toxic elements allowed in acidity, alkalinity, sodicity and, calcium and magnesium carbonate corrective agents	
Cadmium	20.0
Lead	1000.0
ANNEX V: Maximum limit of toxic elements allowed in soil conditioners.	
Cadmium	3.0
Lead	150.0

In addition to the nationally targeted limits, there are also those at the state level, such as those stated by CETESB (Companhia Ambiental do Estado de São Paulo, the term in *English*, Environmental Company of São Paulo State). CETESB provides a guide with values for soil quality control, in which the following are addressed: quality reference values, prevention value, and intervention value divided into three categories such as residential, industrial, and even agricultural (Table 9). Considering the environment's quality, and dealing with an ecosystem, there is an approach to groundwater values for monitoring the area to be studied (CETESB, 2016).

Table 9 - Guiding values for soil and ground water in the State of São Paulo 2016. Adapted: CETESB, 2016.

Element	Soil ($mg.kg^{-1}$ dry weight)					Ground water ($\mu g.L^{-1}$)
	Quality reference value (VRQ)	Prevention value (VP)	Intervention value (VI)			
			Agricultural	Residential	Industrial	
Cadmium	<0.5	1.3	3.6	14	160	5
Lead	17	72	150	240	4,400	10

Table 10 shows the limits of elements considered toxic according to some countries in a study carried out by Shi-bao et al., (2018). In which there is a variation of each place. As a comparison for the limits approached in Brazil regarding soil quality - soil on agricultural and residential land. The values presented in the Soil Environmental Quality Standards (SEQSs) were set out as criteria for investigation or remediation of the soil due to the presence of toxic metals. The difference in parameters between countries may be due to exposure of fish and crustaceans which are used for consumption by groundwater or soil contaminated. Other reasons are due to political and socio-cultural factors in each country. For example, Pb and Cd have limits in the range of 40 to 1,000mg.kg^{-1} and 0.15 to 150mg.kg^{-1}, respectively.

Table 10 - Comparison of some countries on the limits of toxic metals using Soil Environmental Quality Standards. Adapted from Shi-bao et al., (2018).

Country	**Standard values of toxic metals in soil (mg.kg^{-1})**							
	Cadmium	Arsenic	Chromium III	Copper	Mercury	Lead	Zinc	Nickel
Australia	2	20	50 (total)	100	2	100	200	70
Belgium	6	110	300	400	15	700	1000	470
Bulgaria	0.6	15	90	50	0.05	40	110	6
Canada	10	12	64	63	6.6	140	200	50
Czech	0.5	20	90	60	0.3	60	120	50
Denmark	0.5	20	500 (total)	500	1	40	500	3
Finland	1	5	100	100	0.5	60	200	50
France	20	37	130	190	7	400	9,000	140
Germany	20	50	400	NA	20	400	NA	140
Japan	150	150	250 (Cr(VI))	NA	15	150	NA	NA
Republic of Korea	12	75	15	450	12	600	900	300
Netherlands	12	55	380	190	10	530	720	210
Norway	3	2	25	100	1	60	100	50
Poland	4	20	150	150	2	100	300	100
Russia	0.76	4.5	3.8	3.5	1.9	55	16	2.6
Sweden	0.4	15	120	100	1	80	350	35
Switzerland	20	NA	NA	1,000	NA	1,000	2,000	NA
Thailand	0.15	30	80	45	0.1	55	70	45
UK	8	20	130	NA	8	450	NA	50
USA	37	22	100,000	3,100	23	400	23,000	1,600

3 OBJECTIVES

The objective of this work was to obtain $MgSO_4$ and $CaSO_4$ from a real flotation tailing generated in zinc beneficiation. To obtain the byproducts a route that was composed of physical processing, hydrometallurgical extraction (leaching), and purification was evaluated with a low toxic metal content for subsequent use for agricultural purposes.

The objectives to be achieved are listed as follows:

- To perform physical and chemical characterization of the tailing.
- To obtain a dolomite concentrate in physical processing.
- To study the leaching conditions of dolomite by thermodynamic simulations and experimental tests assessing magnesium extraction.
- To verify the non-leached fraction as calcium sulfate concentrate;
- To evaluate methods to eliminate toxic metals from magnesium and calcium sulfates, such as lead and cadmium.

4 MATERIALS AND METHODS

During the development of this work, a route was investigated to produce magnesium sulfate from the assessed tailing. The route consisted of a characterization step, followed by physical processing, hydrometallurgical processing, and purification. Hydrometallurgical processing was evaluated along with thermodynamic simulations. Finally, a mass balance was proposed, estimating the mass of $MgSO_4$ produced from a pre-fixed amount of tailing. The material and methodology used in each stage are described in detail as following.

4.1 TAILING MATERIAL

A tailing from a flotation process of a zinc beneficiation plant located in Brazil was studied. Firstly, the acquired tailing was dried in an oven at 100°C for 48h. The moisture content was calculated considering the difference between its mass before and after drying, in which a water content of 27.07% was found.

Then, the dried tailing was submitted to quartering for rates, then for characterization and physical processing, comparing two techniques: magnetic separation and gravity separation.

4.1.1 Zn tailing characterization

For a better representation of the tailing samples, homogenization was carried out through three-stage quartering. In the first stage, the material was spread over a plastic fabric, forming large agglomerates (Figure 15a). This material was disaggregated manually (Figure 15b) and then forwarded to the second stage, in which a conical pile was formed and divided into four parts (Figure 15c and d). The material was then homogeneously distributed in the form of a longitudinal pile (Figure 15e). Two features from opposite directions of the pile were joined and the other parts were discarded. The joined fractions that were submitted to the first-stage procedure again, as shown in Figure 15. The distributed sample was measured, and each divided part was quartered in the Jones type quarter (Figure 15f).

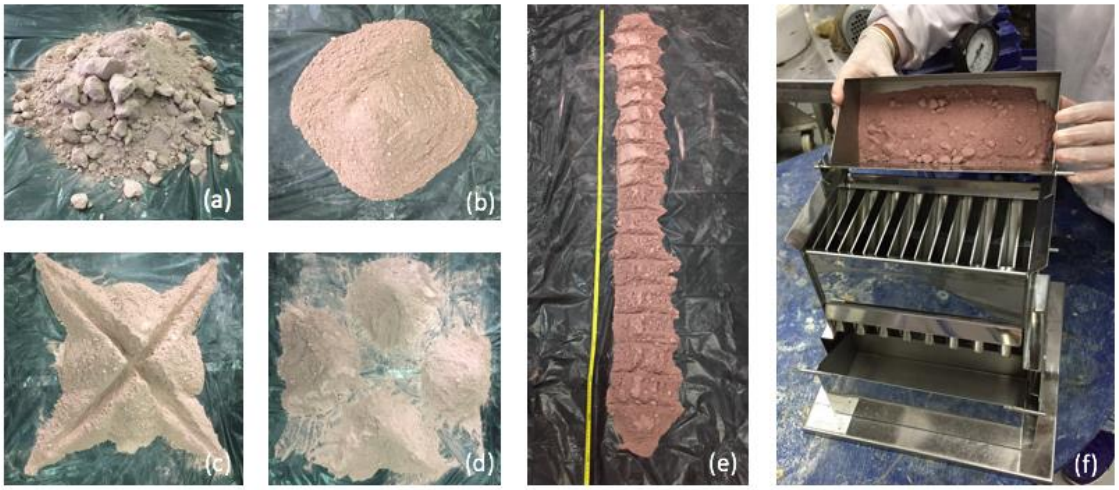

Figure 15 - Quartering sample in three-stages: (a) (b) (c) (d) Conical pile, (e) longitudinal pile and, (f) Jones-type quartering.

Then, qualitative, and quantitative characterizations were performed, as well as granulometry. The quantitative characterization (item 4.7) was intended to identify the main elements present in the material. Thus, EDX equipment was used to scan the composition and approximate percentage of the tailings. Then, the tailings were characterized in ICP-OES, with the aid of the microwave for sample digestion. Carbon and sulfur were also analyzed by Ultra S and C. The qualitative characterization was analyzed by SEM-EDS and XRD, as described in item 4.7.

The granulometric analysis of the zinc tailing was performed in the Malvern equipment, model mastersizer, which uses the Low Angle Laser Light Scattering (LALLS) technique to determine the sample's particle size, and the analysis was performed via wet using water as a dispersant. The determination of carbon and sulfur by infra-red spectrometry using the Eltra equipment model CS2000.

4.2 PHYSICAL PROCESSING

The physical processing is intended to obtain a concentrate of dolomite from the Zn tailing. Thus, magnetic separation technique and gravity separation were studied and compared. In magnetic separation, two routes were performed: *rougher scavenger* and *rougher cleaner*.

4.2.1 Magnetic separation

Magnetic separation was used for removing impurities, such as iron, and for a pre-concentration of the material on interest - dolomite. Thus, allowing the formation of two concentrates, one containing iron and the other, dolomite. The equipment used was the Wet High-Intensity Magnetic Separator, as shown in Figure 16, found in the Department of Mines (PMI-USP), in Laboratório de Tratamento de Minérios (LTM). The method is to separate the material in two fractions: magnetic and non-magnetic fraction by water. In the separator, a coupled container holds the magnetic material, known as a matrix (2.5mm opening), and the funnel that helps in feeding together with the water added when directing the material to the matrix.

Figure 16 – Equipment used for the magnetic separation for the *rougher scavenger* and *rougher cleaner* route, Wet High Intensity Magnetic Separator (WHIMS).

The intensities covered in the study were 8000, 10000, 11500, and 13000G. It was added a 100g of sample for the test for each intensity. Afterward, two routes for magnetic separation were investigated, namely, the *rougher scavenger* and *rougher cleaner*, as shown in Figure 17 and 18.

Both routes were processed with 100g of material, obtaining a magnetic and non-magnetic fraction. In the *rougher scavenger* route, the non-magnetic fraction is reprocessed in a new magnetic separation. Finally, after the second separation, the obtained non-magnetic fraction is added to the non-magnetic fraction from the first step,

as represented in Figure 17. The non-magnetic and magnetic fractions were characterized (in triplicates) by ICP-OES with the microwave aid for sample digestion as is described in item 4.7.4.

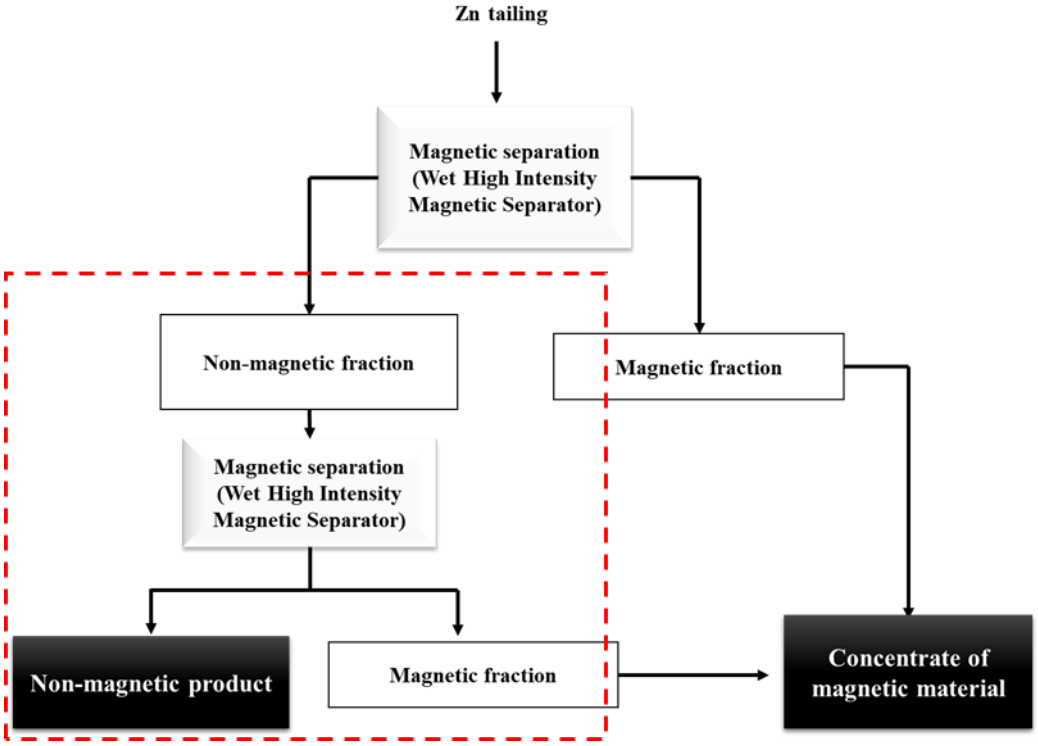

Figure 17 – Flowsheet of magnetic separation using the rougher scavenger route.

In the *rougher cleaner* route, magnetic and non-magnetic fractions are obtained; however in this case, the magnetic fraction is reprocessed in the separation. In the end, a magnetic fraction and a non-magnetic concentrate are acquired, being the non-magnetic fraction the result from the first and the second separations, as shown in Figure 18. The non-magnetic and magnetic fractions were characterized (in triplicates) by ICP-OES with the microwave aid for sample digestion as described in item 4.7.4.

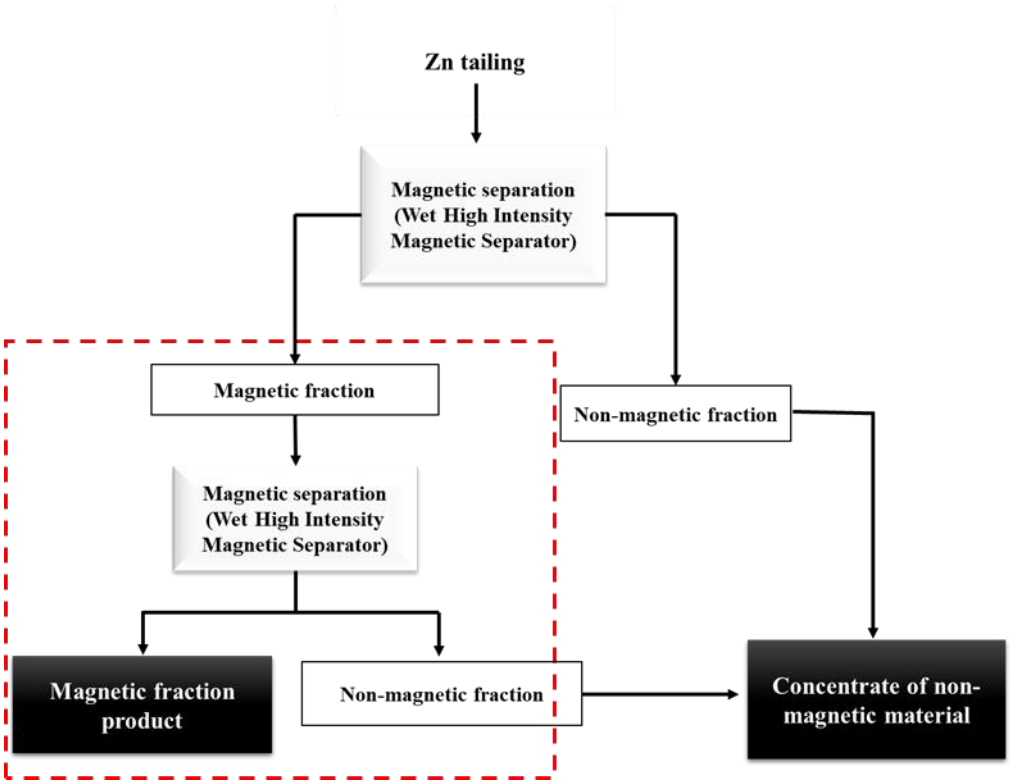

Figure 18 - Flowsheet of magnetic separation using the *rougher cleaner* route.

From the evaluated routes, the one that presented higher efficiency in concentrating dolomite was compared to the efficiency achieved in gravity separation.

4.2.2 Gravity separation

Since hematite, dolomite and quartz have different densities, 4.9-5.3g.cm^{-3}, 2.84g.cm^{-3}, and 2.65g.cm^{-3}, respectively (Lide, 1996), gravity separation was a possibility to separate hematite from dolomite and quartz. The WILFLEY shaking table found in the Department of Mines (PMI-USP), in Laboratório de Tratamento de Minérios (LTM) was used to process 500g of tailing. Three products were obtained in this route: the fraction with lower density, intermediate fraction, and a fraction of higher density, as shown in Figure 19.

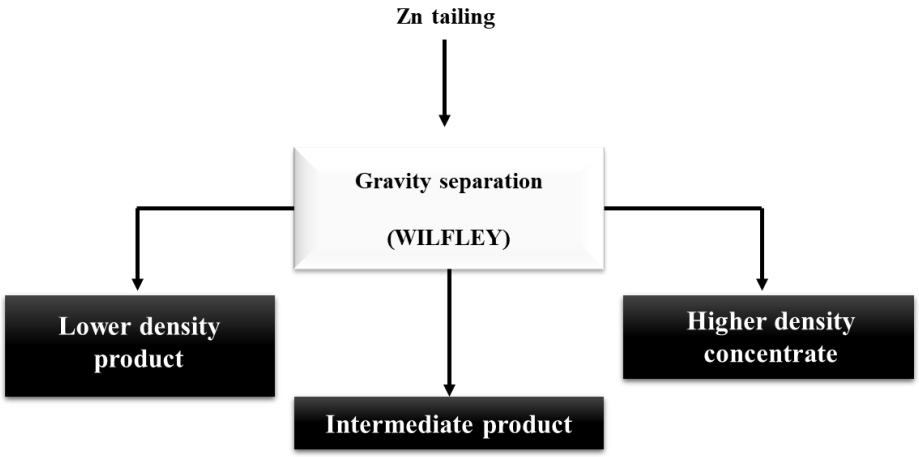

Figure 19 - Flowsheet of gravity separation using WIFLEY shaking table.

The Mg-rich fraction obtained after comparing the physical processing steps was forwarded to the hydrometallurgical stage.

4.3 HYDROMETALLURGICAL PROCESSING

4.3.1 Thermodynamics simulation of leaching parameters

The simulation of the leaching parameters performed with the aid of *FactSage* 7.2, Equilib module software, and the *FactPS*, *FTmisc*, and *FToxid* databases, aimed to establish the optimal leaching conditions of temperature: solid:liquid ratio, and concentration of the leaching agent (H_2SO_4). The purpose of the study was to evaluate the formation of magnesium sulfate from dolomite, according to Equation 12.

$$CaMg(CO_3)_2 + 2H_2SO_4 \rightarrow MgSO_4 + CaSO_4 \cdot 2H_2O\downarrow + 2CO_2\uparrow \qquad \text{Equation 12}$$

The input simulation data were provided considering 100g of dolomite [$CaMg(CO_3)_2$]. Although a fraction of impurities may be found in the tailing, the simulations were first performed considering only the dolomite ore, the study's aim. The initial input data were selected as follows:

- H_2SO_4 concentration: 0.5mol.L^{-1}, 1.0mol.L^{-1} and 2.0mol.L^{-1}
- Solid:liquid ratio: 1:5 and 1:10

- Temperature: from 25ºC to 90ºC, at 5ºC intervals

After an initial screening of the thermodynamic simulations, another set of simulations, closer to the optimal conditions, were performed considering the following parameters:

- H_2SO_4 concentration: 1.0mol.L^{-1}, 1.2mol.L^{-1}, 1.4mol.L^{-1}, 1.6mol.L^{-1}, 1.8mol.L^{-1} and 2.0mol.L^{-1}.
- Solid:liquid ratio: 1:4, 1:5, 1:6, 1:7, 1:8, 1:9, 1:10.
- Temperature: from 25 ºC, 60 ºC and 90 ºC

A simulation of zinc tailing was carried out to evaluate the behavior of the other elements presented in the material. The initial input data were selected as follows parameters:

- H_2SO_4 concentration: 0.5mol.L^{-1}, 1.0mol.L^{-1} and 2.0mol.L^{-1}
- Solid:liquid ratio: 1:10
- Temperature: from 25ºC to 90ºC, at 5ºC intervals.

For each simulation with pure dolomite, the yield of magnesium and calcium was evaluated. Simulation with the zinc tailing, the yield of magnesium, calcium, lead, cadmium, aluminum, zinc, and iron extraction was evaluated and compared to the simulation with only dolomite. The simulated parameters that resulted in the highest predicted $MgSO_4$ formation were chosen to conduct the experimental leaching tests - in which simulations with pure dolomite and zinc tailing were contemplated.

4.4 LEACHING TEST

Firstly, leaching tests were carried out to compare the simulation results and the laboratory tests at different temperatures (25, 50, 75, and 90°C) under constant magnetic stirring. The temperature was measured continuously; approximately every 5min, it was checked. The leaching time was set to 180min. The equipment used to perform the leaching tests was a reactor, a condenser to prevent a volume loss through evaporation, heating and stirring plate and, vacuum filtration. The temperature was measured using a

separate thermometer. For the leaching tests 1L glass reactor having five necks were used. In one of the necks, a condenser connected to a thermostatic bath was placed. The volume used for the tests was 0.5L, and the mass of the residue was 50g. The leaching agent was a 1.2mol.L^{-1} H_2SO solution, as indicated by the simulations.

In these tests, magnesium's extraction was evaluated as a function of time, between 5 and 180 minutes. For this reason, the withdrawn aliquots had 2mL (for each set time), seeking the least interference in the solid:liquid ratio. Samples were collected at fixed time intervals (5, 10, 20, 30 minutes), with the aid of a hydrophobic PTFE-25mmx0.45µm syringe filter.

Leaching tests were also implemented to assess the concentration of sulfuric acid. They were performed varying the concentration of sulfuric acid in 0.8, 1.0, 1.2, 1.5, and 2.0mol.L^{-1} at 50°C, and fixing the reaction time in 35 minutes (all in duplicates). Tests were carried out in 0.25L Erlenmeyer flasks, under constant magnetic stirring, and the temperature was measured continuously at every 5 minutes, approximately. The initial mass was 10g, and the volume was 0.1L. At the end of the tests, the solution was filtrated using a vacuum filtration system equipped with a quantitative paper filter (2 and 6micras). The non-leached fraction was digested according to the procedure described in item 4.7.4.

The leaching liquors and the non-leached fraction were forwarded to chemical analyses, as described in item 4.7.

4.5 PURIFICATION TESTS

To eliminate cadmium in the liquor and lead in the non-leached fraction, they are both designated for the purification stage. The steps used to eliminate cadmium were cementation and sulfide precipitation. For the lead present in the non-leached fraction, the density separation technique was used.

4.5.1 Cementation post-treatment

A post-treatment cementation step was evaluated to remove reminiscent impurities from the leaching liquors, especially cadmium. First, magnesium and cadmium's behavior were considered using a synthetic solution, and subsequently, tests were executed with the real liquor.

According to the liquor's chemical analysis, a synthetic solution simulating the

Mg-rich leaching liquor was prepared. The two main elements acquired were prioritized - Mg and Cd. The synthetic solution was prepared from the dissolution of $MgSO_4.7H_2O$ and $Cd(NO_3)_2.4H_2O$ salts in H_2SO_4 1.2mol.L^{-1} media.

The synthetic solution used a zinc powder, as a cementation agent, at different Zn:Cd ratios – 100:1, 50:1, 10:1, 5:1, 2.5:1, and 1:1 - considering the mass of Cd in grams. A magnetic stirrer was used at 600-800rpm. The temperature and time were fixed at 25°C and 20 minutes, respectively. The effect of time in cadmium cementation was studied through chemical analysis of the aliquots taken in every 5min from the solution at 1 to 50min. The Zn:Cd ratios of 100:1, 50:1, 10:1, and 5:1 was also studied. In each solution was removed aliquot of 0.1mL at times of 1-50min to be analyzed by Atomic Absorption (AA), as described in item 4.7. After the fixed time, the solution was filtered in filter paper. The non-leached fraction was characterized using Scanning Electron Microscopy/ Energy Dispersive X-Ray Spectroscopy (SEM/EDS) described in item 4.7.

A study of the cementation with the real liquor acquired in the leaching step was also performed with conditions as follows. A zinc powder was used as a cementation agent at different Zn:Cd ratios – 100:1, 50:1, 10:1, and 5:1. A magnetic stirrer was used at 600-670rpm and, the temperature was fixed at 25°C. The effect of time in cadmium cementation was studied through chemical analysis of the aliquots taken from the solution at 5, 20, 40, and 50min. For each solution, aliquots of 0.1mL were removed at times of 5-50min to be analyzed cadmium by Atomic Absorption (AA) and magnesium by Ion Chromatography (IC) as described in item 4.7.

4.5.2 Sulfide precipitation

This technique was performed to purify the leached material aiming to precipitate cadmium. The pH for precipitation was selected as pH 1 - 1.5 - 2 - 2.5 and 3 as references to precipitate cadmium as CdS (Jackson, 1986). Sulfide precipitation was carried out with a 1mol.L^{-1} solution of sodium sulfide (Na_2S). The precipitation was compared to the cementation technique to evaluate Cd removal from the liquor.

Therefore, the tests were carried out in duplicate with the tailing liquor after the leaching of 1.2mol.L^{-1} at 50°C to 35min. In preparation, 100mL beakers were used in which 40mL of liquor sampling was added.

Subsequently, the initial liquor's pH was measured, and after 10min of stabilization, the Na_2S 1mol.L^{-1} solution was added gradually with a Pasteur pipette until

it reached the desired pH (Figure 20).

Afterward, the solution was filtered with a 2.0µm filter to separate the precipitated material and the treated liquor. The liquor was analyzed by atomic absorption as described in item 4.7, and cadmium removal was characterized (initial mass of the non-magnetic fraction concerning the final mass obtained in the treated liquor).

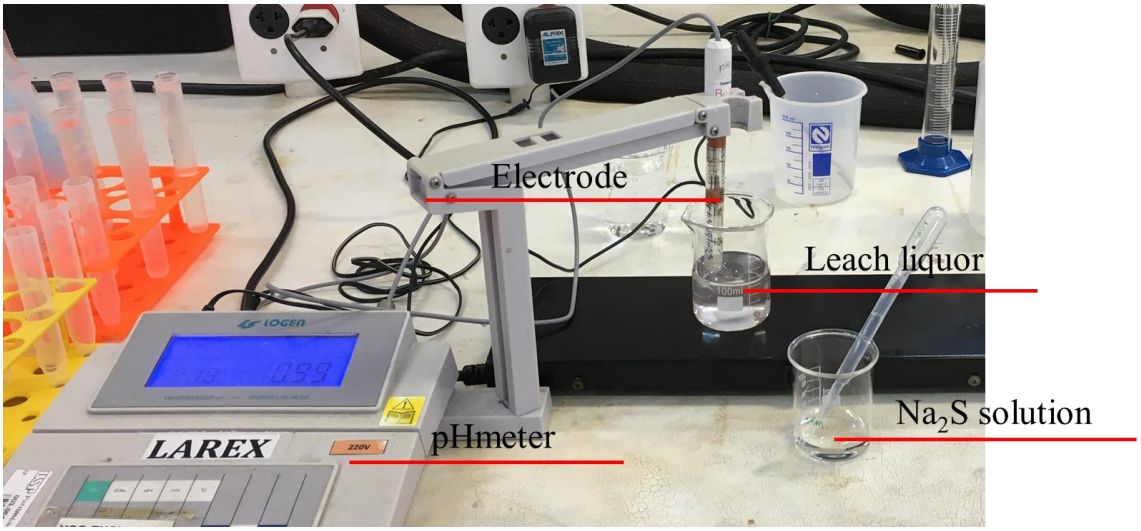

Figure 20 – Sulfide precipitation tests using the pH meter to measure the initial and final pH after adding Na_2S to the leach liquor.

4.5.3 Density separation

The density separation aimed to remove the lead in the fraction of the non-leached fraction. In this stage was obtained a floating and sunk product: lead and calcium sulfate ($CaSO_4$). The organic liquid used for density separation was bromoform (CHBr3).

The tests were performed using 80g of the non-leached fraction, which were divided between 12 fractions and for each sample with approximately 6,67g were weighted. The samples were placed in a centrifuge to obtain floating and sunk products. The samples were placed in a centrifuge to obtain floating and sunk products. For each fraction, 75mL of bromoform was used and, the sample were submitted to the centrifuge for 1min. The material with bromoform was submitted to the centrifuge for 1min and, subsequently, there was the filtration of the suspended material and after the sunk. After the solution was filtered with a 6.0µm filter. Then, the material was washed with ethyl alcohol to make it possible to reuse the added bromoform. The material was dried for 12h at 100°C and characterized by ICP-OES or AA as described in item 4.7, to calculate lead removed percentage.

4.7 CHEMICAL ANALYSIS EQUIPMENT

The samples from leaching and cementation tests were analyzed in the following equipment: X-ray diffraction (XRD) and scanning electron microscopy and dispersive energy spectroscopy (SEM-EDS) for the non-leached fraction and cementation steps. The leaching liquor was analyzed by ion chromatography (IC), atomic absorption (AA) and inductively coupled plasma optical emission spectrometry (ICP-OES) for quantification of Mg, Ca, Fe, Pb, Cd, Al, Mn, Si, and Zn.

4.7.1 X-ray fluorescence (XRF)

The analyses of initial material (zinc tailing) was performed with the aid of an energy-dispersive X-ray spectroscope, Panalytical Epsilon 3X-L equipped with a metal (Ag)-ceramic X-ray tube with a 50μm beryllium window and a 135 eV high-resolution silicon drift detector with an 8μm beryllium window.

4.7.2 X-ray diffraction (XRD)

X-ray diffraction was used to evaluate the predominant phases of the material. The samples were scanned using a Rigaku Miniflex 300 diffractometer, configured from 3° to 100° with 0.02 steps at 1.5°/min speed in *step* mode. An agate mortar was used to perform samples' comminution into the most satisfactory particle sample (holder compacting).

4.7.3 Scanning electron microscopy and dispersive energy spectroscopy (SEM-EDS)

Scanning electron microscopy was performed to analyze the particle structure using a Phenon ProX microscope and an EDS instrument coupled to identify and analyze semi-quantitatively the elements.

The SEM-EDS analyses were carried out in a Phenom Pro X benchtop microscope with an accelerating voltage of 15kV, and a Back Scattered Electron detector (BSE). The SEM analyses with Focused Ions Beams (FBI) were performed in a Quanta FEG (Field Emission Gun) from FEI Company with an accelerating voltage of 30kV and a current of 29.6pA for FIB images. Dispersive Spectroscopy (EDS) was used for the qualitative

characterization of the samples.

4.7.4 Inductively coupled plasma optical emission spectrometry (ICP-OES)

ICP-OES analyses were performed to quantitative characterization of the elements from leaching liquors and non-leached fraction. The latest was analyzed after a leaching procedure assisted by microwave digestion using a CEM Corportion Model Mars 6 microwave instrument. The digestion procedure was carried out by weighing 0.25g of solid samples, but with different mixes of acids in three different situations: 1)characterization of the initial tailing (before physical processing); 2)magnetic, intermediate, higher density, and sunk fractions; and 3)the non-magnetic, lower density and, floating fractions. Situation 1 was used mixing with 2mL HCl, 10mL HNO_3, and 2mL HF. Situation 2 a mixing with 8mL HCl, 5mL HNO_3, and 1mL HF. Situation 3 a mixing with 5mL HCl, 3mL HNO_3, and 2mL HF. After digestion, which was set in two stages: a power at 1400 to 1600W, ramp time for 5 to 10min, holding time for 15 to 35 minutes, the temperature at 160 to 210°C, and a TempGuard of 260°C. Then, 20mL H_3BO_3 was used to neutralize the samples (10mL H_3BO_3 is added for each 1mL HF). The digested samples were filtered and diluted to 50mL.

The quantitative chemical to analyzed the aluminum, calcium, cadmium, iron, manganese, lead, silicon, and zinc with varied concentrations were carried out through the ICP-OES technique in Agilent 710 Spectrometer equipment under the following conditions: plasma flow 15.0L.min^{-1}; auxiliary Argon flow 1.50L.min^{-1} and nebulizer pressure 200kPa.

4.7.5 Ion chromatography (IC)

The ion-chromatograph was used to analyze the samples from the kinetic study. The analyses of magnesium (Mg^{2+}), was carried out in an Ion Chromatography system (Metrohm 850 Professional IC AnCat-MCS and 858 Professional Sample Processor).

Magnesium analysis was performed with a Metrosep C4-150/4.0 cation exchange column. The eluent contained dipiconilic acid (117mg.L^{-1}) and nitric acid (1.7mmol.L^{-1}). The system flux was set to 0.9mL.min^{-1}, and the temperature was 30ºC.

4.7.6 Atomic absorption

The atomic absorption was used to determine the quantitative analysis of the liquor of cementation. Therefore, the analyses of cadmium (Cd) were carried out in an Atomic Absorption AA-700 system (Shimadzu). The hollow cathode lamp of cadmium (Hamamatsu Photonics K.K.), with the specifications of a low current peak value of 8mA, a high current peak value of 100mA and a wavelength of 228.80nm, with a flame type of Air-C_2H_2, the C_2H_2 flow rate of 1.8L.min^{-1} with a burner height of 7mm and a slit width of 0.7nm. The analyses of lead (Pb) was also carried out with a hollow cathode lamp of lead (Hamamatsu Photonics K.K.), with the specifications of a low current peak value of 10mA, a high current peak value of 300mA, and a wavelength of 283.30nm, with a flame type of Air-C_2H_2, the C_2H_2 flow rate of 2.0L.min^{-1} with a burner height of 7mm and a slit width of 0.7nm.

4.8 METHODOLOGY FLOWSHEET

Figure 21 presents the methodology in a flowsheet of the methods according to each analysis for the characterization performed in this work.

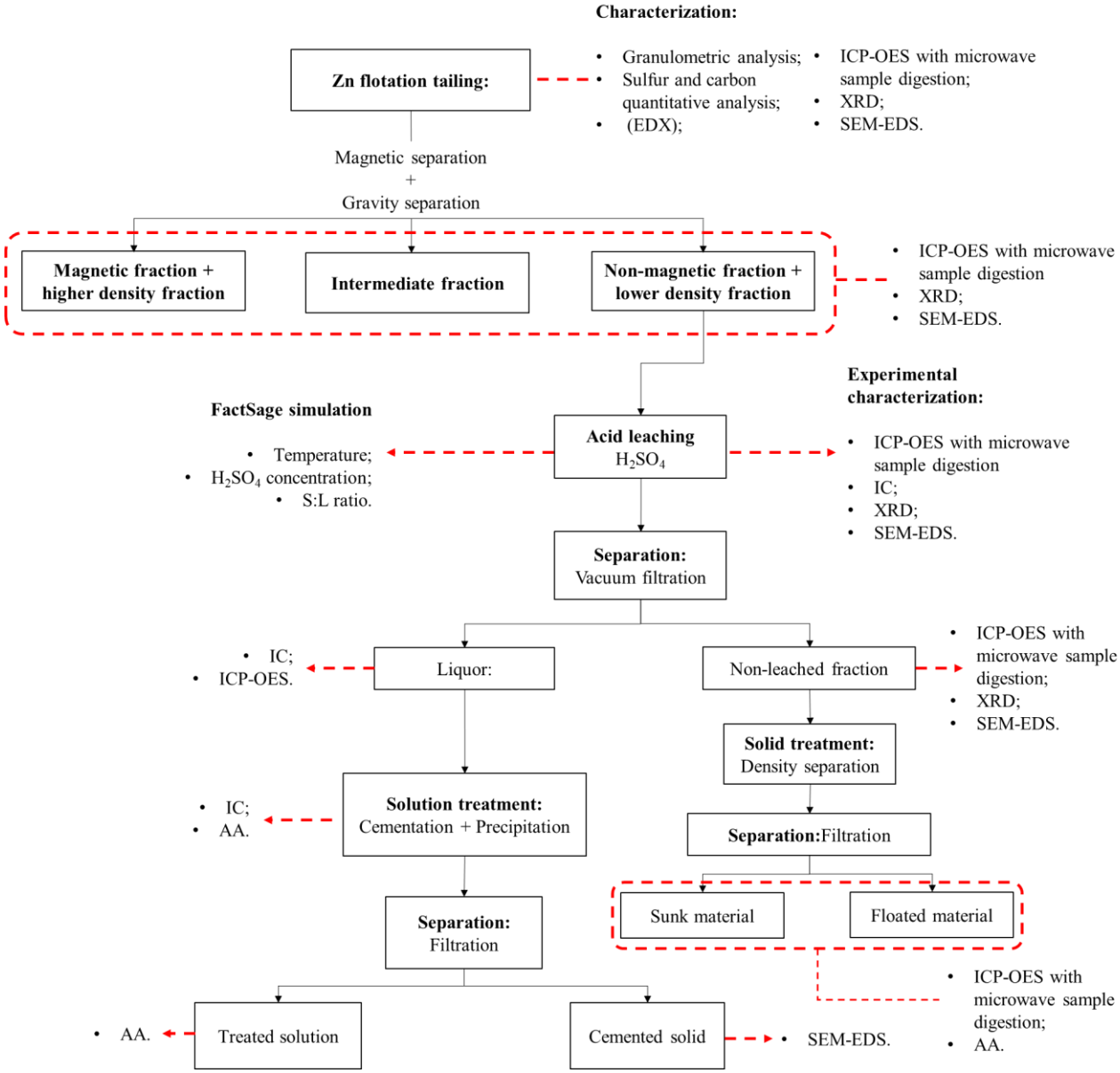

Figure 21 - General flowsheet of the magnetic and gravity separation, simulation stages in the *FactSage* software, leaching stage, purification and separation by density with the due analysis carried out in each stage.

5 RESULTS

5.1 CHARACTERIZATION OF THE TAILING MATERIAL

The first stage of this work consisted of characterizing the acquired zinc tailing. The characterization steps are described as following with the samples properly quartered., which allowed for homogenization of the material.

5.1.1 Particle size analysis

The tailing was obtained from a zinc ore beneficiation in Minas Gerais, Brazil. The tailing characterization was presented as follows. Figure 22 shows the granulometric analysis; in Figure 22a), the particle size distribution of the sample is visualized. The largest peak formed is the particles of the same particle size in greater quantity. These particles with about 16µm represent 4% of the sample volume. Figure 22b) shows the accumulated value of the particle size of the sample. The material had a predominance with the size of particles from 3 to 270µm, which represents 80% of the material.

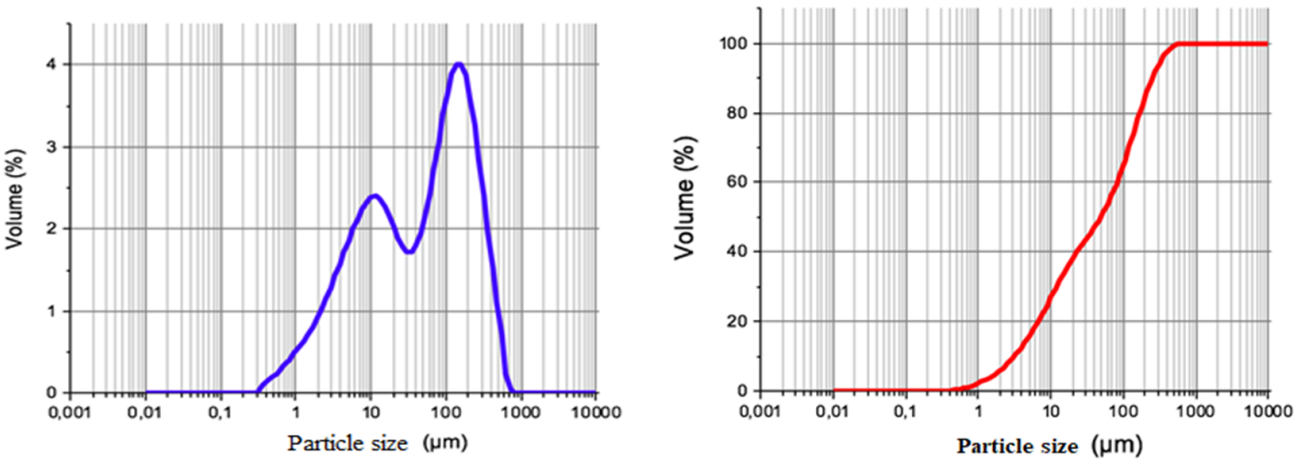

Figure 22 – Particle size analysis of Zn tailing in a) Particle size distribution, and b) Cumulative particle size value.

5.1.2 Sulfur and carbon quantitative analysis and X-ray fluorescence (XRF)

The tailing first went through a semi-quantitative analysis to find out the main elements of its composition. Thus, the best procedures for quantitative chemical analyzes were defined.

The elemental composition of the tailing was analyzed using the X-ray

fluorescence and with Eltra C and S techniques with a solid sampling that was previously dried. The results for the samples of the characterization of the tailing studied are shown in Table 11, and it was observed that the main elements were calcium, iron, magnesium, zinc, and silicon.

In the XRF analyzes, the main elements were analyzed, including calcium and magnesium, which are considered light elements in the XRF analysis. As it is a semi-quantitative analysis, there was digestion of the sample with the aid of microwave in which the ICP-OES characterized it. However, to digest the sample, it was necessary to know the main elements previously. Thereby, knowing the elements were chosen which method to use in the digester and the mixed acids to obtain complete digestion of the sample. For example, silicon was detected in XRF, which requires HF acid for complete digestion. Light elements, especially those with atomic numbers less than 23, e.g. Ca and Mg, have the $K_{(\alpha)}$ and $K_{(\beta)}$ layers filled and are easily excited, in which they have fewer electrons to excite. Thus, these layers are hindered by the other elements with a higher atomic numbers, presenting interference in the reading of the light elements (Beckhoff et al., 2006; Cesareo, 2010).

In Table 11, the characterized elements had a mass balance referring to dolomite (Ca, Mg, C_2 and, O_6, which was presented by the DRX as presented in item 5.1.3) analyzed by EDX. The balance made was quantified the light elements such as Ca and Mg through calculations referring to the total dolomite characterized by XRF, which was 88%. According to this balance in percentage it was presented the other elements with the total mass balance of the standardized elements.

Table 11 - The elementary composition of the zinc tailing by XRF and Eltra C and S.

Element	Weight (%)
Al	0.5
Si	1.5
Ca	18.5
Cd	0.05
Fe	6.9
Mg	13.2
Mn	0.08
Pb	0.2
Zn	1.9
C	11.62
S	0.03

5.1.3 X-ray diffraction (XRD)

The X-ray diffractometry showed characteristic peaks of dolomite [$CaMg(CO_3)_2$]; quartz [SiO_2], and hematite [Fe_2O_3] phases, as verified in Figure 23 and Table 12. The other elements were considered as oxide, as the phases were not identified by diffractogram performed (concentration below 3-5%), being such: ZnO; Al_2O_3; CdO and PbO. The semi-quantitative analysis using the Rietveld approach showed that dolomite was predominant in the mineralogical composition.

Table 12 - Semi-quantitative analysis of the proportions of the main phases with the Rietveld refinement method for the characterization of zinc tailing.

Composition	Percentage (%)
Dolomite	91.6
Quartz	2.9
Hematite	6.1

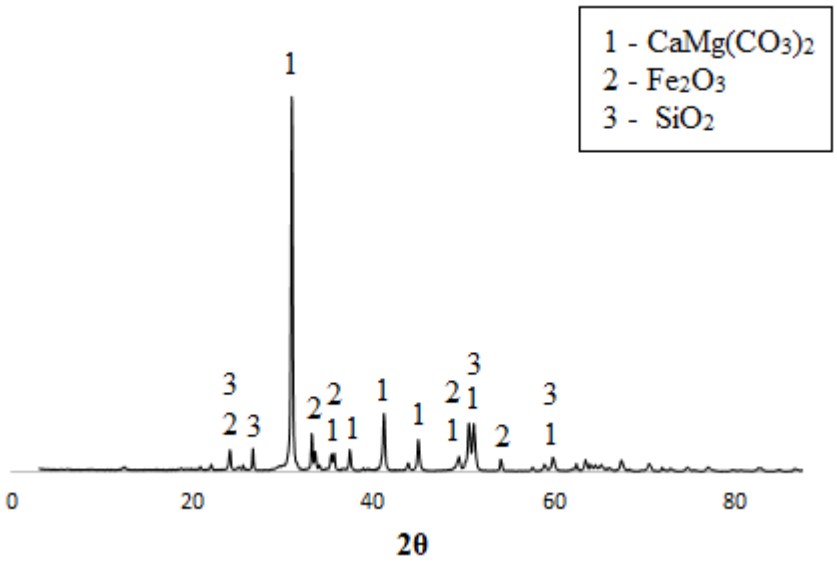

Figure 23 - Diffractometry of the initial sample of Zn tailing and main phases of the material and mineralogical composition.

5.1.4 Scanning electron microscopy and dispersive energy spectroscopy (SEM-EDS)

The SEM-EDS analyses were performed with three different fractions of the quartered material. A total of 40 images were obtained, including images of the sample region and point micro-regions known as spots, all obtained by backscattered (BSE). In

these 40 images obtained, it was analyzed 14 regions and 57 microregions also known as spots. Among these 40 images obtained, an image with the same region was selected, however, with different spots showing the difference of each observed particle.

From scanning electron microscopy, particles present in Zn tailing were punctually analyzed. Firstly, in Figure 24a) was shown the spectrum from EDS coupled to the SEM for a microregion. The SEM provides an image of the microregion that allows the visualization of particles of different sizes. The EDS shows the chemical composition and the content of elements found in the sample.

It was observed in Figure 24b) an EDS spectrum of a punctual particle with a size close to 110µm presents peaks in silicon and oxygen elements. Thus, a possible presence of quartz in the sample was considered. Magnesium was shown in a low concentration in this particle, according to EDS. Figure 24c) shows peaks in the EDS spectrum at a punctual of a particle with a size close to 90µm are the elements oxygen, magnesium, and calcium which indicates the presence of dolomite in the sample. However, elements with lower concentrations were also identified. Figure 24d) shows the spectrum comes from a punctual of a particle with a size close to 150µm, a peak of iron, oxygen in the EDS spectrum, which shows a possibility the presence of hematite, also presented in XRD. Other elements were identified, but with a low concentration compared with those cited above. The EDS for the region and spots in the image in Figure 24 is included in Appendix 1.

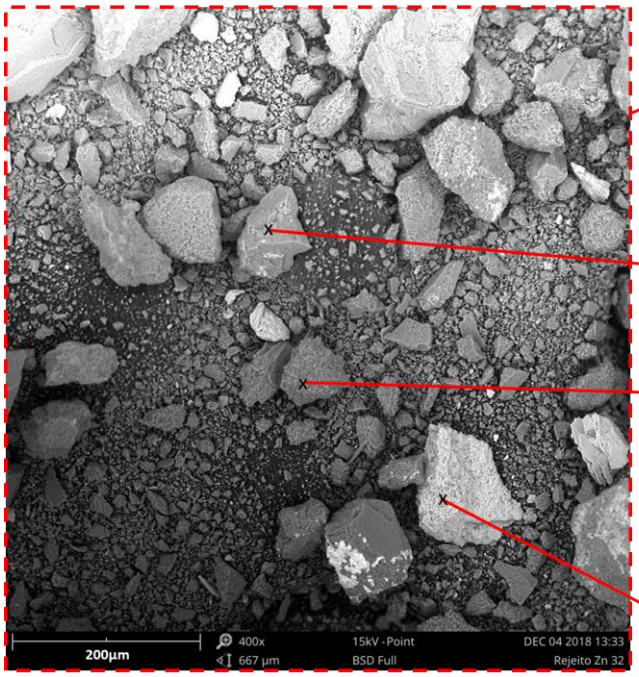

a)

Element	Wt.(%)
O	49.94
C	14.36
Mg	8.56
Ca	12.98
Fe	7.02
Si	2.44
Na	1.33
Zn	2.71
Al	0.64

b)

Element	Wt.(%)
O	63.73
Si	34.59
Ca	1.09
Mg	0.59

c)

Element	Wt.(%)
O	57.77
Mg	15.45
Ca	20.71
Fe	3.60
Na	1.02
Si	0.88
Al	0.57

d)

Element	Wt.(%)
Fe	75.89
O	11.14
Mg	3.50
Ca	3.66
Na	0.82
Zn	2.21
Si	0.77
Al	0.61
Pb	1.41

Figure 24 - Backscattered electron (BSE) image obtained in the scanning electron microscope with a composition of the sample, obtained by EDS a) Microregion composition; b) Punctual spectrum of silica particle; c) Punctual spectrum of dolomite particle; d) Punctual spectrum of hematite particle.

5.1.5 Inductively coupled plasma optical emission spectrometry (ICP-OES)

The elementary composition was performed by inductively plasma optical emission spectrometry with the previously digested samples. The results are shown in Table 13. The tests for the zinc tailing characterization by ICP-OES were carried out in triplicates.

Table 13 - The elementary composition as a percentage of the sample characterization.

Elementary chemical analysis by ICP-OES (%)								
Al	Ca	Cd	Fe	Mg	Mn	Pb	Zn	Si
0.33	17.4	0.02	7.96	10.3	0.07	0.2	1.74	1.47

As performed in X-ray diffractometry (XRD) which was presented in phases mainly of dolomite, hematite, and quartz, each element analyzed by ICP-OES was calculated and normalized. Both methodologies contributed to the construction of Table 14. The phases that were not presented in the XRD due to the concentration being below 3% were considered as oxides. Therefore, from the mass balance calculated using Ca and Mg as a reference, which are major elements in the tailing, the other elements that were not identified phases were standardized in oxides, except zinc that was found as willemite

due to the beneficiation of zinc be with this ore. From the mass balance, oxides (alumina, lead, and cadmium oxides) fulfilled a coherent role with the other phases presented.

Table 14 - Composition of the sample characterization phases.

Chemical formula	Composition	Percentage (%)
$CaMg(CO_3)_2$	Dolomite	81.70
Fe_2O_3	Hematite	11.64
SiO_2	Quartz	2.45
Zn_2SiO_4	Willemite	3.06
Al_2O_3	Alumina	0.61
PbO	Lead oxide	0.51
CdO	Cadmium oxide	0.03
Total		**100**

5.2 PHYSICAL PROCESSING

The physical processing consisted of two stages, the magnetic separation using two different routes (*rougher scavenger* and *rougher cleaner*), which was compared, and the gravity separation. Thus, it was intended to produce a concentrate of dolomite to recover magnesium sulfate using the hydrometallurgical route.

5.2.1 Magnetic separation

The magnetic field intensity tests showed that increasing intensity in Gauss resulted in no difference in the amounts of magnetic and non-magnetic fractions, as shown in Figure 25. Thus, the route *rougher scavenger* and *rougher cleaner* were performed at an intensity of 8000G opting for lower energy expenditure.

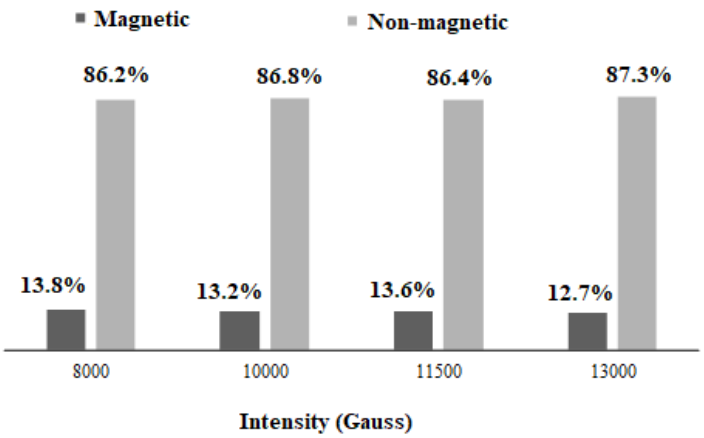

Figure 25 – Magnetic separation intensity field tests.

After the *rougher scavenger* route, the SEM-EDS was carried out, presenting the chemical composition of the micro-regions of (a) tailing before magnetic separation, (b) magnetic fraction and (c) non-magnetic fraction. It was observed that the occurrence of Fe concentration through magnetic separation, which has a Fe peak in the EDS spectrum, Mg and Ca, was also presented in the EDS, in Figure 26b). There was a reduction of Fe in the non-magnetic fraction and, an increase of Mg was lower than Ca. However, both are related to dolomite, showing a concentration of dolomite compared to the tailing before magnetic separation (Figure 26c). The EDS for the region and spots in the image in Figure 26 is included in the Appendix 2.

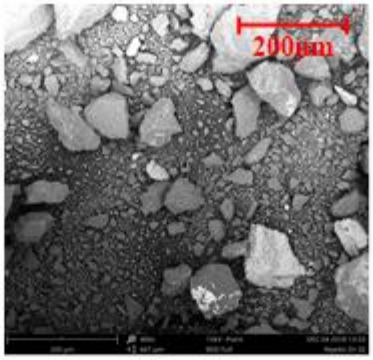

a)

Element	O	C	Mg	Ca	Fe	Si	Na	Zn	Al
Wt.(%)	49.94	14.36	8.56	12.98	7.02	2.44	1.33	2.71	0.64

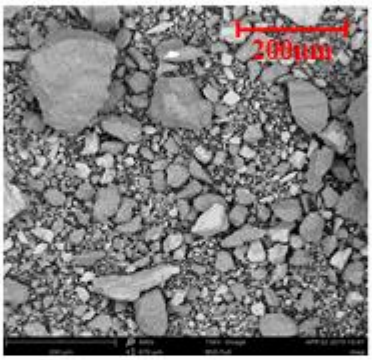

b)

Element	O	Fe	Ca	Mg	Si	Na	Al
Wt.(%)	44.95	26.22	10.57	10.10	3.07	2.75	2.36

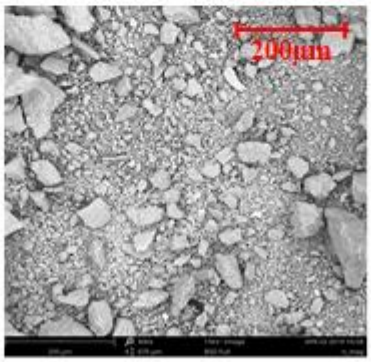

c)

Element	O	Ca	Mg	Zn	Fe	Si	Al
Wt.(%)	56.11	19.13	11.64	4.65	4.36	2.65	1.47

Figure 26 – Backscattered electron (BSE) image obtained in the electron microscope scanning, and EDS spectrum in the *rougher scavenger* route, and EDS of (a) zinc tailing, (b) magnetic fraction, and (c) non-magnetic fraction.

The XRD of the *rougher scavenger* route was also performed, which presented a concentration of Fe, as is shown in Figure 27. Since the peaks of Fe_2O_3 increase in the

magnetic fraction, in the non-magnetic one, the predominance of dolomite was detected, as can be observed in Figure 27.

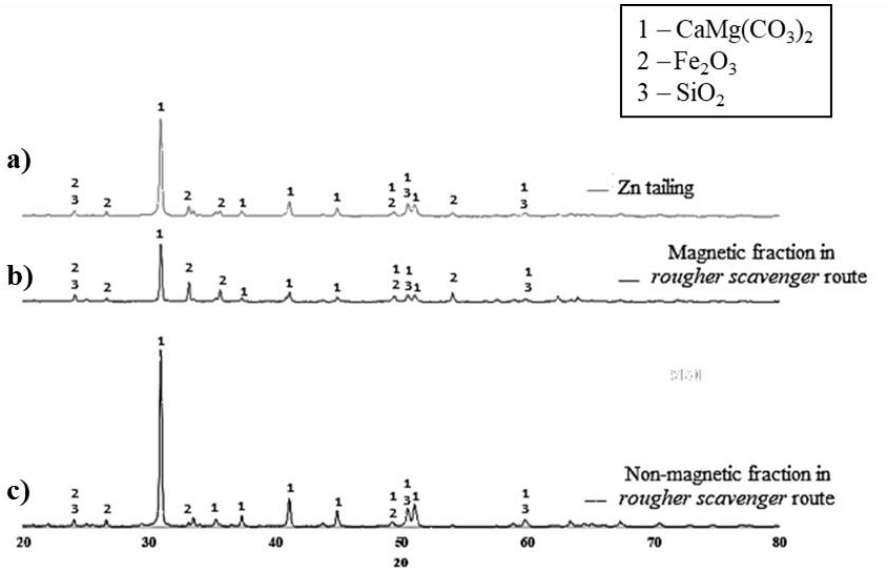

Figure 27 - X-ray diffractometry in *rougher scavenger* route of (a) zinc tailing, (b) magnetic fraction and (c) non-magnetic fraction.

Through the chemical analysis by ICP-OES of the products obtained in the magnetic separation using *rougher scavenger* route compared to the characterization of the zinc tailing (item 5.1.5) in Table 15, there is a concentration of Fe in a magnetic fraction to 33%. The content of each element was identified after the chemical characterization (ICP-OES) which the magnetic and non-magnetic fraction were related to the mass acquired after the *rougher scavenger* magnetic separation. The initial mass was 100g which 82g was designated for the non-magnetic fraction and 18g for the magnetic fraction, so the percentage for each fraction was 82% and 18%, respectively.

In the initial material, Zn tailing the content of Fe was 7.96%. In the non-magnetic fraction, dolomite was concentrated with 11.6% Mg content, and 19% Ca content. Both lead and cadmium had a higher percentage in the non-magnetic fraction, which was 0.2% for both cases.

Table 15 - Elementary concentration of Zn tailing, magnetic and non-magnetic fraction, using *rougher scavenger* route.

Wt.%	Al	Ca	Cd	Fe	Mg	Mn	Pb	Si	Zn
Zn tailing	0.33	17.4	0.02	7.96	10.3	0.07	0.2	1.47	1.74
Magnetic fraction	0.8	8.5	0.02	33.0	5.4	0.05	0.2	1.4	2.0
Non-magnetic fraction	0.5	19.0	0.04	2.0	11.6	0.08	0.2	1.5	1.6

On the next route, *rougher cleaner*, SEM-EDS of the magnetic and non-magnetic fractions were performed, shown in Figure 28. In Figure 28b), the Fe content was equal to 49.94%, which was higher than the obtained by the *rougher scavenger* route that being 26.22%, as previously presented in Figure 28b). In Figure 28c) was observed a higher concentration of Mg and Ca when compared to the magnetic fraction and the tailing before the magnetic separation in Figure 36a) and b). The EDS for the region and spots in the image in Figure 28 is included in the Appendix 3.

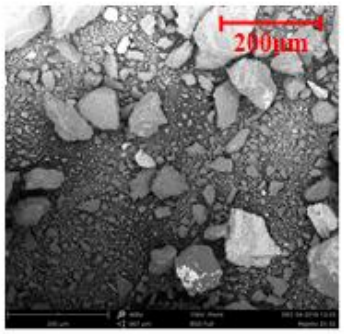

Element	O	C	Mg	Ca	Fe	Si	Na	Zn	Al
Wt.(%)	49.94	14.36	8.56	12.98	7.02	2.44	1.33	2.71	0.64

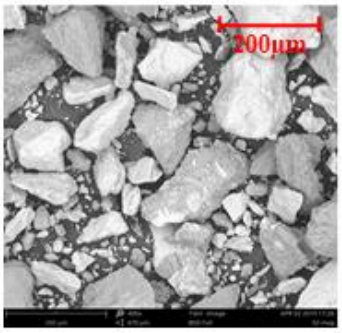

Element	Fe	O	Mg	Ca	Si	Al
Wt.(%)	49.94	35.55	5.74	4.91	2.53	1.32

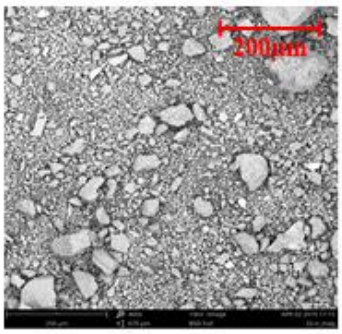

Element	O	Ca	Mg	Fe	Zn	Si	Al
Wt.(%)	58.36	17.06	11.52	5.60	2.99	2.55	1.93

Figure 28 - Backscattered electron (BSE) region image obtained in the electron microscope scanning, and EDS spectrum in the *rougher cleaner* route of (a) zinc tailing, (b) magnetic fraction and, (c) non-magnetic.

In Figure 29, it was analyzed by XRD, the magnetic fraction after the *rougher cleaner* route. Similarly, to the rougher scavenger route, the magnetic fraction had an increase in the intensities of the hematite peak when compared to Zn tailing before magnetic separation. The predominant phase in the non-magnetic fraction is dolomite, which decreased hematite peaks when compared to the tailing before magnetic separation. Hence, there was a concentration of hematite in the magnetic fraction, shown in Figure 29b) showing fewer dolomite peaks and more hematite compared to Figure 29a).

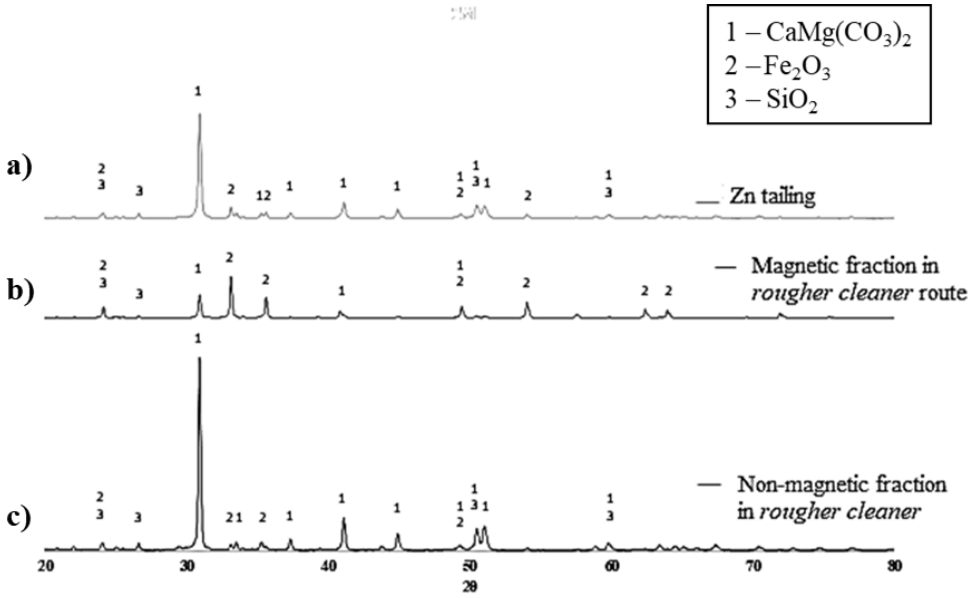

Figure 29 - X-ray diffraction in *rougher cleaner* route (a) Zn tailing, (b) magnetic fraction and, (c) non-magnetic fraction.

Through the chemical analysis by ICP-OES of the products obtained in the magnetic separation using *rougher scavenger* route compared to the characterization of the zinc tailing (item 5.1.5), Table 16 shows the chemical analysis of the magnetic separation with the *rougher cleaner* route. The content of each element was identified after the chemical characterization (ICP-OES) which the magnetic and non-magnetic fraction were related to the mass acquired after the *rougher cleaner* magnetic separation. The initial mass was 100g which 90g was designated for the non-magnetic fraction and 10g for the magnetic fraction, so the percentage for each fraction was 90% and 10%, respectively.

In this separation, the magnetic material has a content of 52% Fe by mass, equivalent to 74.3% Fe_2O_3, considering the only phase identified by XRD for iron. Dolomite presented content of 90.3%, which represents 11.9% Mg and 21.6% Ca.

Table 16 - Elementary concentration of zinc tailing using the *rougher cleaner* route of the magnetic and non-magnetic fraction.

Wt.%	Al	Ca	Cd	Fe	Mg	Mn	Pb	Si	Zn
Zn tailing	0.33	17.4	0.02	7.96	10.3	0.07	0.2	1.47	1.74
Magnetic fraction	0.36	3.3	0.01	52.0	1.88	0.02	0.18	1.29	1.73
Non-magnetic fraction	0.34	21.6	0.04	2.7	11.9	0.08	0.2	1.37	1.73

From the sample of the non-magnetic fraction in *rougher cleaner* route, the elements that were not characterized by XRD were considered as oxides, as shown in Table 17.

Table 17 - Approximate composition (weight %) of the zinc flotation tailing.

Composition	**Weight (%)**
[$CaMg(CO_3)_2$]	90.3 %
[Fe_2O_3]	3.9 %
[SiO_2]	3.0 %
[ZnO]	2.2 %
[Al_2O_3]	0.6 %
[PbO]	0.2 %
[CdO]	0.05 %

Through the qualitative analyses by SEM-EDS, it was observed that Pb's presence was added to dolomite. Despite the SEM and EDS images showing Pb in the magnetic fraction, as they were associated with dolomite, there was a concentration of this element in the non-magnetic fraction, as shown in Table 15 and 16.

Both routes achieved results that concentrated dolomite. However, as observed by SEM-EDS images, particles of the magnetic material in the *rougher cleaner* route in Figure 28b), are larger when compared to the magnetic material in the *rougher scavenger* route, in Figure 26b). Makhula. et al., (2016) processed a low-grade iron ore with the presence of Fe_2O_3 in a grinding roll, obtaining in the chemical granule analysis an increase in the Fe content from 40.43% to 44.63% in ranges between 53µm and 850µm. Thus, there is an interference with a resistance to fragment this ore. Therefore, the large granulometry of the magnetic material in the *rougher cleaner* route had a higher Fe content analyzed by EDS, which means a greater amount of Fe_2O_3.

5.2.2 Gravity separation

Gravity separation was carried out aiming to compare with the magnetic separation, considering both as physical processing.

From the gravity separation step, three products were obtained: denser material, less dense material, and intermediate material. A mass of 500g of the initial zinc tailing was added to the shaking table, which is used as a wet method to obtain the three products. After going through the shaking table using water as an aid to separate the materials, each product was dried. At the end of the process, 34.4g of material with higher density, 207.6g of intermediate, and 258g of material with lower density were dried separately to carry out chemical analysis.

In Figure 30a-c), it was presented the table mounting configurations such as the three outlets – lower density concentrate, intermediate material, and higher density concentrate. In Figure 30a), there is the feeding of the material in the separation process. Also, there are less dense particles such as dolomite and quartz, according to theoretical densities, being dragged by the water flow until the particles leave as a dolomite concentrate, in Figure 30b). A concentrate of hematite in higher density concentrate is shown in Figure 30d) shows the concentrated material with higher densities such as hematite.

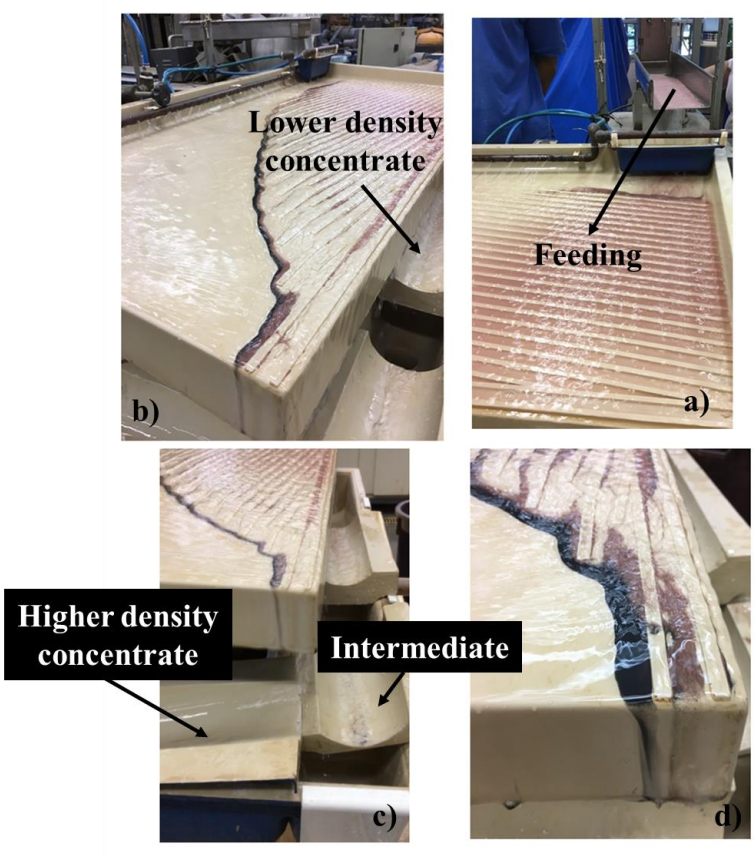

Figure 30 - Gravity separation using WILFLEY shaking table: a) Feeding material with Zn tailing, b-c) materials output; b) particles with lower density being dragged by the water flow, d) particles with higher density being a concentrate.

Figure 31 shows the microregion images obtained by SEM-EDS in which the higher density fraction and intermediate material are composed of larger particles if compared with the zinc tailing and lower density fraction. According to the chemical composition provided by EDS, there was an increase in the concentrations of Mg and Ca in the lower density material and a reduction of Fe content. In the higher density material Figure 31b), an inverse behavior was shown, in which the Mg and Ca contents were reduced and increased the Fe content. The content of 7.02% Fe was concentrated to 44.52%, which is equivalent to 63.60% Fe_2O_3. The EDS for the region and spots in the image in Figure 31 is included in the Appendix 4.

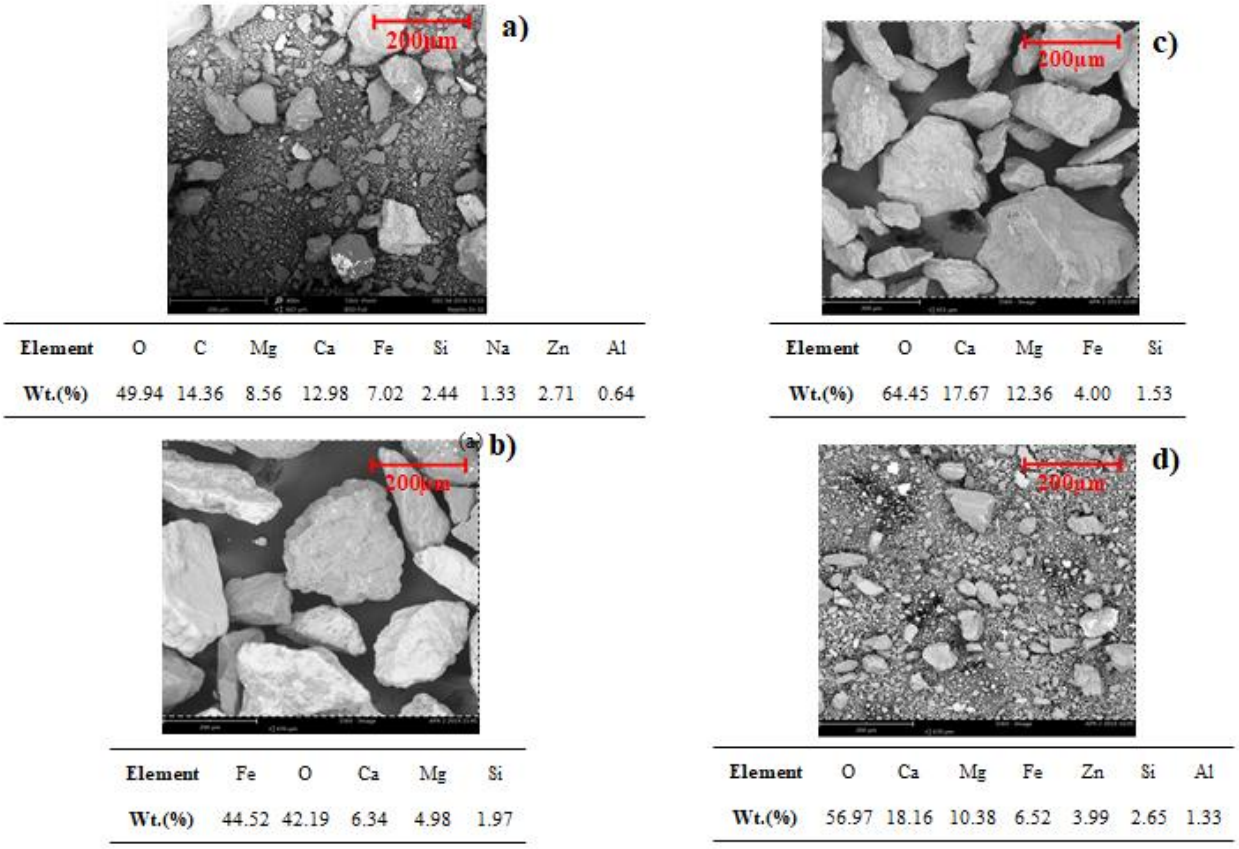

Figure 31 – Backscattered electron (BSE) region image obtained in the electron microscope scanning and EDS spectrum, using gravity separation of (a) Zn tailing, (b) higher density fraction, (c) intermediate material and, (d) lower density fraction.

Figure 32 shows the XRD of the zinc tailing and the products obtained in gravity separation. The higher density material Figure 32b) showed an increase in Fe_2O_3 peaks comparing with the initial zinc tailing. The lower density fraction, Figure 32d) presented an increase in the peaks of the dolomite phase comparing with zinc tailing, Figure32a), corroborating the results of the EDS.

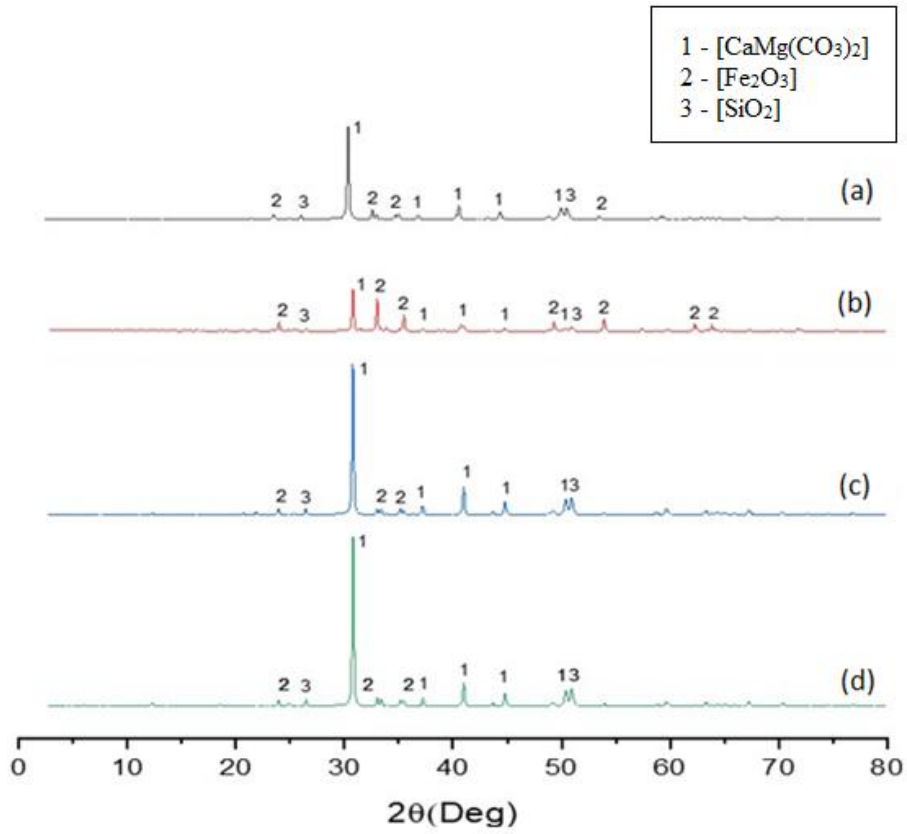

Figure 32 – X-ray diffractometry of the samples before and after gravity separation with (a) Zn tailing, (b) lower density fraction, (c) intermediate material, (d) higher density fraction.

Through the chemical analysis by ICP-OES of the products obtained in the gravity separation compared to the characterization of the zinc tailing (item 5.1.5), in Table 18 the chemical analysis of the lower density fraction indicates the concentration of Mg and Ca and the reduction of Fe content. The content of each element was identified after the chemical characterization (ICP-OES) which the lower density fraction, intermediate material and the higher density fraction were related to the mass acquired after the gravity separation. The initial mass was 500g which 258g was designated for the lower density fraction, 208g for the intermediate material and, 34g for the higher density fraction, so the percentage for each fraction was 51.6%, 41.6% and 6.8% respectively.

In this fraction the composition of Mg, Ca, and Fe were 11.6%, 20.5%, and 4.5%, respectively. The intermediate material contained 9.90% Mg, 17.90% Ca, and 4.40% Fe.

Table 18 – Chemical analysis by inductively coupled plasma optical emission spectrometry of the products obtained in the gravity separation.

Wt. (%)	Al	Ca	Cd	Fe	Mg	Mn	Pb	Si	Zn
Zn tailing	0.33	17.40	0.02	7.96	10.3	0.07	0.20	1.47	1.74
Higher density fraction	0.20	9.00	0.01	40.4	3.50	0.02	0.20	1.50	2.00
Intermediate material	0.30	17.90	0.04	4.40	9.90	0.10	0.20	2.00	1.60
Lower density fraction	0.40	20.50	0.04	4.44	11.60	0.10	0.20	1.60	1.60

Elements such as calcium and magnesium were preferably concentrated in the lower density fraction, 20.5% and 11.6%, respectively. In the higher density fraction iron was concentrated to 40.4%. However, this technique produced an intermediate product, which often does not have an ideal element concentration to be studied. In this case, calcium, magnesium, and iron had a content of 17.90%, 9.90%, and 4.4%, respectively.

Considering that the material's selectivity focusing at first in the Mg, Ca, and Fe, using the magnetic separation *rougher cleaner*, the non-magnetic fraction of this route was chosen for the following tests.

5.3 HYDROMETALLURGICAL PROCESSING

5.3.1 Thermodynamic simulation of leaching parameters

5.3.1.1 Magnesium extraction

Thermodynamic simulations were performed with the aid of *FactSage 7.2* software. According to the database available in *FactSage*, it was possible to simulate the leaching process of dolomite using sulfuric acid and the effect of the temperature. These databases refer to the calculations of the activation energy and Gibbs free energy of all the possible formed compounds (Bale et al., 2016, 2009; Havlik, 2001; Paliwal and Jung, 2019; Walle et al., 2018) and comprise reactions in aqueous media. Figure 33 to 36 shows the results for the first set of simulations which evaluated the H_2SO_4 concentration, solid:liquid ratio and the temperature to optimize the leaching conditions of Mg from dolomite. According to (Ramalingom et al., 2001), the $MgSO_4$ has greater solubility until 90°C. Above this temperature, it becomes insoluble and starts to precipitate. For this reason, the chosen range of temperatures varied from 25 ºC to 90 ºC.

The simulation presented in Figure 33 was carried out with the S:L ratio of 1:5 evaluating the thermodynamic behavior at concentrations of 0.5, 1.0, and 2.0mol.L^{-1}. In the S:L ratio of 1:5, none of the conditions reached 100% extraction, and low extraction of magnesium was observed, mainly at concentrations of 0.5 and 1.0mol.L^{-1}, being around 20% at temperatures below 50°C.

While increasing temperature, the percentage of extraction decreased to 1%. The explanation for that is magnesium sulfate's solubility decreases at temperatures higher than 90°C (Ramalingom et al., 2001; D´Ans, 1933). In this case, in an S:L ratio of 1:5, without the excess of acid, even at lower temperatures (75 to 90°C) the behavior of magnesium sulfate shows an extraction below 10%.

Hence, it was demonstrated that the H_2SO_4 concentration had greater influence on Mg extraction than the temperature. In Figure 33, for 1.0mol.L^{-1} H_2SO_4 the Mg extraction decreased when increasing the temperature above 50°C. Besides, the Mg extraction for this condition was lower than 20% for all modeled temperatures. The highest Mg extraction was around 85% for 2.0mol.L^{-1} H_2SO_4.

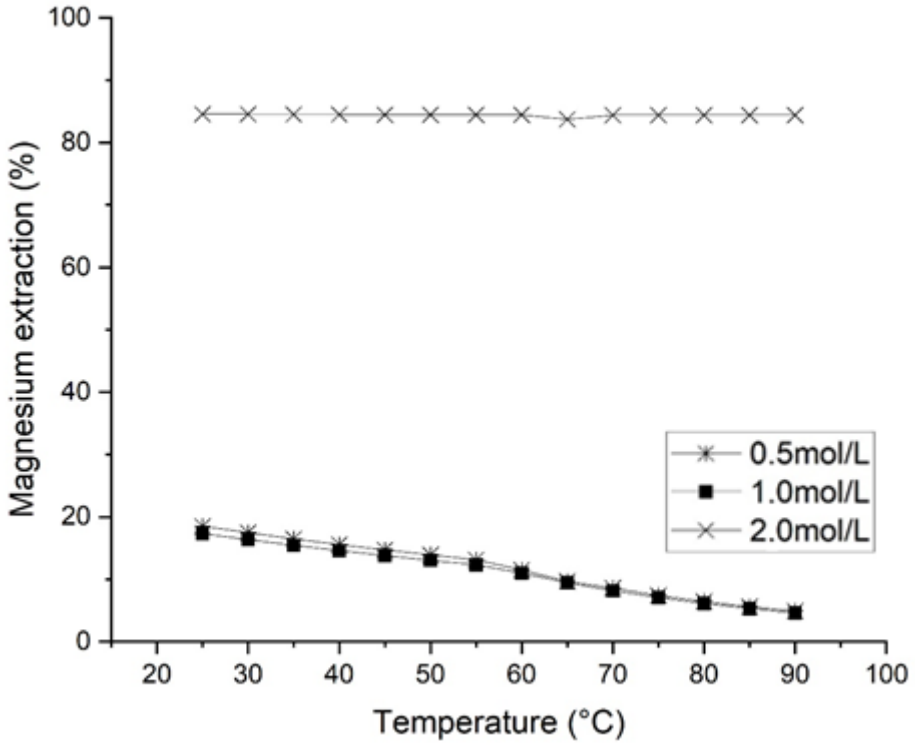

Figure 33 - Simulation of Mg leaching from dolomite (%) as a function of the temperature at 25-90°C and H_2SO_4 concentration in a solid:liquid ratio of 1:5.

Unlike the first simulation, in Figure 34, a magnesium extraction of 100% was achieved with 2.0mol.L^{-1} H_2SO_4 concentration and an S:L ratio of 1:10. The percent extraction for both concentrations, 0.5 and 1.0mol.L^{-1}, were close to 85% and less than 40%, respectively. According to the reaction stoichiometry (Equation 12), at least 1 mol.L^{-1} of H_2SO_4 is used to react with dolomite in an S: L = 1:10 ratio, allows Mg leaching (Xiong et al., 2014).

Figure 34 shows the modeled conditions considering S:L = 1:10. For H_2SO_4 concentration of 0.5mol.L^{-1} the Mg extraction decreased as the temperature increased, especially above 60°C. The highest Mg extraction was found for an acid concentration of 2.0mol.L^{-1}. The $MgSO_4$ solubility increases in temperatures between 25 – 60 °C. However, at temperatures above 60°C, the $MgSO_4$ is reprecipitated because its solubility is lower at such temperatures (Ramalingom et al., 2001; D'Ans, 1993).

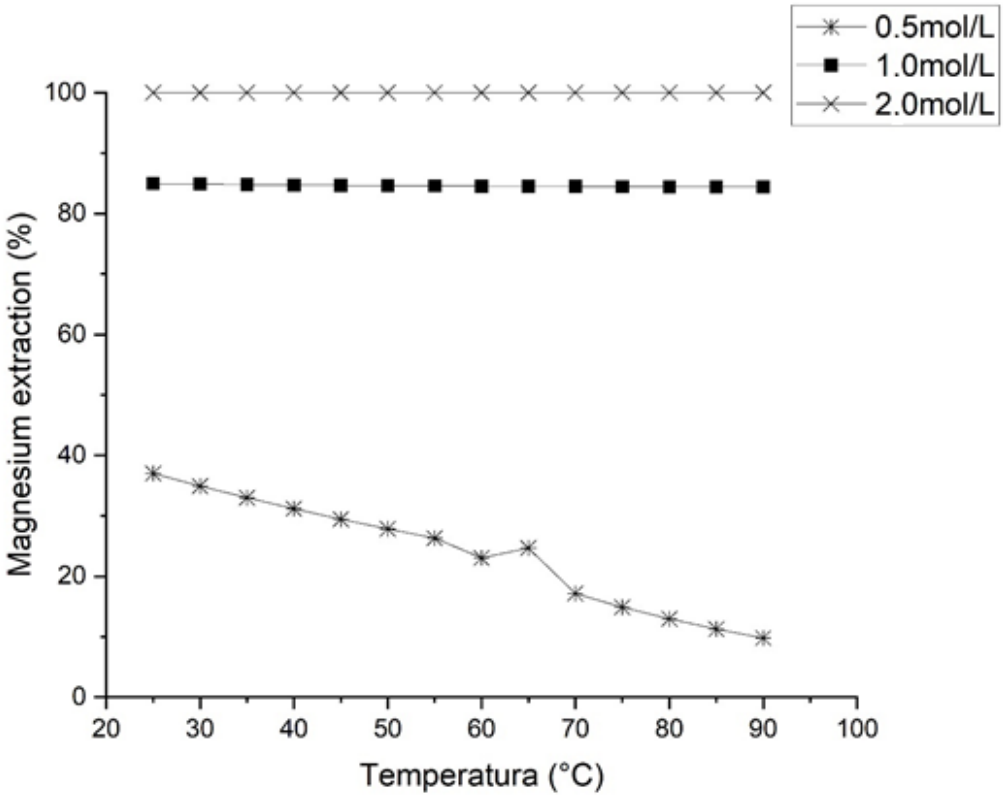

Figure 34 - Simulation of Mg extraction from dolomite (%) as a function of the temperature at 25-90°C and H_2SO_4 concentration in a solid:liquid ratio of 1:10.

Different S:L ratios were evaluated in Figures 35 and 36 for concentrations of 1.0mol.L^{-1} and 2.0mol.L^{-1} of H_2SO_4. The concentration of 0.5mol.L^{-1} was disregarded, since in both simulations, Figure 33 and 34, it yielded a magnesium extraction below

40%.

In Figure 35, the condition of 1.0mol.L^{-1} H_2SO_4 concentration was evaluated, in the range of the S:L ratio from 1:4 to 1:10. Even using the highest 1:10 ratio, the maximum magnesium extraction was around 80%. The temperature showed no influence on the extraction in the S:L ratios from 1:7 to 1:10.

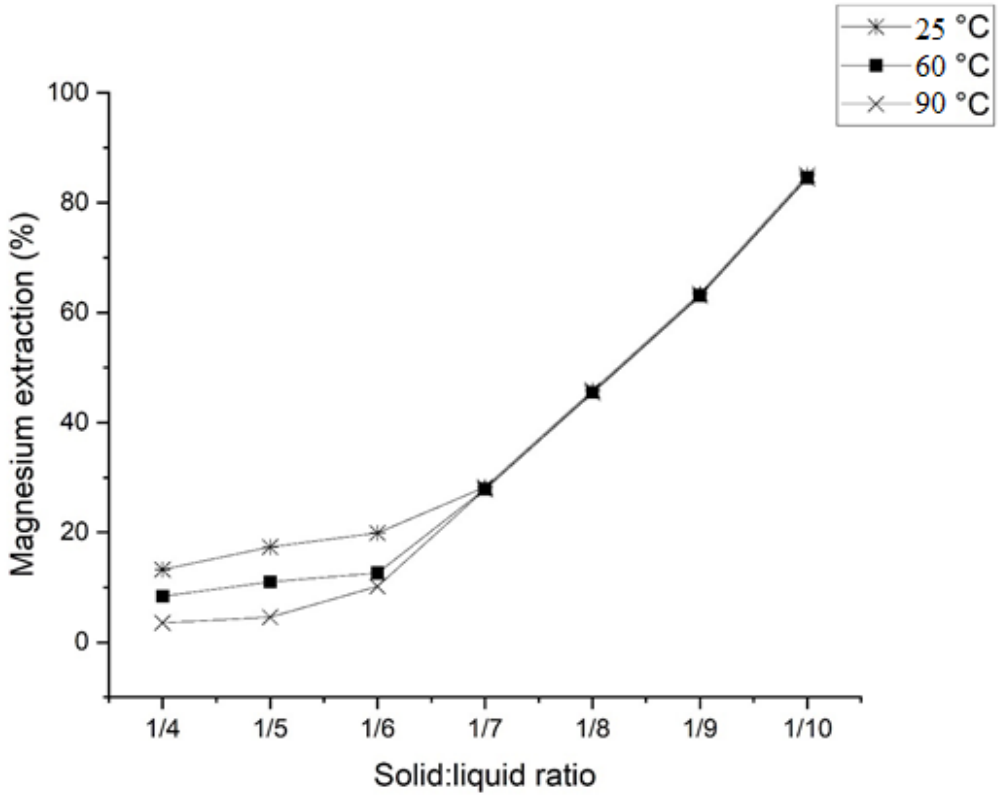

Figure 35 - Simulation of Mg extraction from dolomite (%) as a function of the temperature at 25, 60 and 90°C, and solid:liquid variation in a 1.0mol.L^{-1} H_2SO_4 concentration.

It was shown in Figure 36 the effect of the S:L ratio when fixing the concentration of H_2SO_4 in 2.0mol.L^{-1}. It was observed that from 1:6 to 1:9, the extraction was close to 100%. Therefore, only in the simulations comprising a 1:10 ratio, 100% extraction was reached. The temperature had no influence on any of the S:L ratios.

The slight influence of temperature on Mg leaching can be confirmed from Figure 35 and 36. Figure 35 shows the modeled curve considering an H_2SO_4 concentration of 1.0mol.L^{-1}, and it is noticed that, at S:L ratios higher than 1:7, the temperature does not influence Mg leaching. For an H_2SO_4 concentration of 1.0 mol.L^{-1}, the temperature showed no influence on Mg extraction throughout the whole evaluated S:L range.

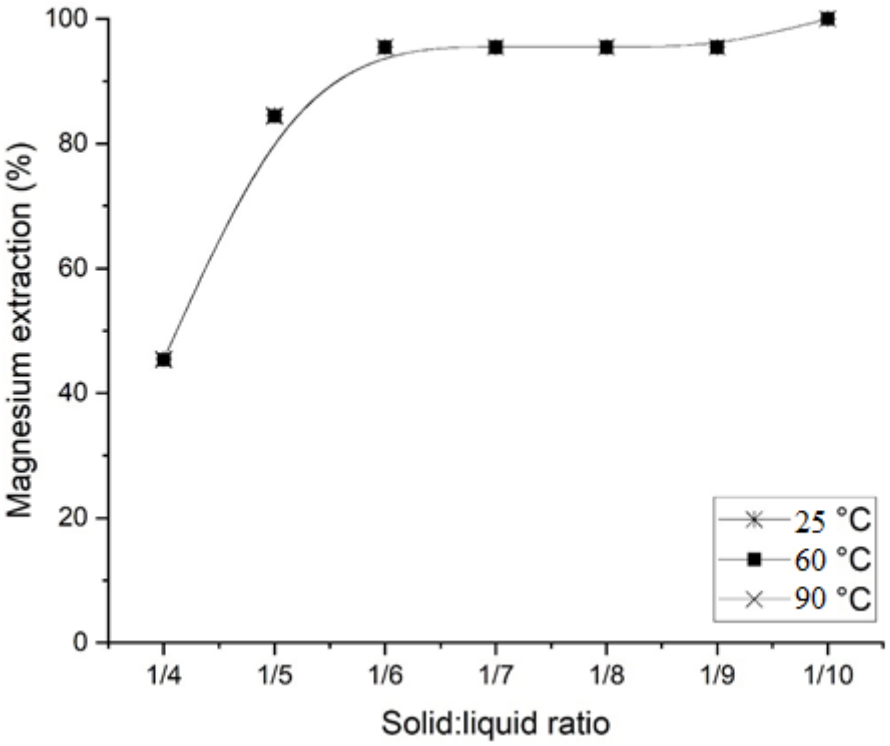

Figure 36 - Simulation of Mg extraction from dolomite (%) as a function of the temperature at 25, 60 and 90°C, and solid:liquid variation in a 2.0mol.L^{-1} H_2SO_4 concentration.

From the previous results, it was observed that in the acid concentration between 1 and 2mol.L^{-1} was possible to obtain a 100% Mg extraction. In Figures 37 and 38, the excess of acid used to achieve 100% Mg extraction was investigated. The effect of H_2SO_4 concentration for both S:L ratios = 1:5 and 1:10 was studied.

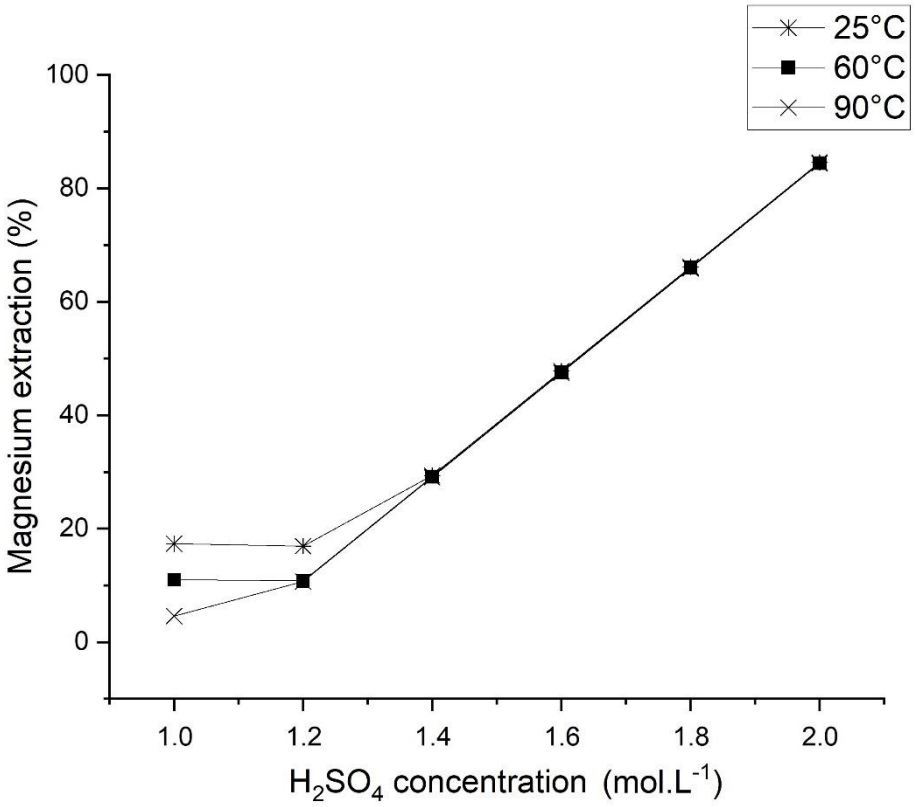

Figure 37 - Simulation of Mg leaching (%) from dolomite as a function of the temperature at 25, 60 and 90°C, and H_2SO_4 concentrations from 1.0 to 2.0mol.L^{-1} in a solid:liquid ratio of 1:5.

The results from Figure 37 and 38 show that for an S:L ratio of 1:5, the Mg extraction increased linearly when increasing the acid concentration from 1.2mol.L^{-1} to 2.0mol.L^{-1} while Figure 38 indicates that, for an S:L ratio of 1:10, the Mg extraction achieved a maximum value for 1.2 mol.L^{-1} H_2SO_4. Therefore, if the solid:liquid ratio is lower than 1:10, the acid concentration must be increased, in accordance with the stoichiometry of Equation 12 (Xiong et al., 2014).

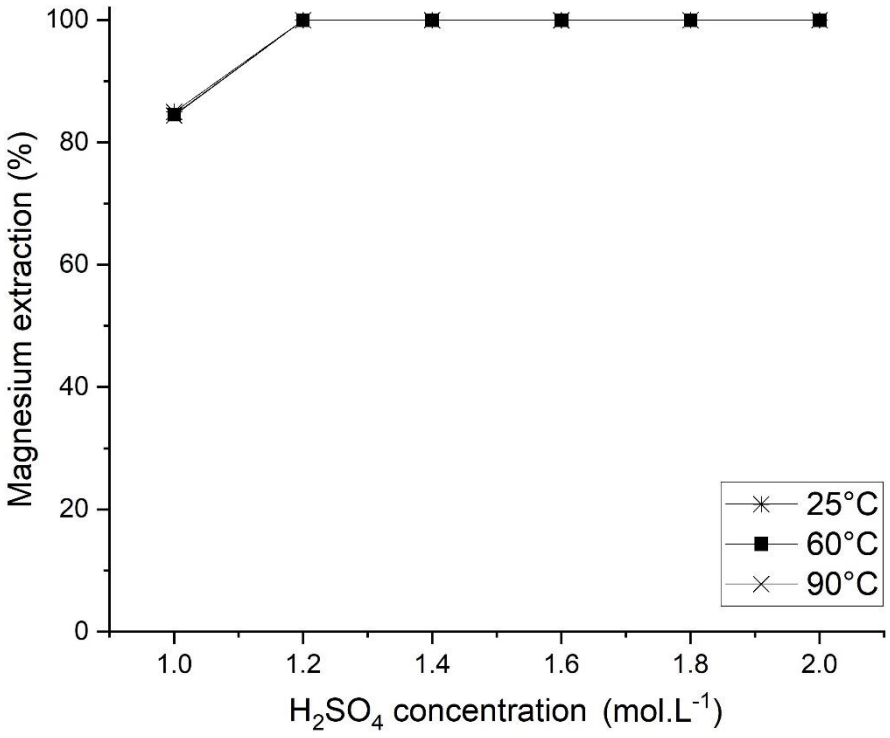

Figure 38 - Simulation of Mg leaching (%) from dolomite as a function of the temperature at 25, 60 and 90°C, and, H_2SO_4 concentrations from 1.0 to 2.0mol.L^{-1} in a solid:liquid ratio of 1:10.

By analyzing the results from Figures 33 - 36 and 37 -38, the optimal parameters for experimental leaching tests were established as follows.

- Temperature = 25ºC, since increasing the temperature does not influence the Mg extraction. Nonetheless, experimental leaching essays were performed at higher temperatures to validate the results.
- S:L = 1:10 and H_2SO_4 concentration of 1.2 mol.L^{-1}, which allowed using the less concentrated leaching agent and reached 100% Mg extraction according to the modeled results shown in Figure 38. Similarly, experimental leaching tests using higher H_2SO_4 concentrations were carried out to validate the results.

5.3.1.2 Calcium extraction

Considering that the predominant material (90.3wt.%.) is dolomite -

[$CaMg(CO_3)_2$], the reaction with H_2SO_4 would produce $MgSO_4$ which solubility is higher at temperatures between 50 to 80°C , and $CaSO_4$ which is insoluble. The phases of calcium sulfate are mostly gypsum and anhydrite; for example, at temperatures between 25 and 75°C, the gypsum phase is found, and at temperatures between 75 to 100°C, the anhydrite phase is formed (Abali et al., 2006; Freyer and Voigt, 2003; Ramalingom et al., 2001). Figures 39 and 42 show the thermodynamic simulation for Ca extraction in three different concentrations of H_2SO_4. From Figure 39, it was observed that the temperature showed no influence in Ca extraction. Besides, less than 0.25% Ca was obtained due to the solubility of calcium sulfate.

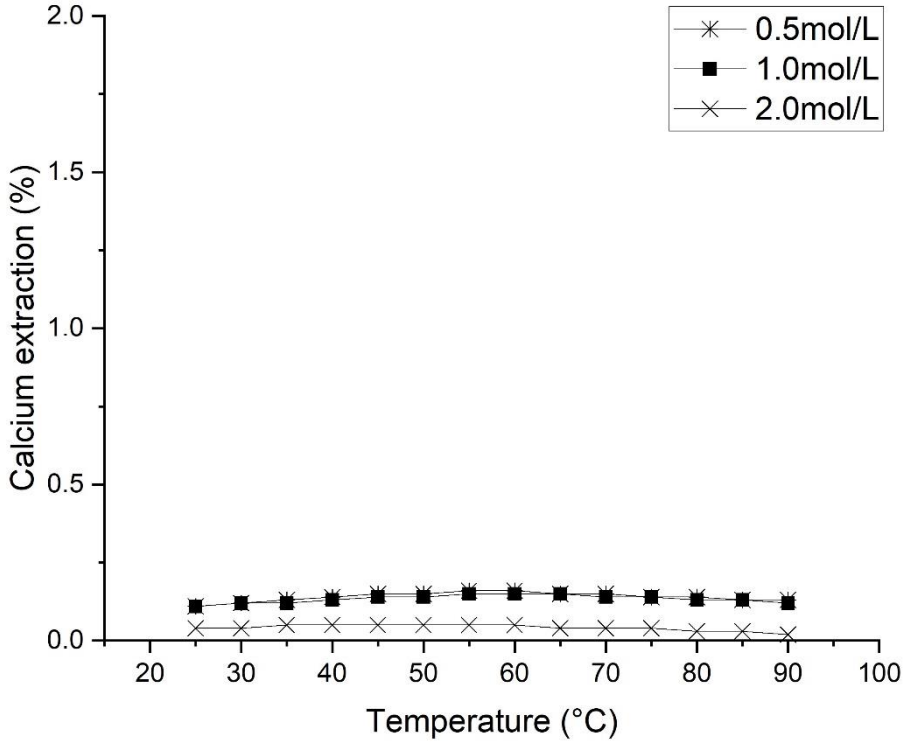

Figure 39 - Simulation of Ca leaching from dolomite (%) as a function of the temperature at 25-90°C and H_2SO_4 concentration in a solid:liquid ratio of 1:5.

When an S:L ratio = 1:10 was tested (Figure 40), the Ca extraction increased to 1% at temperatures from 50 to 90°C. Even though the calcium extraction is lower than the magnesium extraction.

Even when modeling the conditions that could increase the Ca extraction, as the S:L ratio, the yield of calcium extraction was lower than magnesium, Figures 41 and 42.

Calcium extraction was evaluated as a function of temperature behavior at 25 to

90°C in three different acid concentrations. The highest extraction yield was around 1% for 2mol.L^{-1} at 90 °C and an S:L ratio of 1:10, Figure 40, and no influence of temperature for Ca extraction was noticed in Figure 41.

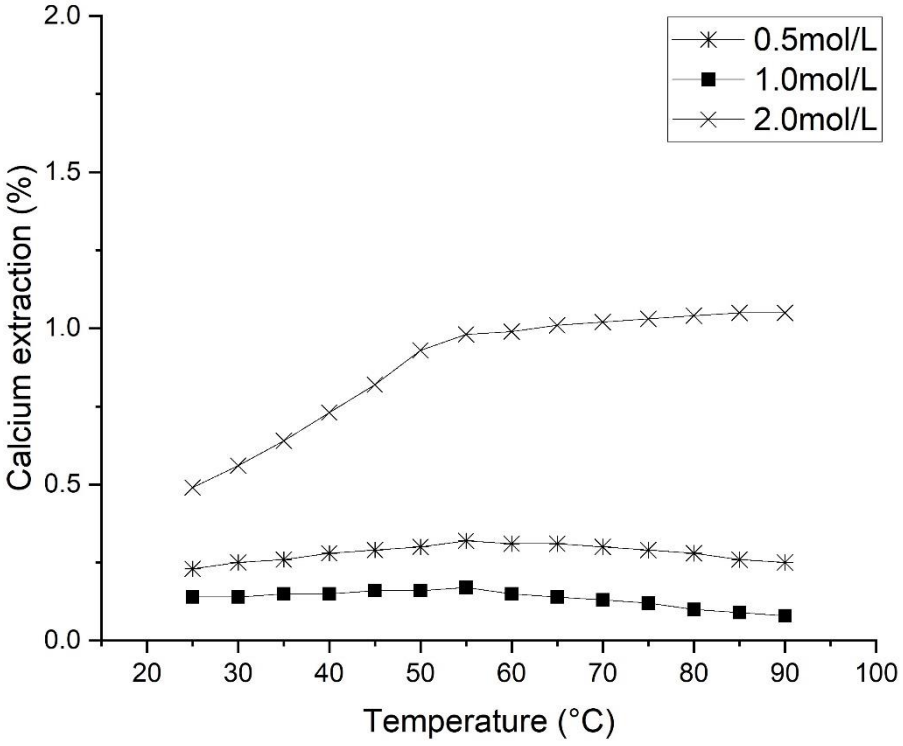

Figure 40 - Simulation of Ca leaching from dolomite (%) as a function of the temperature at 25-90°C and H_2SO_4 concentration in a solid:liquid ratio of 1:10.

The study of the intervals of the S: L ratio in two concentrations of H_2SO_4 (1.0mol.L^{-1} and 2.0mol.L^{-1}) were presented in Figures 41 and 42. For 1.0mol.L^{-1}, the Ca extraction showed no effect either with the S:L and temperature increase.

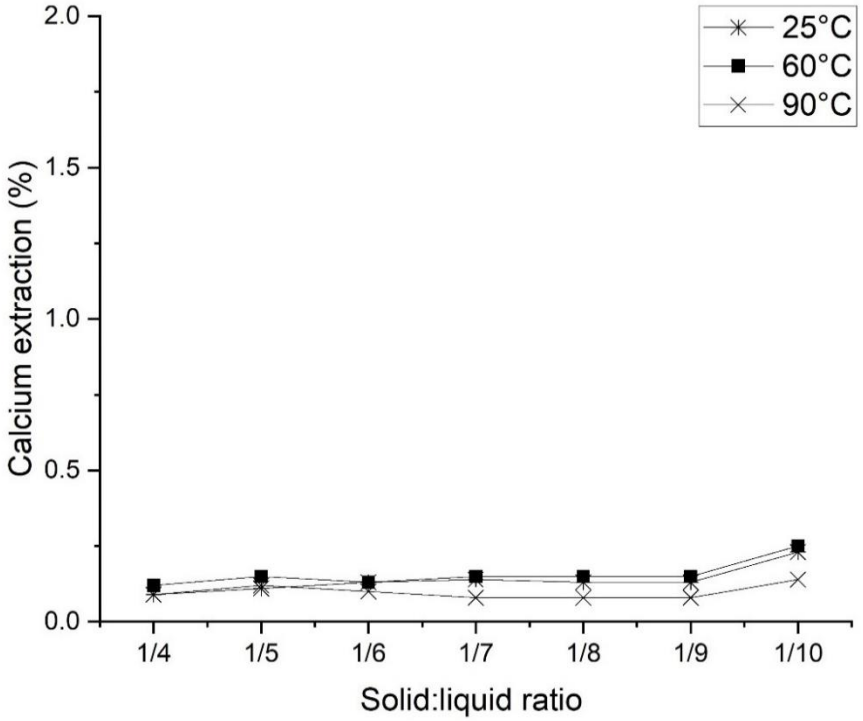

Figure 41 – Simulation of Ca extraction from dolomite (%) as a function of the temperature at 25, 60 and 90°C, and solid:liquid variation in a 1.0mol.L^{-1} H_2SO_4 concentration.

The highest Ca extraction was obtained for an S:L ratio = 1:10 at 60 and 90°C which was about 2%, as shown in Figure 42. It was shown that regardless of temperature and S:L ratio, the Ca extraction was close to 0% due to the low solubility of $CaSO_4$. From the difference in solubilities, it is possible to separate the calcium and magnesium sulfate, which turns this dissimilarity advantageous, thus obtaining purified $MgSO_4$.

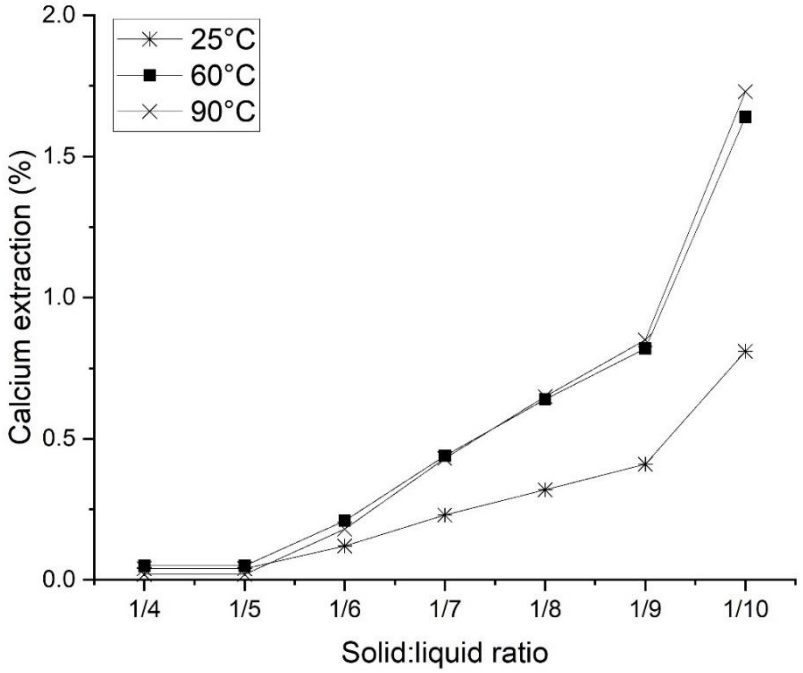

Figure 42 – Simulation of Ca extraction from dolomite (%) as a function of the temperature at 25, 60 and 90°C, and solid:liquid variation in a 2.0mol.L^{-1} H_2SO_4 concentration.

FactSage simulation showed that data were compatible with the information mentioned above about Ca phases. The simulations at temperatures above 75°C suggested the formation of anhydrite instead of gypsum.

The acid variation to investigate the behavior of calcium in the conditions selected using excess acid was also studied in Figures 43 and 44. In Figure 43 was observed the same behavior of calcium which was that either temperature or acid concentration increased the Ca extraction in an S:L ratio = 1:5.

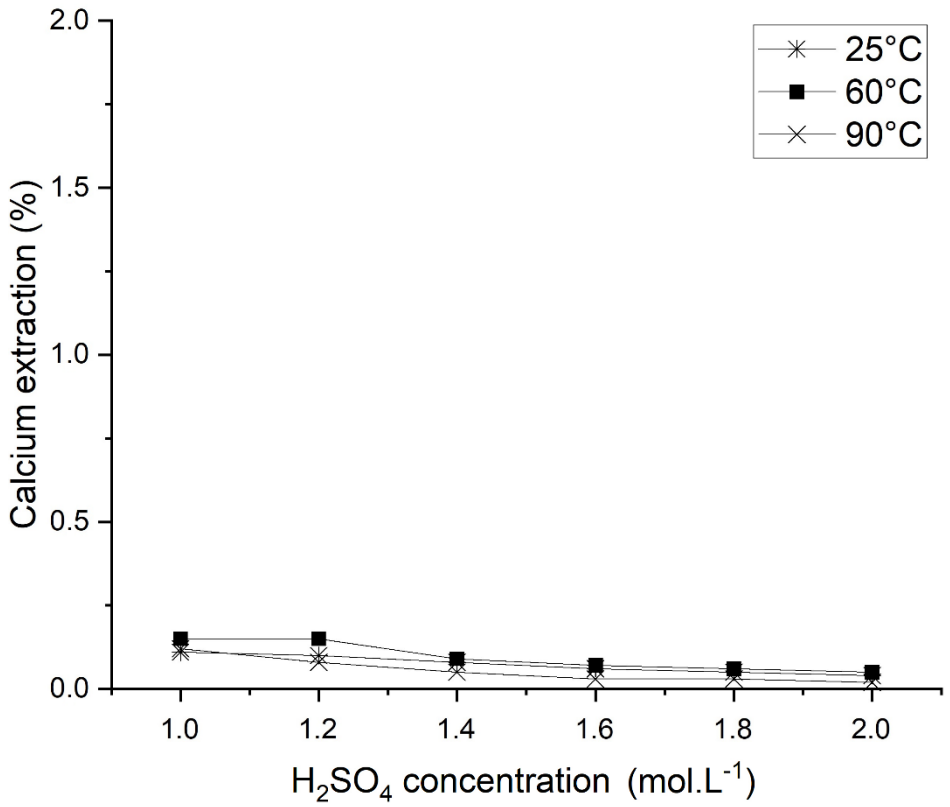

Figure 43 – Simulation of Ca leaching (%) from dolomite as a function of the temperature at 25, 60 and 90°C, and H_2SO_4 concentrations from 1.0 to 2.0mol.L^{-1} in a solid:liquid ratio of 1:5.

On the other hand, the conditions set to evaluate the leaching of magnesium, which were 1.2mol.L^{-1}, S:L = 1:10, and T = 25°C, were assessed for Ca extraction, and the results are presented in Figure 44. Using an excess of 20% acid, which is equivalent to 1.2mol.L^{-1}, the Ca extraction was below 0.5% at all simulated temperatures. The behavior of calcium using 2.0mol.L^{-1} H_2SO_4 concentration in an S:L ratio = 1:10 did not indicate an extraction above 1%. To obtain magnesium sulfate in the liquor generated from the leaching of dolomite, as simulated in *FactSage*, since calcium showed no extraction (<2%), it could be obtained a second product, the gypsum ($CaSO_4$).

Hence, the simulations indicated that dolomite leaching using 1.2mol.L^{-1} H_2SO_4 at 25ºC and an S:L ratio of 1:10 could produce soluble $MgSO_4$ and insoluble calcium sulfate – gypsum or anhydrite - which may be potential resources.

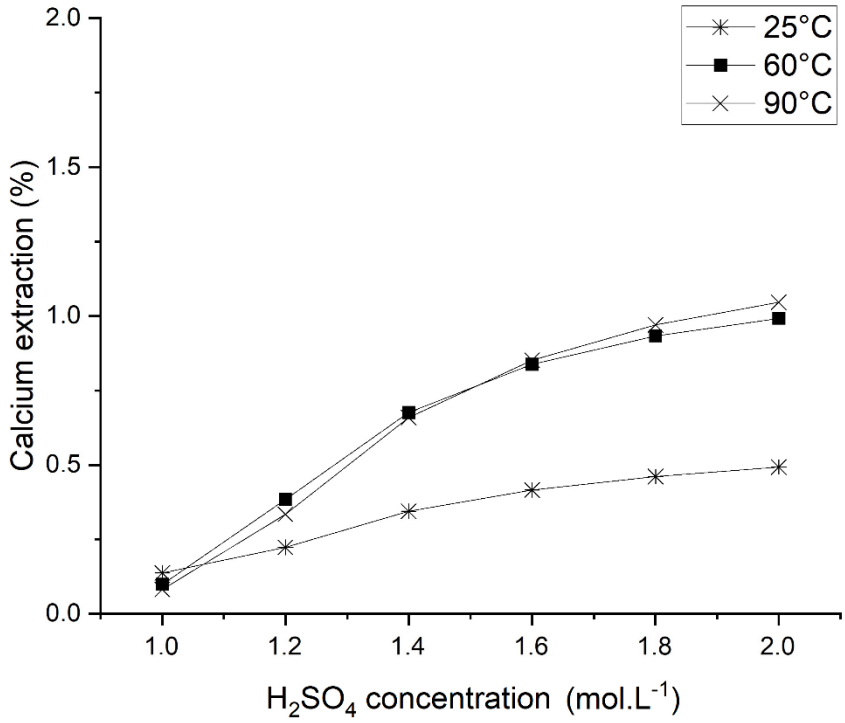

Figure 44 - Simulation of Ca leaching (%) from dolomite as a function of the temperature at 25, 60 and 90°C, and H_2SO_4 concentrations from 1.0 to 2.0mol.L^{-1} in a solid:liquid ratio of 1:10.

5.3.1.3 Zinc tailing

The simulations carried out for the composition of the real Zn tailing aimed to verify the behavior of the elements, in addition to Ca and Mg. Therefore, to study the phases of the main compounds, also to observe the toxic metals - allowing to identify which elements were in the liquor ($MgSO_4$) or the non-leached fraction ($CaSO_4$). The chosen parameters were S:L ratio = 1:10 and H_2SO_4 0.5, 1.0 and 2.0mol.L^{-1}. The extractions of Mg, Ca, Fe, Zn, Al, Pb and Cd were assessed for a range of temperatures from 25 to 90°C. Such conditions were set based on the previous simulations for dolomite.

Figure 45 presents the results of the condition with the least effect on the extraction of magnesium. Even with the interference of the other elements (Ca, Fe, Zn, Al, Pb and Cd) magnesium had the highest leaching yield, at 25°C, obtaining 40% of extraction. In this case, Cd and Pb had almost zero extraction, following the same behavior for Fe, Al, Ca, and Zn at temperatures higher than 60°C.

During the simulation with the composition of the real Zn tailing, it was observed that the other elements had little influence on Mg leaching. Thus, the extraction of Mg

was similar to the simulation performed with pure dolomite.

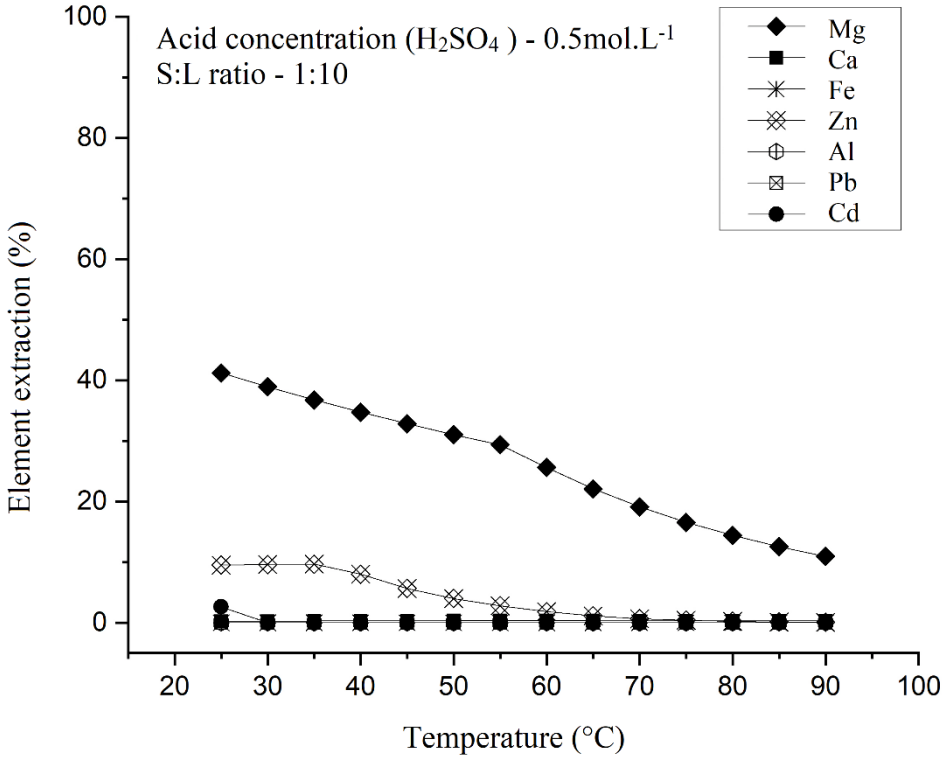

Figure 45 - Conditions of Zn tailing simulation in relation to the Mg, Ca, Fe, Zn, Al, Pb, and Cd extraction yield in percentage as a function of the temperature at 25-90°C in 0.5mol.L^{-1} H_2SO_4 concentration in a solid:liquid ratio of 1:10.

When the acid concentration was increased to 1mol.L^{-1} (Figure 46), cadmium showed 100% extraction. At temperatures above 60°C, magnesium and zinc were also extracted in 100% and 75 to 80%, respectively, at any temperature studied, ranging from 25 to 90°C. Calcium followed the same behavior of the previous simulations, in which the extraction was close to zero, as lead followed the same trend. Both elements form low solubility compounds when compared to magnesium and cadmium, for example.

According to Apelblat and Korin (2007), cadmium in the $CdSO_4 \cdot 8/3H_2O$ phase and temperatures above 44°C becomes cadmium sulfate monohydrate ($CdSO_4 \cdot H_2O$). At higher temperatures (1000°C), phases associated with $CdSO_4$ decompose, thus obtaining $2CdO.CdSO_4$ (Aurivillius, 1980). The cadmium phases, such as $CdSO_4$, $CdSO_4 \cdot 8H_2O$, and $CdSO_4 \cdot H_2O$, have solubility equal to 767g.L^{-1} at 25°C (Lide, 1996).

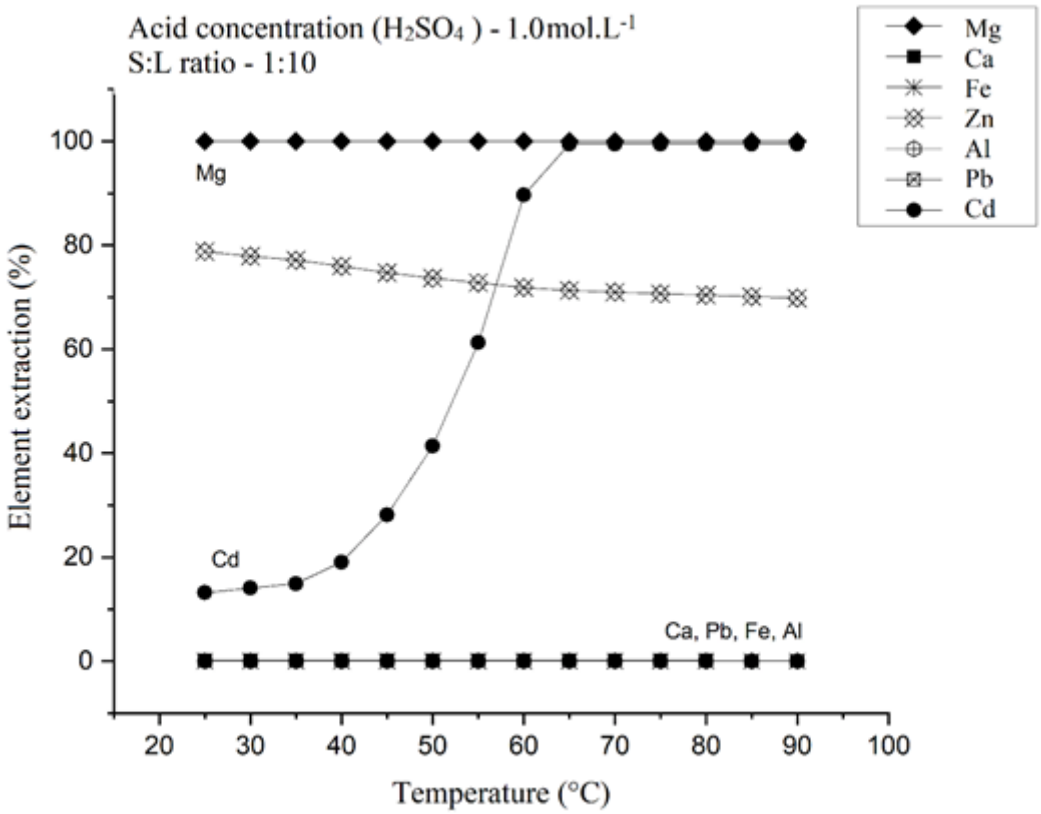

Figure 46 - Zn tailings leaching simulation for Mg, Ca, Fe, Zn, Al, Pb, and Cd extraction yield in percentage as a function of the temperature at 25-90°C in 1.0mol.L^{-1} H_2SO_4 concentration and a solid:liquid ratio of 1:10.

In the simulations carried out in Figures 46 and 47, divergence in the extraction of magnesium was found if compared with the modeled Mg leaching from dolomite (Figure 38). Comparing the simulations considering dolomite and the non-magnetic fraction of the Zn tailing (90.3% dolomite) for 1.0mol.L^{-1} H_2SO_4, the latter achieved 100% of Mg extraction. This was due to the mass of dolomite being smaller in the Zn tailing. Simulations for dolomite achieved 100 % Mg extraction with 1.2mol.L^{-1}, while for Zn tailing it was possible to reach 100% of the extraction using 1.0mol.L^{-1}

The behavior of Ca and Pb with 2.mol.L^{-1} was the same, which achieved zero extraction in all temperatures (25 to 90°C), as shown in Figure 47. Both Figures 46 and 47 suggest that the non-leached fraction generates a predominance of $CaSO_4$ and Pb.

Figure 47 shows that Zn, Al, and Cd reached 100% extraction along with Mg. Fe presented 100% extraction until 65°C. From 65 to 90°C Fe extraction decreased to values lower than 40%. It is well known that iron has two oxidation numbers, Fe^{2+} and Fe^{3+}, which reacts with the aqueous medium. In this case, an aqueous acid medium (Duarte, 2019). In some cases, because the electrochemical potential of iron equals to +0.77V,

Fe^{3+} may be reduced to Fe^{2+} in an aqueous medium (Pourbaix, M., 1974). Therefore, Fe^{2+} was oxidized to Fe^{3+} which may be explained by the presence of CO_2 in the reaction then, the solubility of Fe^{2+} is 7.2g.L^{-1}, and Fe^{3+} is considered insoluble (Duarte, 2019; Lide, 1996). This may explain the possibility for Fe to decrease its extraction, as shown in Figure 47.

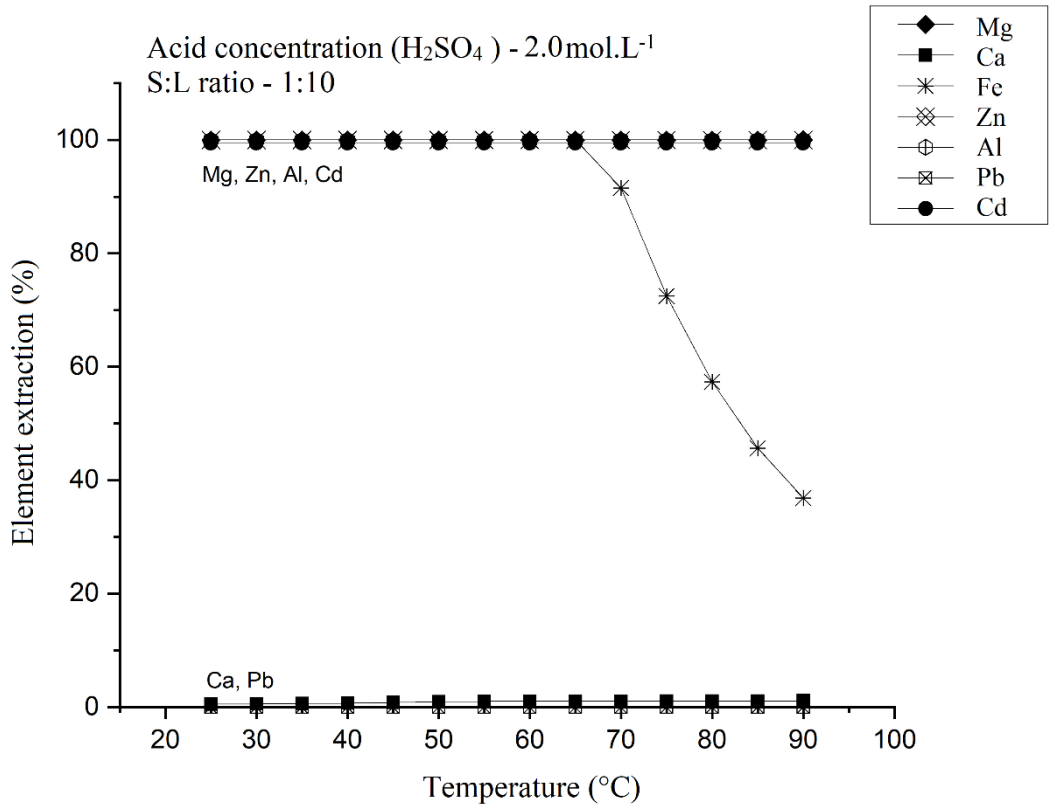

Figure 47 - Leaching simulation of Zn tailing for Mg, Ca, Fe, Zn, Al, Pb, and Cd extraction yield in percentage as a function of the temperature at 25-90°C and 2.0mol.L^{-1} H_2SO_4 in a solid:liquid ratio of 1:10.

FactSage software provided the formed phases in the studied temperature range. Tables 19, 20, and 21 show the behavior of the elements and the compounds that present thermodynamic tendency to be formed in the non-leached fraction.

In Table 19, it is shown that the amount of Mg not leached would form the solid phases: $CaMg(CO_3)_2$, $MgCO_3$, and $Mg_5Al_2Si_3O_{10}(OH)_8$. However, as previously discussed, dolomite did not obtain complete solubilization at temperatures from 25 to 90°C using H_2SO_4 0.5mol.L^{-1}, magnesium carbonate would be formed from the incomplete dissolution of dolomite.

Calcium is initially presented as dolomite and as calcium sulfate. At temperatures from 25 to 60°C, it is found as gypsum ($CaSO_4(H_2O)_2$) and from 65 to 90°C as anhydrite ($CaSO_4$), losing water from its composition as the temperature increased.

In the simulation with 0.5mol.L^{-1} of H_2SO_4 more compounds (non-leached phases) in the non-leached fraction was obtained, comparing with the simulations with 1.0 and 2.0mol.L^{-1}, shown in Table 19. Cadmium, for instance, behaved as a carbonate after adding acid, while lead was obtained as sulfate, regardless of the set temperature. Zinc was found as carbonate at T=25 to 35°C and silicate at T=40 to 90°C. Iron remained as hematite in all temperatures.

Table 19 – List of solid phases thermodynamically predicted by *Factsage* considering H_2SO_4 0.5mol.L^{-1} , S:L ratio 1:10 and varying temperature from 25 to 90°C.

Temperature	**Compounds**						
(°C)	**Ca**	**Pb**	**Fe**	**Mg**	**Zn**	**Al**	**Cd**
25	$CaSO_4(H_2O)_2$ and $CaMg(CO_3)_2$	$PbSO_4$	Fe_2O_3	$CaMg(CO_3)_2$ and $MgCO_3$	$ZnCO_3$	$Al_2O_3(H_2O)$	$CdCO_3$
30							
35							
40					Zn_2SiO_4		
45							
50							
55							
60							
65	$CaSO_4$ and $CaMg(CO_3)_2$					$Mg_5Al_2Si_3O_{10}(OH)_8$	
70							
75							
80							
85							
90							

Increasing H_2SO_4 concentration to 1.0mol.L^{-1} resulted in the phases listed in Table 18, in which the dolomite phase was no longer present in the simulation Table 20. The behavior of the formed compounds from Table 19 remained the same in the conditions presented in Table 20, except for magnesium, which achieved 100% leaching.

Table 20 – List of solid phases thermodynamically predicted by *Factsage* considering H_2SO_4 1.0mol.L^{-1} , S:L ratio 1:10 and varying temperature from 25 to 90°C.

Temperature	**Compounds**					
(°C)	Ca	Pb	Fe	Zn	Al	Cd
25	$CaSO_4(H_2O)_2$	$PbSO_4$	Fe_2O_3	$ZnCO_3$	$Al_2O_3(H_2O)$	$CdCO_3$
30						
35						
40				Zn_2SiO_4	$Al_2O_3(H_2O)$	
45						
50						
55	$CaSO_4$					
60						
65						
70						
75						
80						
85						
90						

In Table 21, considering H_2SO_4 2.0 mol.L^{-1}, phases with Ca, Pb and Fe were presented in the non-leached fraction. Two phases of calcium sulfate were acquired, namely gypsum ($CaSO_4(H_2O)_2$) and anhydrite ($CaSO_4$). Iron remained as hematite and lead as a sulfate. In this case, even increasing the concentration of sulfuric acid, such compounds are considered insoluble.

Table 21 - List of solid phases thermodynamically predicted by *Factsage* considering H_2SO_4 2.0mol.L^{-1} , S:L ratio 1:10 and varying temperature from 25 to 90°C.

Temperature	Compounds		
(°C)	**Ca**	**Pb**	**Fe**
25	$CaSO_4(H_2O)_2$	$PbSO_4$	Fe_2O_3
30			
35			
40			
45			
50			
55	$CaSO_4$		
60			

65			
70			
75			
80			
85			
90			

Tables 19 to 21 show the phases that possibly constitute the non-leached fraction. In which, there was the presence of $CaSO_4(H_2O)_2$ (gypsum) or $CaSO_4$ (anhydrite), and $PbSO_4$ in the acid concentration of 0.5, 1.0, and 2.0mol.L^{-1}. Iron was presented as hematite in all cases of simulation. The influence on temperature was observed in relation to the calcium sulfate phase may be $CaSO_4(H_2O)_2$ (gypsum) or $CaSO_4$ (anhydrite). Also, the incomplete reaction of dolomite with 0.5mol.L^{-1} H_2SO_4.

5.3.2 Eh-pH diagrams for thermodynamic modelling of impurities

The thermodynamics of leaching considers the chemical equilibrium of all possible species involved in every reaction (Havlik, 2001). By means of phase/species and Eh-pH diagrams it was possible to understand the fate of the impurities from the tailing before the experimental leaching tests. In particular, the behavior of $PbSO_4$ and $CdSO_4$ were investigated since their presence must be avoided in the leaching liquor. In Figure 48, the Eh-pH diagram constructed according to the composition of the tailing is presented.

In Figure 48, it is shown that cadmium assumes its ionic form in an aqueous medium [Cd^{2+}] in the same pH range as Mg^{2+} and Pb^{2+} (pH 0 to 4) at 25°C. On the other hand, the solubility of $CdSO_4$ at 25°C is around 767g.L^{-1} while the solubility of $PbSO_4$ is much lower, 0.04g.L^{-1}. Likewise, the solubility of $MgSO_4$ and $CaSO_4$ is approximately 357g.L^{-1} and 2.05g.L^{-1} respectively (Dutrizac, 2002; Lide, 1996). Considering the main compounds mentioned, $MgSO_4$ and $CdSO_4$ have high solubility, unlike $CaSO_4$ and $PbSO_4$ which have lower solubility, as previously mentioned. Therefore, the leaching liquor is expected to present negligible amounts of Pb, but the dissolution of Cd must be considered (Ramalingom et al., 2001; Shen et al., 2019; Williams, 1996).

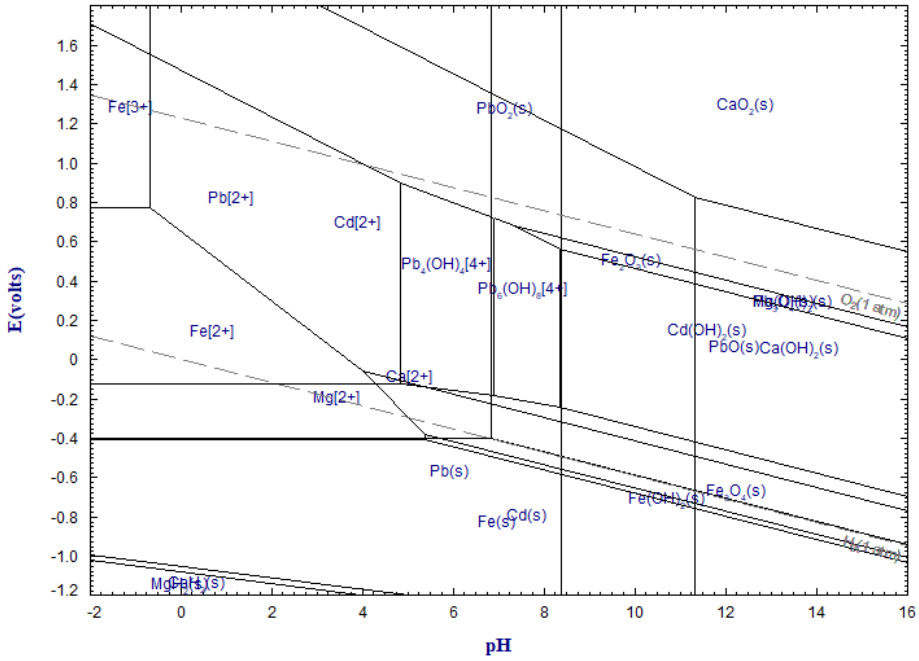

Figure 48 - Speciation diagram – *FactSage* EpH module with the main compounds of the zinc flotation tailing

The reactions between the compounds found in the tailing and the sulfuric acid are represented by Equations 13 to 19 as follows:

$$MgCO_{3(s)} + H_2SO_{4(aq)} \leftrightarrow H_2O_{(l)} + CO_{2(g)} + MgSO_{4(aq)} \quad \text{Equation 13}$$

$$CaCO_{3(s)} + H_2SO_{4(aq)} \leftrightarrow H_2O_{(l)} + CO_{2(g)} + CaSO_{4(s)} \quad \text{Equation 14}$$

$$Fe_2O_{3(s)} + 3H_2SO_{4(aq)} \leftrightarrow 3H_2O_{(l)} + Fe_2(SO_4)_{3(s)} \quad \text{Equation 15}$$

$$ZnO_{(s)} + H_2SO_{4(aq)} \leftrightarrow H_2O + ZnSO_{4(aq)} \quad \text{Equation 16}$$

$$Al_2O_{3(s)} + 3H_2SO_{4(aq)} \leftrightarrow 3H_2O_{(l)} + Al_2(SO_4)_{3(aq)} \quad \text{Equation 17}$$

$$CdO_{(s)} + H_2SO_{4(aq)} \leftrightarrow H_2O_{(l)} + CdSO_{4(aq)} \quad \text{Equation 18}$$

$$PbO_{(s)} + H_2SO_{4(aq)} \leftrightarrow H_2O_{(l)} + PbSO_{4(s)} \quad \text{Equation 19}$$

5.4 LEACHING TESTS

The leaching tests were performed to ascertain the results of the thermodynamic simulation and to evaluate the kinetic effects. Besides, to compare the simulation and the leaching tests, and then, following with the purification stage.

In Figure 49, the leaching step using a five-neck reactor and the products obtained are shown. The volume of acid used for the tests was 0.5L, and the tailing mass was 50g.

The leaching agent was a 1.2mol.L^{-1} H_2SO_4 solution, as indicated by the simulations (item 5.3.1). The solid:liquid ratio was fixed in 1:10 to all assays.

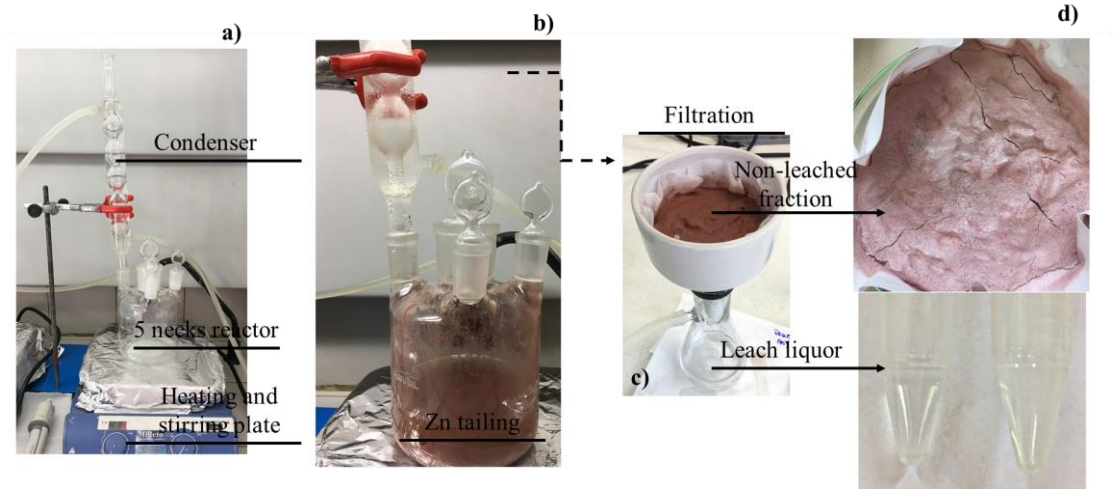

Figure 49 - (a) Main equipment used in leaching step consisting of a five-neck reactor, (b) Zn tailings leaching in the five necks reactor (c) and (d) the products obtained: non-leached fraction and liquor.

Dolomite was dissociated with H_2SO_4 acid to remove magnesium. The kinetics and thermodynamics of such a reaction were evaluated. Figure 50 shows the results of percent extraction of Mg under the mentioned conditions. According to Figure 50, after 60min, the magnesium extraction tended to stabilize. At 25°C, the extraction was lower than the other temperatures until 50min, then, it stabilized similarly/at similar yields than to the different temperatures.

According to Figure 50, the Mg extraction using 1.2mol.L^{-1} of H_2SO_4 achieved higher rates after approximately 30 to 50min. After 60min, a slight decrease in Mg extraction was noticed. Such a tendency is in accordance with the simulated results, which showed that increasing the temperature could result in lower extraction rates due to the precipitation of Mg. Aside from the temperature, the reaction time appears to have an influence on Mg precipitation. The tests performed at 25°C showed lower percent extraction than the others up to 50 minutes, when it stabilized, reaching an extraction rate close to the other evaluated temperatures. The parameters that resulted in the highest yield of Mg extraction were 35 minutes and 50°C, leading to an Mg extraction of 72% ± 5%.

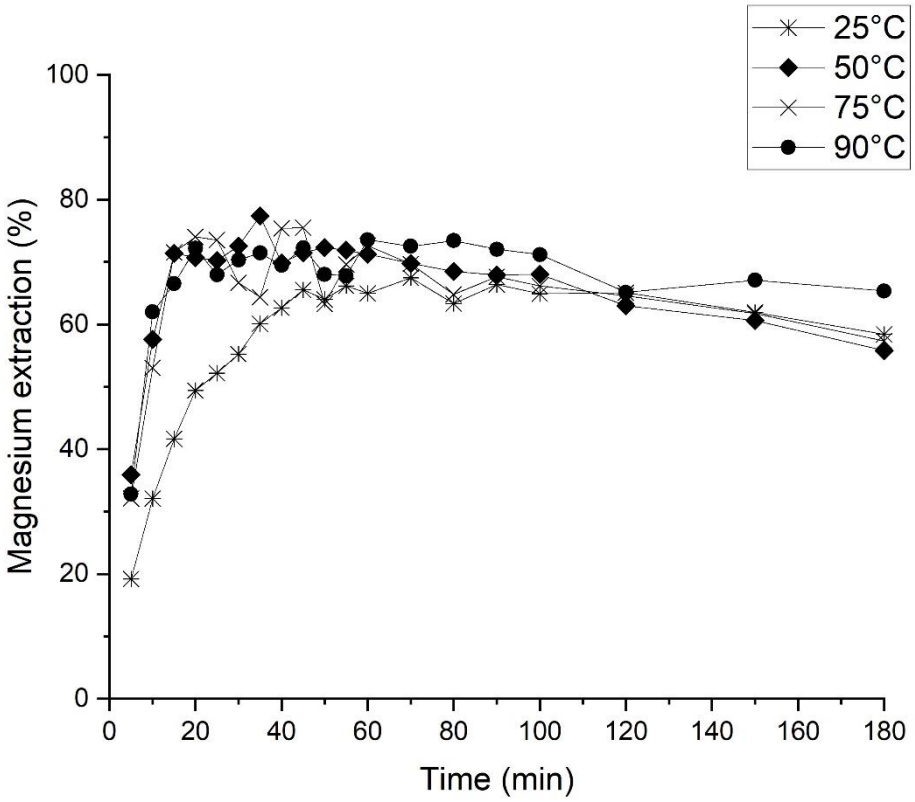

Figure 50 - Yield of magnesium extraction in the leaching step. Evaluation of the magnesium extraction in relation to the temperature and reaction time.

The effect of acid concentration aiming to provide an excess of acid was also studied. From the stoichiometric reaction presented in Equation 12, five different acid concentrations were evaluated and compared: 0.8, 1.0, 1.2, 1.5 and 2mol.L^{-1}. The second one represents the stoichiometric relation between H2SO4 and dolomite/tailing. The last three provided excess acid of 20, 50 and 100% respectively.

In Figure 51 the variation of the concentration of H_2SO_4 shows that from 1.0mol.L^{-1} to 2.0mol.L-1 there was a yield above 60%. The variation of H_2SO_4 concentration showed that from 1.0 mol.L^{-1} the extraction yield reached more than 70%. The highest magnesium extraction was reached using H_2SO_4 1.5 and 2.0mol.L^{-1}, which was around 75-80 %.

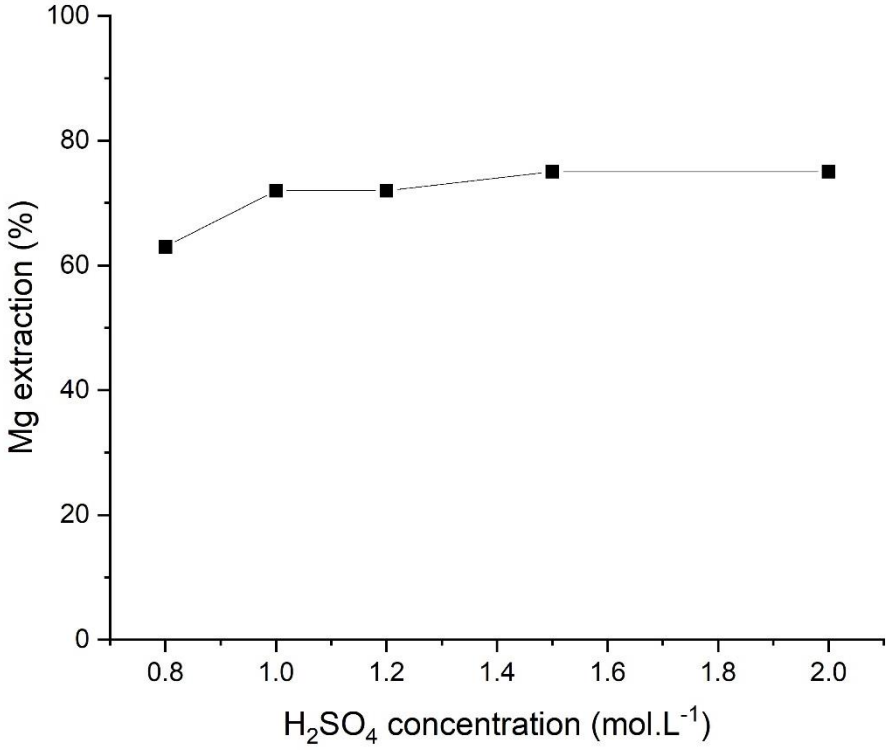

Figure 51 - Yield of magnesium extraction from zinc tailing leaching at 50°C in 35min for H2SO4 concentration from 0.8 to 2.0mol.L^{-1}.

Hence, the optimal conditions for Mg extraction from dolomite were 1.2mol.L^{-1}, 35min, and 50ºC. The obtained results are in good agreement with other researches that aimed at the recovery of Mg from different ores. (Abali et al., 2006) found the best conditions for Mg extraction from $MgCO_3$ as 60min, using a higher H_2SO_4 concentration (5.0mol.L^{-1}), and the temperature was 65°C. In the study of Luo et at (2015), the authors used H_2SO_4 to recovery K and Mg from biotite. The temperature was found to enhance the reaction yield and a longer contact time (150 minutes) was reported. As a result, the authors achieve an extraction of around 95 % Mg (Luo et al., 2015). In the production of $MgCl_2.6H_2O$, from a magnesite tailing, it was shown that 85-90% of the Mg was solubilized after 20 minutes when using hydrochloric acid (HCl), the concentration was between 1.5 to 2.0 mol.L^{-1} at a temperature of 40 °C (Özdemir et al., 2009).

The results of the leaching tests were also compared to the results of the simulations. The main point observed was that the Mg leaching had a lower extraction yield than expected in simulation. The parameters for dolomite leaching and the optimal H_2SO_4 concentration were considered. However, the kinetic effects are not possible to be

simulated but are the main factors to be considered as an influence on the results by decreasing the Mg extraction in experimental tests.

Another hypothesis to explain the differences in Mg extraction yield is due to the lower availability of SO^{4-} in the leaching solution after the formation of gypsum ($CaSO_4$). Therefore, a lower Mg extraction rate and a slight difference in the optimal leaching temperature were observed during the experimental leaching tests. Nevertheless, the simulations showed to be a reliable basis for selecting the experimental leaching parameters. It is worth mentioning that calcium was virtually not detected in the leaching liquor, which is in accordance with the thermodynamic simulations and the reaction described in Equation 12 (Xiong et al., 2014).

Subsequently, leaching tests with H_2SO_4 concentrations from 0.8 to 1.5mol.L^{-1} were performed at 50°C in 35min. The results are shown in Figures 52 and 53.

In Figure 52, the result of the quantitative analysis of the leaching liquor is presented. There was a low extraction of Ca, Pb, and Al (<5%), as expected. On the other hand, Mg and Cd had an extraction above 60% in the conditions of H_2SO_4 from 1.0mol.L^{-1}. The extraction of Fe was around 10%, and Zn ≥50%. Therefore, it was found that the results are compatible with the behavior presented in the simulation. Thus, there was a tendency for Mg, Cd, and Zn to appear in the liquor fraction and the non-leached fraction to be composed mainly of Ca, Pb, Fe, and Al. Al was extracted only when using an H_2SO_4 concentration equal to 2.0mol.L^{-1} in the simulation.

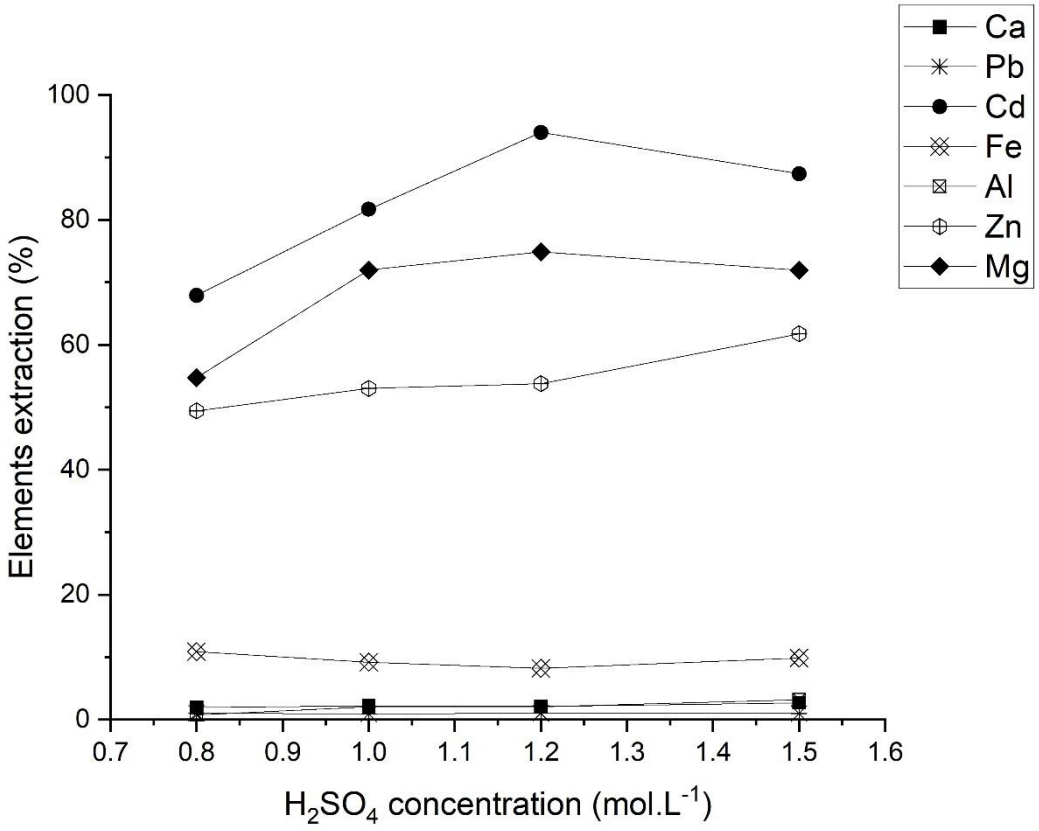

Figure 52 – Yield of elements extraction after leaching at 50°C in 35min evaluating the variation of H_2SO_4 concentration from 0.8 to 1.5mol.L^{-1}.

Despite the fact, leaching has shown to be efficient in the extraction of Mg from dolomite, the presence of impurities was detected in the leaching liquor, especially Cd. The chemical analyses showed that the leaching liquor for 1.2mol.L^{-1} H_2SO_4 presented about 400mg.L^{-1} of Cd. Besides, the analyses of the non-leached fraction in the filter showed that 100% Cd was leached.

During the assays, the pH was measured, as presented in Table 22. The compounds were acquired as solid/precipitated; were $CaSO_4$ and $PbSO_4$ in the non-leached fraction and was leached Mg and Cd in a pH <2. In the dolomite leaching, some challenges are found due to the control of the partial pressure of the CO_2 generated, as well as the pH measurement, because there is a disparity in the values of solubility product of dolomite in an acid medium above room temperature (Abali et al., 2006; Puthiya et al., 2017).

Table 22 - Molar concentration of H_2SO_4 acid in leaching and pH in 5, 20, and 35min.

	0.8mol.L^{-1}	**1.0mol.L^{-1}**	**1.2mol.L^{-1}**	**1.5mol.L^{-1}**	**2.0mol.L^{-1}**
pH_{5min}	0.94	0.68	0.59	0.66	1.05
pH_{20min}	1.66	0.91	0.57	0.62	0.67
pH_{35min}	2.46	1.13	0.63	0.60	0.57

The other analysis step was carried out with the non-leached fraction with acid digestion with the microwave aid.

Thus, Figure 53 showed that Cd was not present in the non-leached fraction. If evaluated by the non-leached fraction, Mg had a higher extraction rate, being greater than 80%. And, as previously discussed, the same tendency was observed for Pb and Ca, which is not be extracted. The mass balance of the stages was presented in item 5.6.

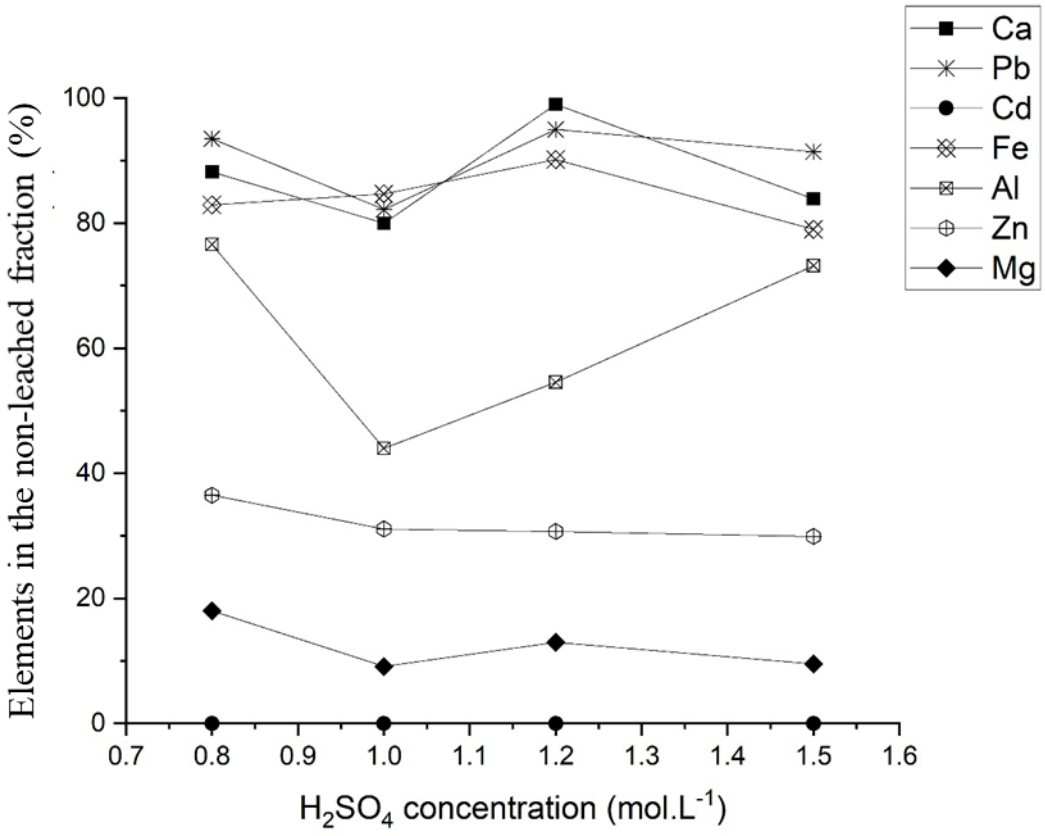

Figure 53 - Yield of elements in the non-leached fraction at 50°C in 35min evaluating the H_2SO_4 concentration from 0.8 to 1.5mol.L^{-1}.

Although leaching has shown to be efficient in the extraction of magnesium from the dolomite. The presence of impurities was detected in the process of leaching liquors, especially cadmium. Chemical analyses showed that the leaching liquors in 1.2mol.L^{-1} concentration was presented about 400mg.L^{-1} of cadmium. The non-leached fraction

analyses retained in the filter showed that 100% of cadmium was leached.

For a better investigation, the XRD of the non-leached fraction in filter paper was performed, as shown in Figure 54. The peaks numbered as 1 and 2 in Figure 54 indicate the formation of calcium sulfate phases, $Ca(SO_4)\cdot 2H_2O$, in all evaluated H_2SO_4 concentrations (Tolonen et al., 2015).

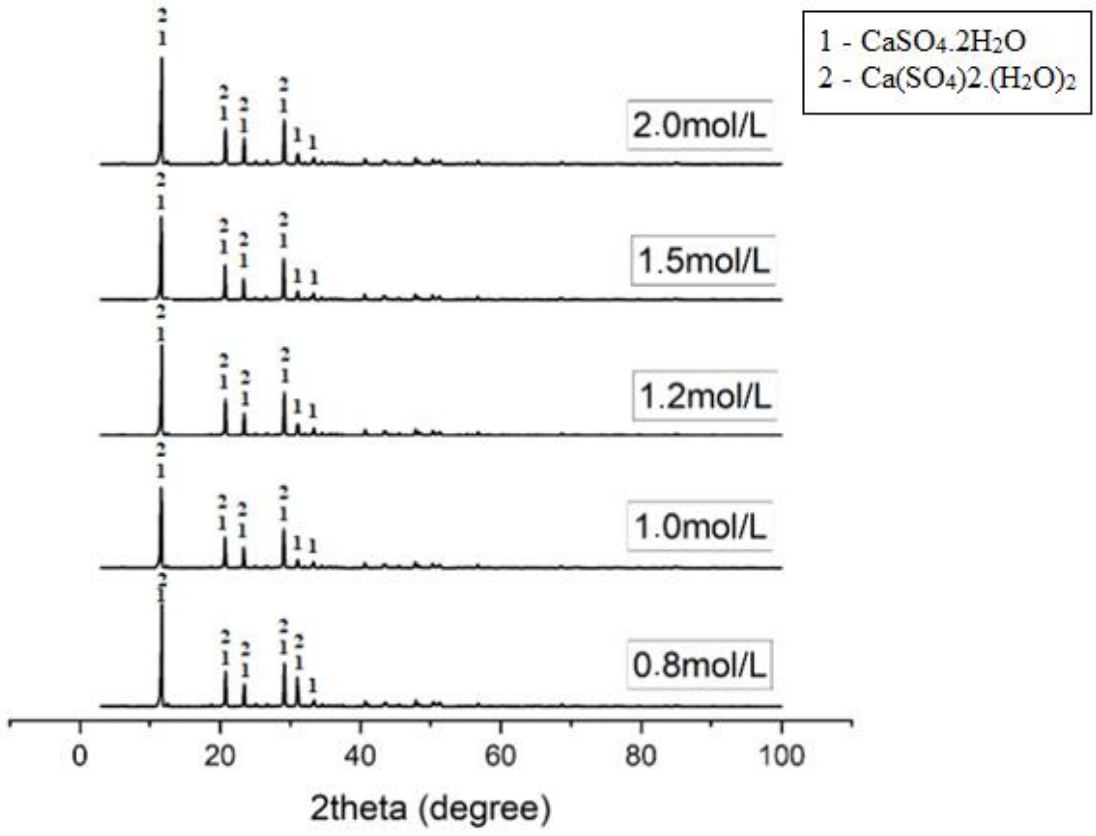

Figure 54 - XRD of the non-leached fraction for acid concentration from 0.8 to 2.0mol.L^{-1}, 50°C in 35min.

Figures 55 to 59 present the SEM images showing the non-leached fraction in all evaluated concentrations of H_2SO_4. According to the EDS semi-quantitative analysis, there is a concentration of Ca and S, representing the leaching tests performed using H_2SO_4. The non-leached fraction has a lamellar shape which is supposedly $CaSO_4$. No concentration greater than 1wt.% of Mg was found by EDS in the non-leached fraction.

The analysis of a 300µm microregion that describes a particle formed by calcium sulfate is shown in Figure 55. The EDS spectrum did not present Mg in the observed particle.

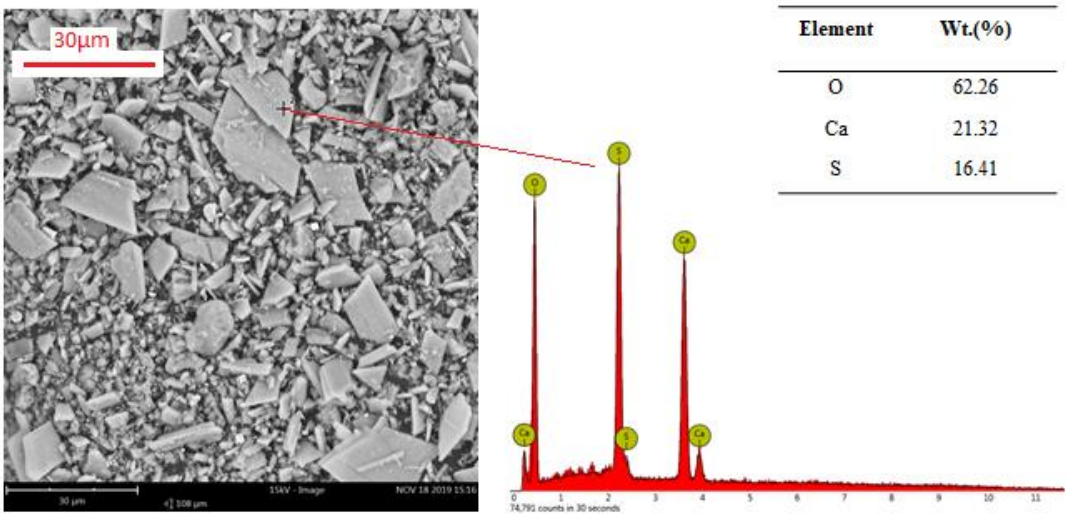

Figure 55- Backscattered electron (BSE) spot image obtained in the electron microscope scanning with a composition of the sample, obtained by EDS of the non-leached fraction in 0.8mol.L^{-1} H_2SO_4 concentration in 35min at 50°C.

In Figure 56 a particle was also observed in which it predominantly contained Ca, S and O. However, a mass concentration of 0.48% Mg was also presented. This may represent remnants of the Mg that was not leached. Silicon was also found with a mass concentration of 0.35%.

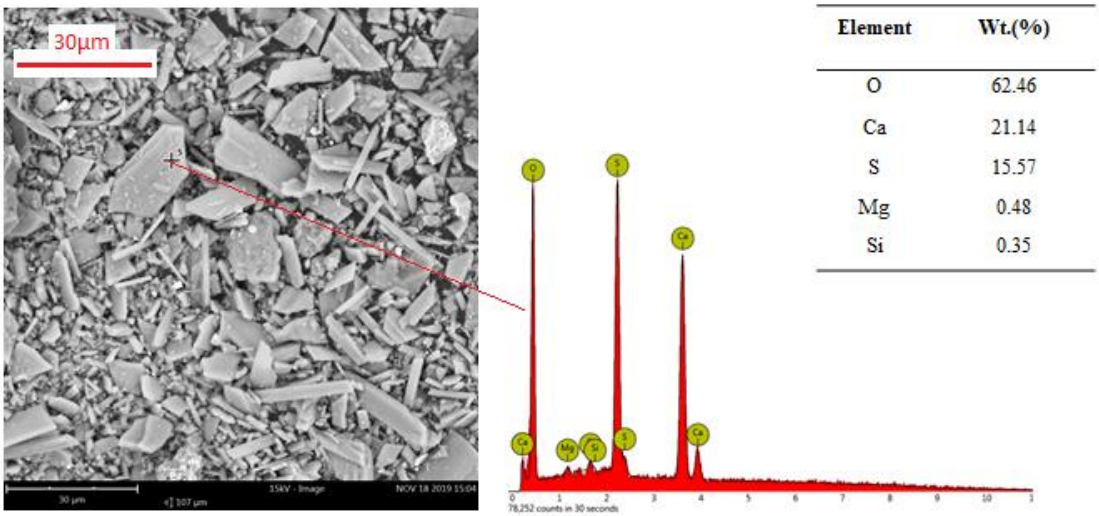

Figure 56 – Backscattered electron (BSE) spot image obtained in the scanning electron microscope with a composition of the sample, obtained by EDS of the non-leached fraction in 1.0mol.L^{-1} H_2SO_4 concentration in 35min at 50°C.

Figure 57 refers to the non-leached fraction in 1.2mol.L^{-1} of H_2SO_4, and a detail that could be observed was the presence of a Pb particle, being one of the elements of interest for the purification step.

In Figure 57a), the mass concentrations of Pb and Ca were 50 and 11%, respectively. Therefore, since the concentration of Pb is predominant along with other elements, such as S, and O, it is possible to assume that Pb is found as $PbSO_4$ with a size of about 30µm and free from the remnant material that was observed in the SEM. In Figure 57b), the Pb particle's presence was also observed with a concentration of 83%. The other elements, Ca, and Fe appeared with concentrations below 3%. In both situations, the surrounding material is presented by lamellas, which are characteristic of $CaSO_4$ seen in Figure 55 and 56.

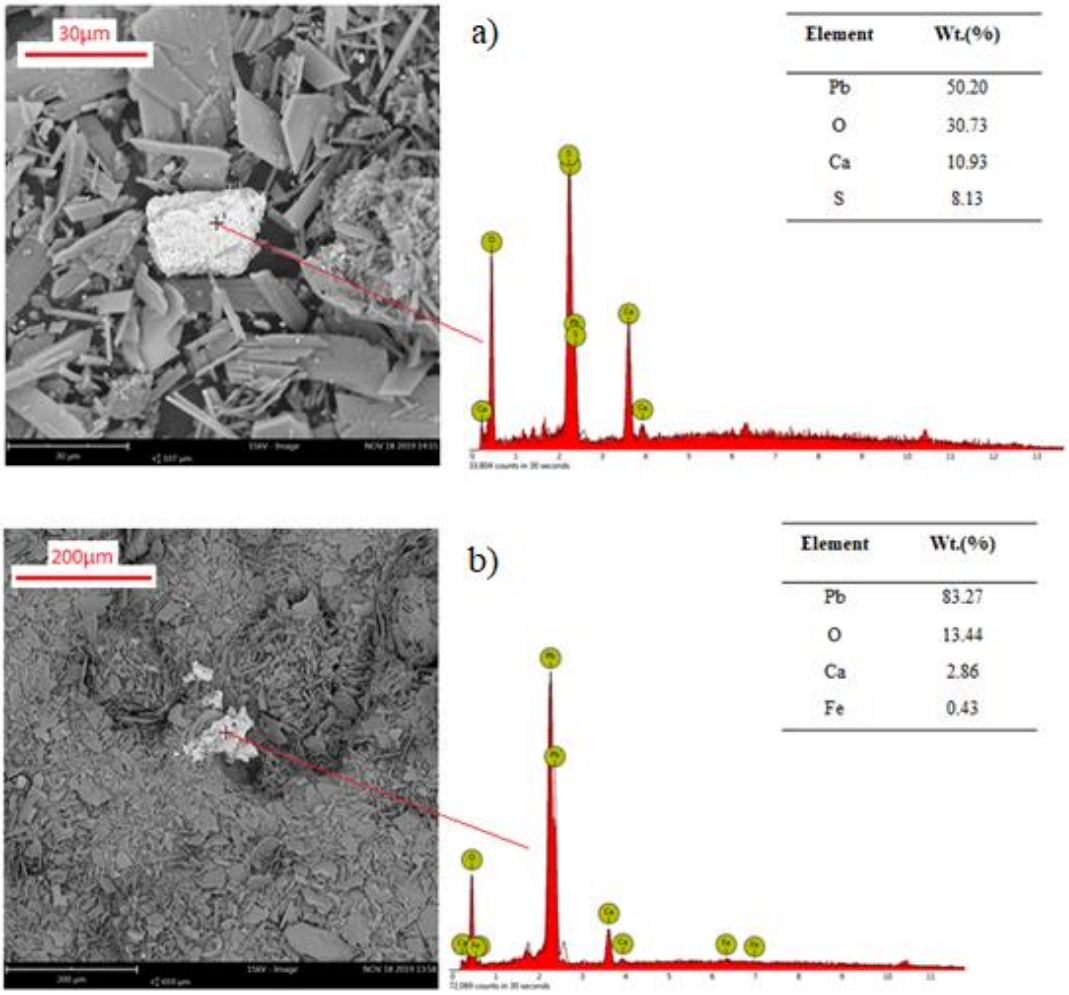

Figure 57 – Backscattered electron (BSE) spot image obtained in the scanning electron microscope with a composition of the sample, obtained by EDS of the non-leached fraction in 1.2mol.L^{-1} H_2SO_4 concentration in 35min at 50°C – a) and b) a spot is representing a Pb particle.

In Figure 58, the non-leached fraction analysis in 1.5mol.L^{-1} H_2SO_4 also presented particles of Ca, S and O in EDS and lamellar aspects.

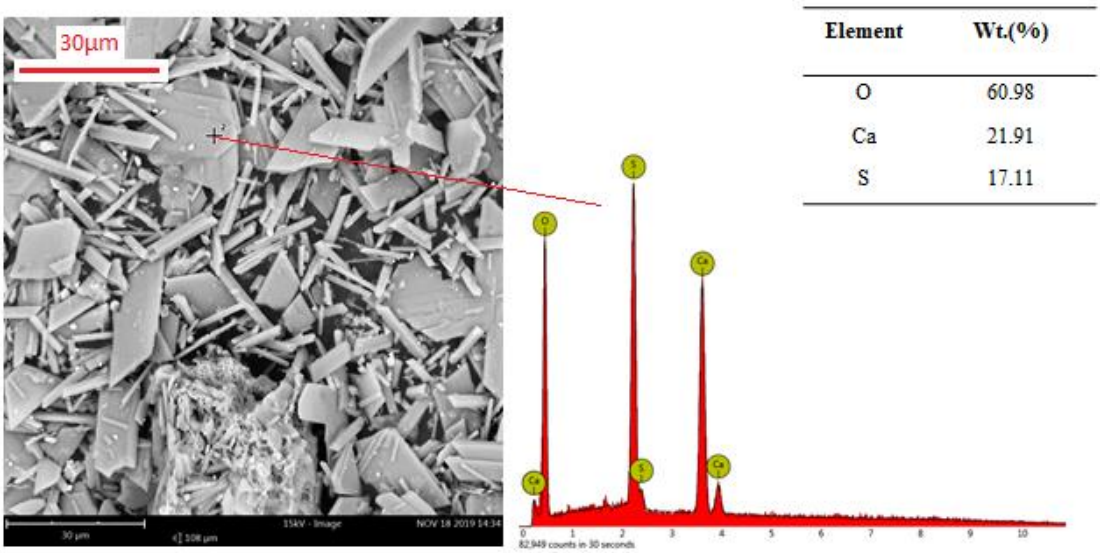

Element	Wt.(%)
O	60.98
Ca	21.91
S	17.11

Figure 58 - Backscattered electron (BSE) spot image obtained in the scanning electron microscope with a composition of the sample, obtained by EDS of the non-leached fraction in 1.5mol.L^{-1} H_2SO_4 concentration in 35min at 50°C.

In Figure 59, an analysis was made with another perspective of the material. The particles were observed with a scale of 80µm, and the predominance of particles with the same aspect mentioned above, of lamellas. The EDS analysis was carried out of a microregion with Ca, Pb, Al, and Si in a particle.

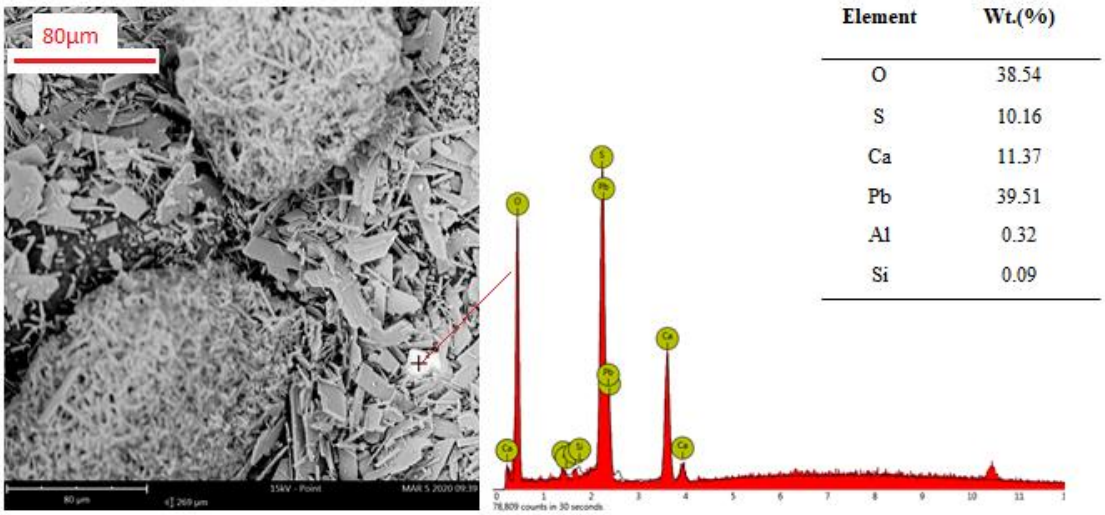

Element	Wt.(%)
O	38.54
S	10.16
Ca	11.37
Pb	39.51
Al	0.32
Si	0.09

Figure 59 - Backscattered electron (BSE) spot image obtained in the scanning electron microscope with a composition of the sample, obtained by EDS of the non-leached fraction in 2.0mol.L^{-1} H_2SO_4 concentration in 35min at 50°C

Leaching proved to be efficient in the extraction of magnesium from dolomite. However, elements such as cadmium were found in the liquor (94%wt.).

From the chemical analysis, the calcium extraction was 2.7% in an H_2SO_4 concentration of 1.2mol.L^{-1} in 35 min at 50°C. In the non-leached fraction, calcium formed gypsum, although lead was found as an impurity.

Thus, purification steps for the liquor ($MgSO_4$) and to a non-leached fraction ($CaSO_4$) were carried out to remove Cd from the liquor and Pb from the non-leached fraction as following in item 5.5.

5.5 PURIFICATION TESTS

In this stage, three purification techniques were used: cementation, sulfide precipitation and density separation. In the liquor, two purification steps were carried out to be compared, the cementation with the sulfide precipitation. The non-leached fraction was carried out using the density separation step.

5.5.1 Cementation post-treatment

Since the aim of the study is to produce $MgSO_4$, which is a potential candidate to be used in agriculture as a fertilizer, it is necessary to eliminate the remaining Cd of the leaching liquor. Hence, the cementation was evaluated as a possible post-treatment step.

Cadmium cementation using zinc powder is a well established method, and it has been evaluated in different conditions (Havlik, 2001; Ku et al., 2002; Sadegh Safarzadeh et al., 2007; Younesi et al., 2006). Zinc being less noble than cadmium is oxidized while cadmium is reduced. The global reaction is shown in Equation 20.

$$Cd^{2+} + Zn_{(s)} \rightarrow Cd_{(s)} + Zn^{2+} \qquad \text{Equation 20}$$

5.5.1.1 Cementation using synthetic solution

Figure 60 shows the material before filtering in the 100:1 Zn:Cd ratio and the final material cemented.

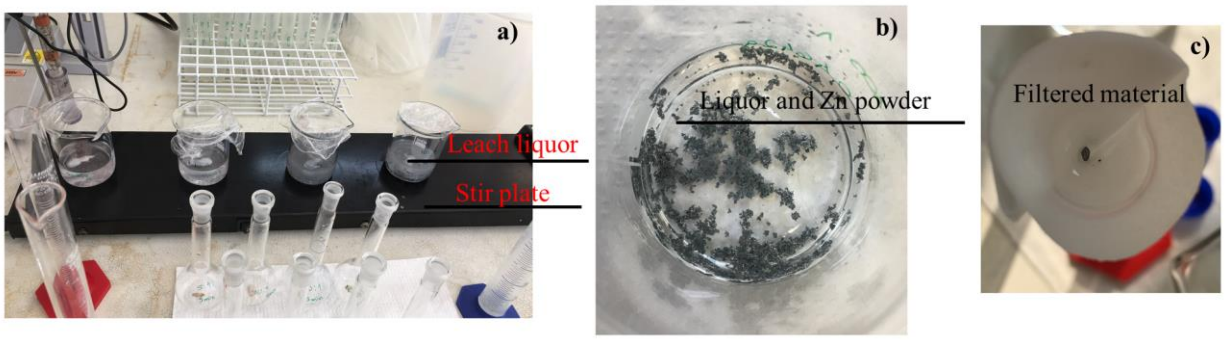

Figure 60 - Cementation tests with Zn powder with (a) Equipment for cementation with the liquor of the synthetic solution; (b) Cementation with the liquor; (c) Cemented material after filtration.

The assays performed using a synthetic solution containing Mg and Cd in sulfuric medium and the same concentration as the leach liquor are presented in Figures 61 and 62. Figure 61 shows the Cd removal results during the cementation for four different Zn:Cd ratios: 1:1, 2.5:1, 5:1, 10:1; and 100:1. It is evidenced that the 100:1 ratio yielded the highest Cd removal, equivalent to approximately 100%.

According to (Younesi et al., 2006), 100% Cd removal was achieved after 15min, when using a sulfate solution initially containing 7250mg.L^{-1} of Cd and a Zn:Cd ratio equals to 10:1. When decreasing the initial Cd concentration to 246mg.L^{-1}, the authors obtained 100% Cd removal after 16s. Thus, to evaluate the influence of time on Cd cementation, the second set of tests was performed, and aliquots were withdrawn each 5min and forwarded to chemical analysis. The results are detailed in Figure 62.

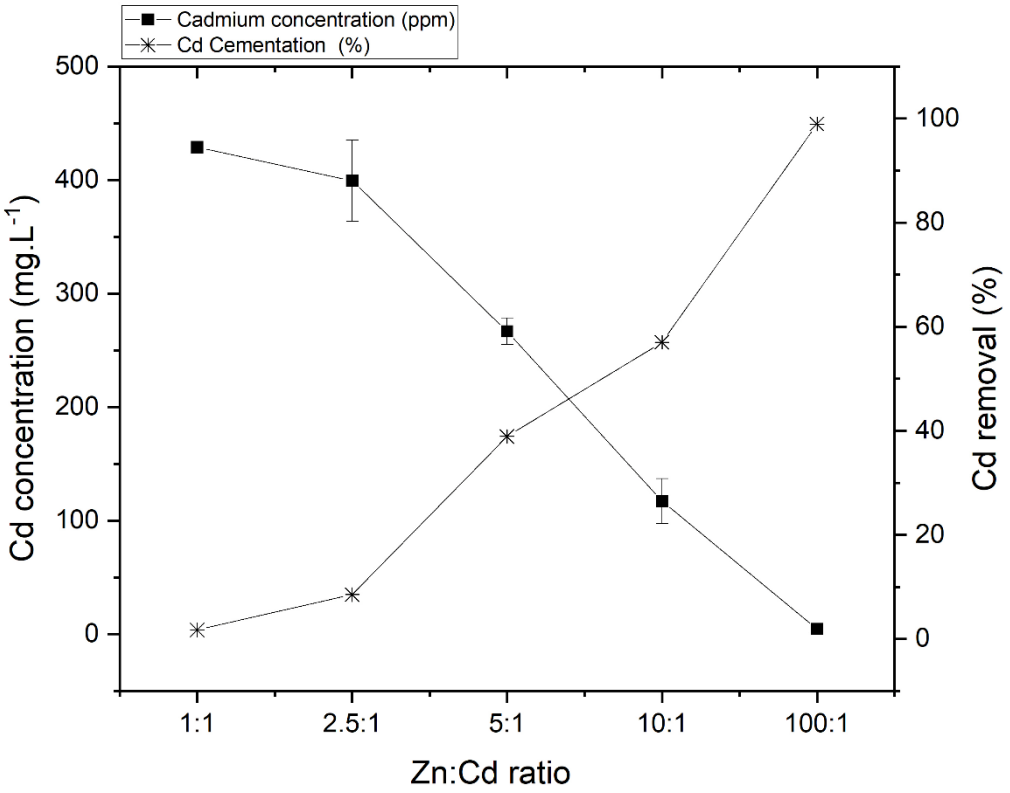

Figure 61 – Cementation of Cd from a synthetic solution containing 400mg.L^{-1} Cd and 9,600mg.L^{-1} Mg after 20minutes.

Younesi et al., (2006) carried out a study in which there was a tendency to increase the removal of Cd with time and higher Zn:Cd ratio, as shown in Figures 61 and 62. However, the 50:1 and 100:1 ratio showed that from 35min obtained a Cd removal around 90%, Figure 62.

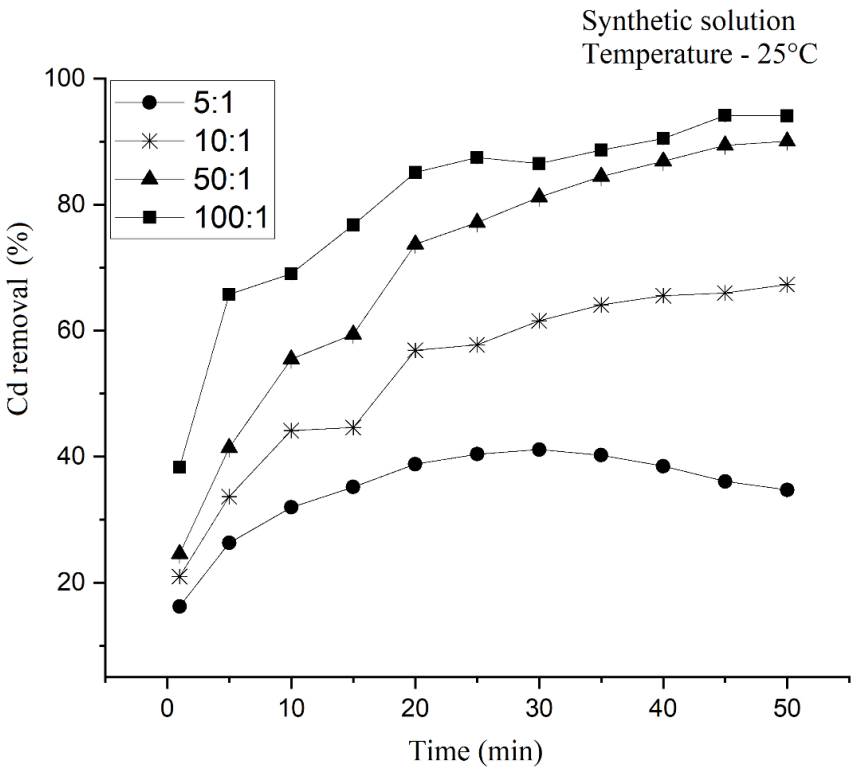

Figure 62 - Cd removal from the synthetic solution from 1 to 50 min for different Zn:Cd ratios.

According to Younesi et al (2006), the increase of Cd cementation in relation to time may be attributed to different mechanisms that control the cementation. In their study, the effect of Cd concentration was investigated, using a Zn:Cd ratio of 5:1 and zinc powder with a particle size -170 + 325#. The authors reported that different kinetic models might describe the cementation process, depending on the Cd concentration. For example, the ash diffusion model was suitable for Cd concentration higher than 1000mg.L^{-1}. Concentrations between 500mg.L^{-1} and 1000mg.L^{-1} presented a mixed kinetic mechanism of the reaction while at concentrations below 500mg.L^{-1}, the data adjustment was best for film diffusion control. Thus, it is observed that the percentage extracted increases with time instead of decreasing.

SEM-EDS analysis was performed to investigate better and observe the differences between the initial material used for cementation, as well as the final process, Figure 63. For comparison to the cementation tests, the analysis of the Zn powder revealed a spherical shape with a size of approximately 20µm, in Figure 63a).

Figure 63a) to f) show the difference in the zinc powder structure when increasing the Zn:Cd ratio. The appearance of spicules is observed as cadmium is cemented. Spicules begin to emerge in the lower Zn:Cd ratio (Figure 63b) and it becomes more evidenced as

the ratio increases.

A spot region image analysis was performed in the Zn:Cd ratio equal to 5:1, and the presence of Cd was observed in Figure 63c), in a concentration lower than the previous 2.5:1 ratio. The spheres mentioned in Figure 63a) were presented in a modified way in relation to Figures 67b) to f). The spicules mentioned above end up forming a cluster of this material, and in this same cluster, the Cd and Zn were identified. So, it represents Cd cementation. A particle was found in the 10:1 Zn:Cd ratio in a spot region image, represented as 79% Cd, in Figure 63d). The same particle has a different shape than the surrounding material, and the spheres that were showed previously changed their shape, forming clusters. Figure 63e) refers to the 50:1 Zn:Cd ratio, which obtained cementation in the synthetic solution of 75% in 20min. Due to the increase in the mass of Zn powder, the tendency was to increase the removal of Cd. In images by SEM-EDS, a spot region image identified Cd and Mg. The surrounding material it was again changed its shapes and lighter also, agglomerates with different spike and sphere shapes.

The Zn:Cd ratio with the best condition for cementation was shown in Figure 63f). It was observed that the material formed a spherical agglomerate and the other part of the material is represented as a smooth aspect, representing most of the material, therefore, zinc after cementation. That was the sample that contained the largest mass of Zn powder. In the EDS, Zn and Cd were analyzed with a mass concentration equal to 75 and 17%, respectively. Even with, Cd was cemented as shown in the spot region image by SEM.

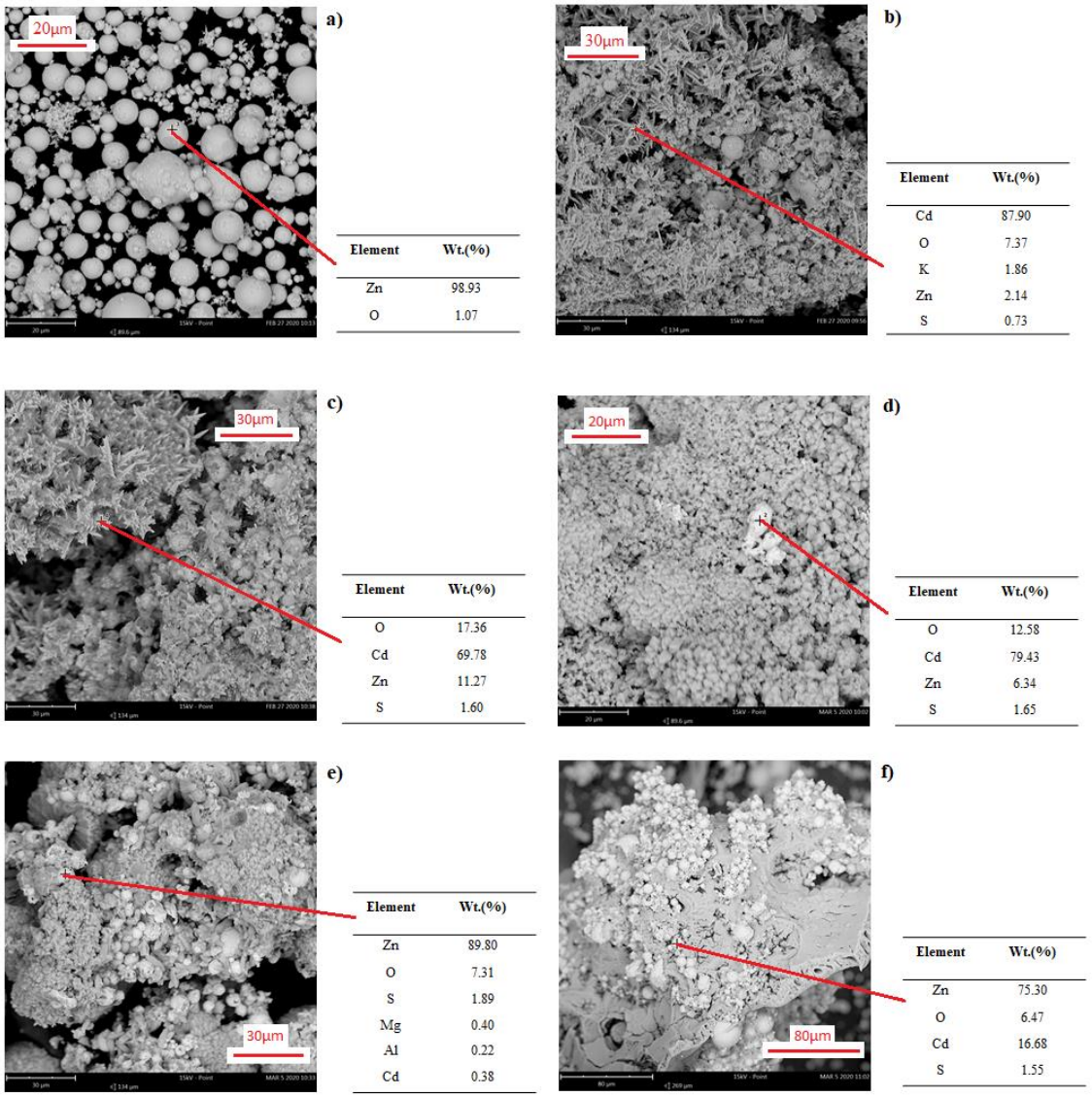

Figure 63 - Backscattered electron (BSE) spots images obtained in the scanning electron microscope with a composition of the sample, obtained by EDS of the interaction of zinc powder with cadmium in the cementation step. (a) Zinc powder before cementation; Cementation in 20min at 25°C with a (b) Zn:Cd ratio of 2.5:1; (c) Zn:Cd ratio of 5:1; (d) Zn:Cd ratio of 10:1; (e) Zn:Cd ratio of 50:1; (f) Zn:Cd ratio of 100:1.

Despite the EDS semi-quantitative analysis indicated higher Cd wt% in lower Zn:Cd ratio, this occurs merely because of the lower mass of Zn used in those conditions. Comparing Figure 63b) and Figure 63f), the amount of Zn is 40 times higher in Figure 63f). Hence a higher wt% of Zn was detected by the EDS analysis. The EDS of each spot in the image in Figure 67 is included in Appendix 5.

5.5.1.2 Cementation using leaching liquor

The tests with the leaching liquor (leaching conditions: 1.2mol.L^{-1} H_2SO_4 at 50°C in 35min) were performed and the effect of Zn:Cd ratio and time were evaluated.

The cementation tests with the leaching liquor are shown in Figure 64. The percentage of Cd removal was studied according to the Zn: Cd ratio as a function of time using room temperature (25°C).

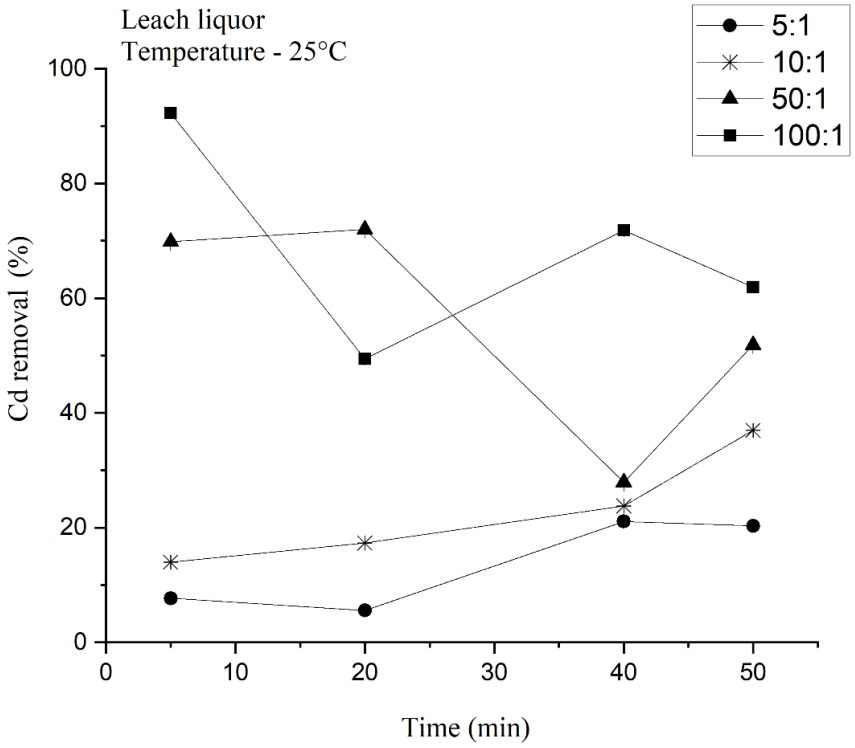

Figure 64 - Cadmium removal in the function of time with the leach liquor generated at 50°C with 1.2mol.L^{-1} in 35min.

In Figure 64, the behavior of Cd removal in cementation was efficient in times shorter than that of the synthetic solution. Mainly, in the Zn:Cd ratio of 100:1 being the closest to remove 100% Cd. The Zn:Cd ratio 5:1 and 10:1 were up to 40min, and had a 20% Cd removal., and in 50min only the 10:1 ratio obtained a removal close to 40%. It was aiming to use the least Zn powder. These two options were shown insufficient to remove Cd in the liquor. It was also observed that Zn:Cd ratios that were equal to 50:1 and 100:1 presented a removal of 70% and above 90%, respectively, in 5min. As time increased, there was a decrease in Cd removal for both ratios. The difference in the behavior between the synthetic solution and the leaching liquor may be due to the

presence of Fe (E_0 = -0.44V, SHE) or even other elements present in the liquor that may undergo an electrochemical reduction on Zn particles along with Cd (Havlik, 2001).

The analysis of Mg in the liquor was also carried out during the cementation to evaluate if there was a loss of Mg during the technique. Thus, in Figure 65, the results of Mg removal during the cementation are presented. The cementation of Mg close to zero was already expected due to the standard reduction potential of Mg (E_0 = -2.37V) being less than that of zinc (E_0 = -0.76V). Thus, it tends to remain in the oxidized state.

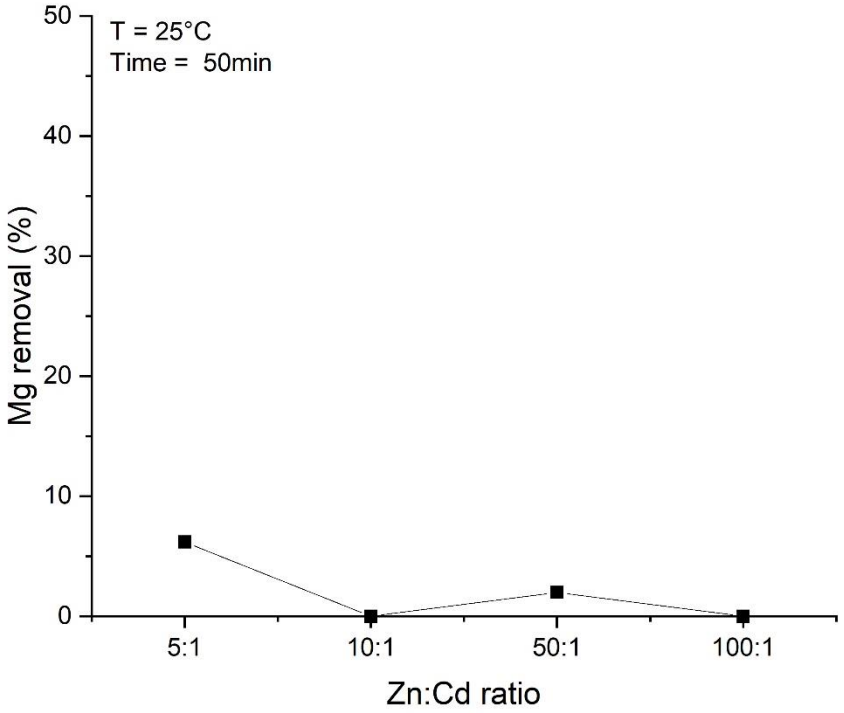

Figure 65 – Magnesium removal during cementation, after 50min, for different Zn:Cd ratios

In the case of a material with a concentration of Cd, which is less than or equal to 400mg.L^{-1}, the estimative of the amount of Zn required for Cd removal may be calculated as described in Table 23. Based on the Brazilian legislation, Cd limits are given in mg/kg. Therefore, the Cd concentration was calculated in reference to the total solid obtained from 81% of the crystallized $MgSO_4 \cdot 7H_2O$ and 100% of the crystallized $CdSO_4 \cdot H_2O$ after the cementation step, allowing for comparison of the values provided in Table 8 (item 2.6) with the values in Table 23. Considering that a 92% Cd removal may be obtained, each 1L of liquor would require 23g of Zn powder, the solution after cementation would reach 50mg/kg of Cd in a Zn:Cd ratio of 100:1 in 5min. Then, these

values of Cd must be used 40% of the byproduct obtained which achieves values within the legislation for the use of solid magnesium sulfate as a fertilizer, which the limits of the Brazilian legislation are describes in Table 8 (Annex II) for CONAMA and Table 9 for CETESB.

Table 23 – List of the best cementation conditions (Zn:Cd ratio and time) with the leach liquor with Zn powder in grams for each 1L of the solution and the removal of Cd (%) with values in $mg.kg^{-1}$.

Zn:Cd	Time (min)	Zinc used in grams for 1L	Cd in mg/kg	Cd removal (%)
100: 1	5	23g	50	92
50:1	20	11.6g	200	72
10:1	50	2.32g	400	37

5.5.2 Sulfide precipitation

A method for comparison with the cementation technique was sulfide precipitation, evaluating which one removed a higher percentage of Cd in the leaching liquor solution.

According to a study by Ennaassia et al., (2002), Cd^{2+} was precipitated using a Na_2S solution of 0.1 and $1mol.L^{-1}$. It was concluded that the precipitation of CdS decreases while the concentration of H_3PO_4 and H_2SO_4 increases, but it also occurs when there is an increase in temperature, and the CdS decreases. As more Na_2S solution was added in the medium, the percentage of Cd removal was increased. The reaction that describes the formation of the precipitate is presented as follows in Equation 21. Even with the excess of S^{2-} ions from the addition of Na_2S in an acidic medium with H_3PO_4 or H_2SO_4, the kinetics to form CdS can last up to 1h due to the formation of CdS colloids, interrupting the precipitation of the metal as a sulfide (Ennaassia et al., 2002; Lewis, 2010).

$$Cd^{2+} + S^{2-} \Leftrightarrow CdS_{(s)} \qquad \text{Equation 21}$$

Firstly, a speciation diagram was constructed with Hydra-Medusa software's aid, to investigate the sulfide precipitation, Figure 66.

The diagram was constructed considering the concentrations of Mg and Cd of the leaching liquor, being $9.6g.L^{-1}$ and $0.4g.L^{-1}$, respectively. Then, the formed species and their relationship with the pH could be estimated. In Figure 66, $CdS_{(s)}$ was shown to be precipitated at a range of pH from -1 to 5 while the decrease of $CdSO_4$ was shown to be

from pH -1 to 2, at a concentration equals to $1x10^{-5}$ to $1x10^{-9}$mol.L^{-1}.

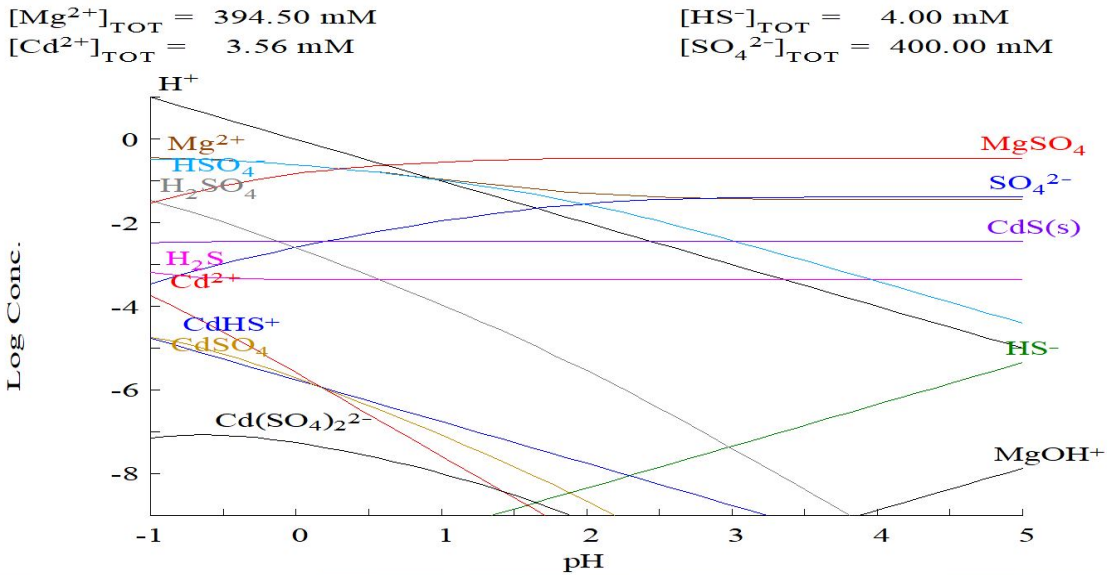

Figure 66 – Speciation diagram for magnesium and cadmium, obtained in the leach liquor using H_2S for the precipitation of CdS.

The tests were performed with a 1.0mol.L^{-1} Na_2S solution using the leaching liquor. The precipitation of Cd and Mg are shown in Figure 67. The solution medium was 1.2mol.L^{-1} of sulfuric acid, and the tests were performed at room temperature. The Cd showed a maximum removal of 22.6% at pH 2.5, and in this same condition, there was also precipitation of Mg equals to 4%.

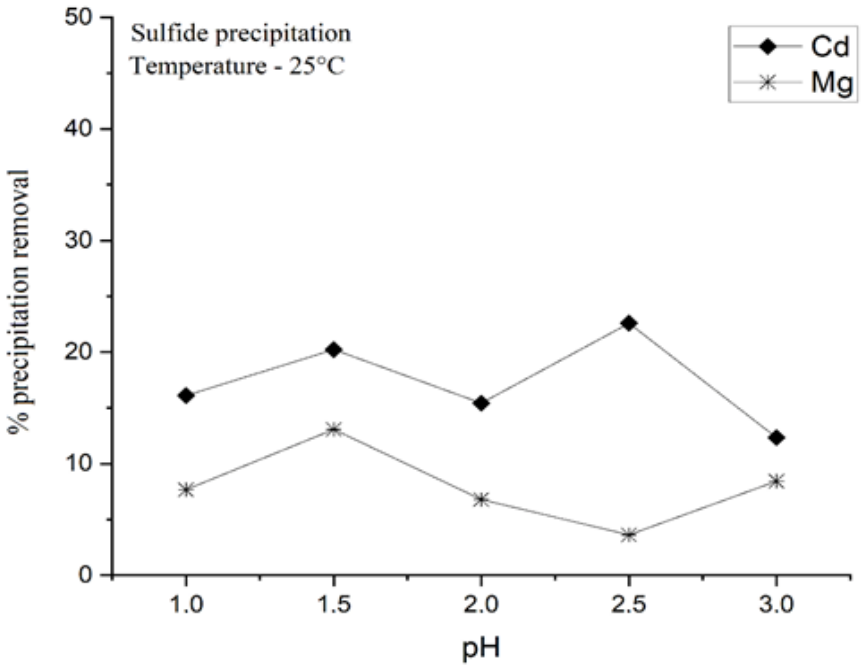

Figure 67 – Sulfide precipitation of magnesium and cadmium in the leaching liquor, using Na_2S 1mol.L^{-1} at room temperature.

Comparing the cementation tests that achieved a 92% Cd removal in the 100:1 ratio in 5min, the technique that reached the value below the limit suggested by CONAMA in Table 8 (Annex II) using 40% of the fertilizer as a byproduct. On the other hand, the sulfide precipitation showed that, at pH 2.5, 22.6% of Cd removal was achieved. The limits of Cd in the Brazilian legislation are given in mg/kg. Therefore, the Cd concentration was calculated (theoretical) in reference to the total solid obtained from 81% of the crystallized $MgSO_4 \cdot 7H_2O$ and 100% of the crystallized $CdSO_4 \cdot H_2O$ after the sulfide precipitation step; the final Cd reaches a content of $300mg.kg^{-1}$ – above allowed in Table 8 and 9 (item 2.6) which can be used with 6.5% as a fertilizer byproduct.

5.5.3 Density separation

Density separation was the technique to perform the non-leached fraction tests to eliminate the Pb in the sample. In this method, it is essential to assess whether the material to be eliminated, the Pb, presented with the release particle size, as well as the difference in density of the materials (Inácio et al., 2010; Sampaio et al., 2007). The non-leached fraction, which contains mainly $CaSO_4$ is characterized by a density lower than that of $PbSO_4$, which is the element of interest to be eliminated, being $2.31\text{-}2.33g.cm^{-3}$ and $6.29g.cm^{-3}$, respectively (Lide, 1996).

As shown in Figure 68, two fractions were obtained. The sunk material, with higher density, was represented with 2% of Pb. In the floated material, less dense, the Pb content was 98%. There was a greater concentration of Pb than 0.20%, it became 0.21%, which represents $2100mg.kg^{-1}$ of Pb - there was a concentration of the material, with the removal of the iron instead of the lead in the sunk fraction.

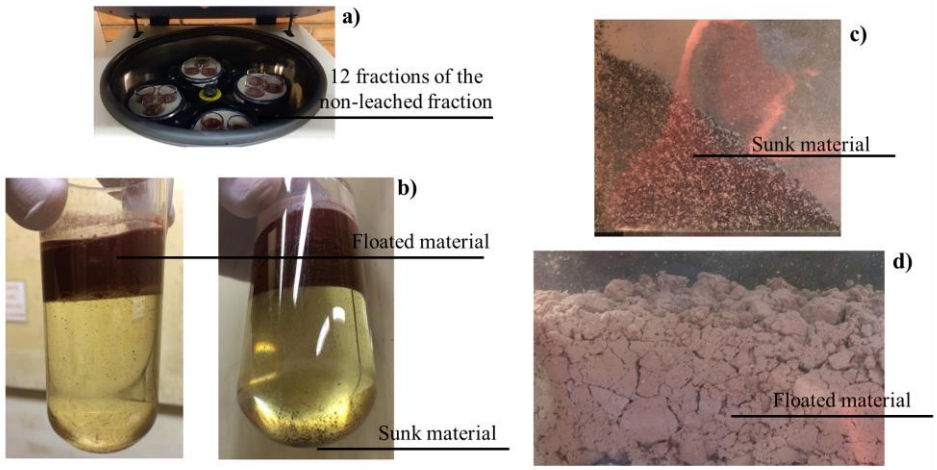

Figure 68 - Density separation test of the non-leached fraction to remove lead. (a) Fractions divided for the centrifuge; (b) Products separated by the density difference; (c) Denser product – sunk material; (d) Less dense product - floated material.

The gypsum may be used in the fabrication of the cement along with the clinker. In this clinker, usually, 5% gypsum is added to obtain the mortar product (Gesoglu et al., 2016; Nouairi et al., 2018). The types of Portland cement which has gypsum in their composition are varied, such as Common Portland Cement (CP I); Compound (CP II); Blast Furnace (CP III); Pozzolanic (CP IV); High Initial Resistance (CP V-ARI); Sulfate Resistant (RS) and Low Heat Hydration (BC), (ABNT, 2018).

In a study carried out by Nouairi et al., (2018), a mining tailing containing Pb was evaluated to be immobilized in the final mortar. The immobilization reached 70-75% of Pb. The immobilization was achieved following the acceptance standards for waste in landfills, regarding Law n° 12,305 according to NBR 10004. Considering the gypsum obtained in the non-leached fraction being added to the mortar with the immobilization, the content of Pb in 5% of the material is equivalent to 100mg.kg^{-1}, and with the Pb immobilization of 70-75% the concentration is 26mg.kg^{-1}, but following NBR 10004, the solubilization with immobilization of 75% did not achieve the limits allowed of 0.01mg.L^{-1} Pb (Nouairi et al., 2018).

Meurer et al., (2019) applied a reused water from sewage treatment plants in the manufacture of hollow concrete blocks for sealing masonry using Portland cement. It was demonstrated the possibility to apply a material containing elements such as Zn and Pb, in which some criteria such as setting time and compressive strength for kneading concrete is followed by NBR 15900-1 (ABNT, 2008).

Thus, for each application and specific characteristics, such as consistency,

plasticity, water retention and mechanical resistance, specific testing standards and minimum requirements must be investigated. These specifications for each type of cement can determine the maximum concentration of Pb present in the composition. In cement, the Pb may interfere in the concrete's hydration, causing a delay in the material hardness (ABNT, 2018; Carpio, 2005).

Considering the uses of concrete (such as foundations and pavements) during its useful life, as well as in its disposal and final destination, Pb leaching or eventual solubilization must be investigated through NBR 10004 (ABNT, 2018; Carpio, 2005; Guedes et al., 2014; Psomopoulos and Themelis, 2016; Vaillant, 2013). According to Carpio, (2005); Mantus, (1992); Tanna and Schipholt, (2003), the accepted levels for Pb in cement is 5,000mg.L^{-1}. Based on that, the 5% of Pb added as gypsum in the cement manufacture, the accepted limits, which is 100mg.L^{-1} Pb is allowed.

A study that evaluated a CP II showed 2.72% Pb in the total composition due to the substitution of primary fuels for alternatives ones during the Portland cement manufacturing process (Guedes et al., 2014). According to Psomopoulos and Themelis, (2016), the cement clinker production can be replaced by alternative fuels, whether solid or liquid. Those with solid characteristics are agricultural biomass residues, non-agricultural biomass residues, petroleum residues, chemical and hazardous residues. Therefore, it is essential to know the material and, preferably, to have a similar property in the substitution, e.g. the gypsum contaminated with Pb as a substitute for common gypsum. For each alternative there is an adaptation of the process using this replacement. Hence, the importance of determining which material will be used as a cement to carry out specific tests in the Portland cement manufacturing process.

Even if the density separation method did not obtain enough Pb removal to use the material according to Table 8 (item 2.6), in the same Table in Annex V, gypsum can be used in a diluted form as another alternative. The maximum limit of Pb is 150mg.kg^{-1}; therefore, using 7.5% of the gypsum obtained in 1kg, the limit of Pb would be within the legislation as a soil conditioner.

5.6 GENERAL FLOWSHEET AND MASS BALANCE

From the leaching tests, a characterization for a mass balance was carried out with the best conditions of the physical processing in the non-magnetic fraction, the leaching

assays with a concentration of 1.2mol.L^{-1} H_2SO_4 carried out at 50°C in 35min.

In Figure 69, an input of 100g of Zn tailing material from the non-magnetic fraction (*rougher cleaner* route), which contains 11.9wt.% Mg was presented. In each step, the amount of magnesium in grams of mass and the percentage of each fraction (non-leached fraction, leach liquor and mass loss) are shown. In the leaching of magnesium was observed a mass loss of 15%. There was also a portion of the material, that was not leached, found in the non-leached fraction, being represented by 16% of the initial material, and the Mg extraction was 68.5%.

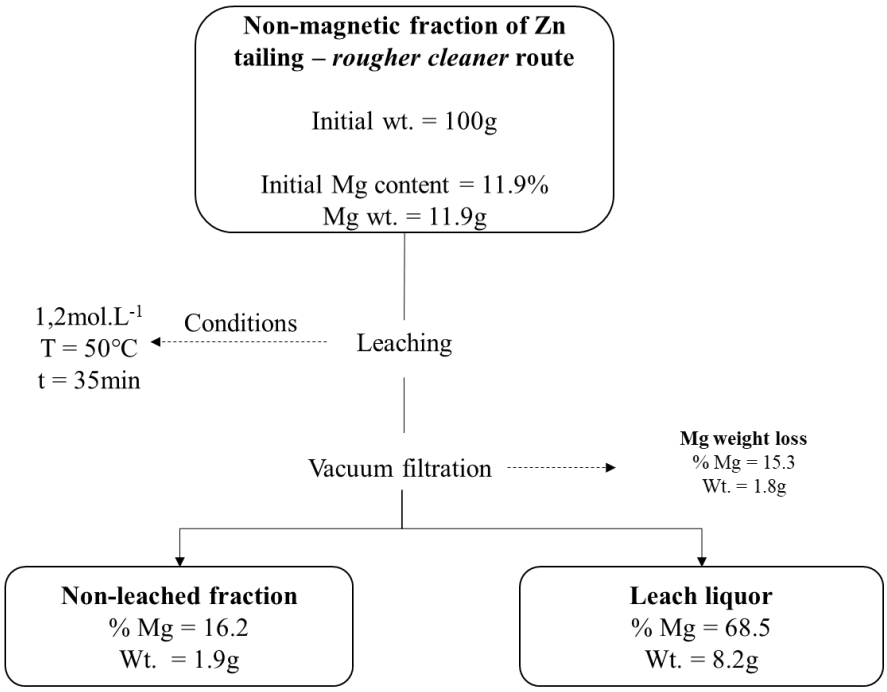

Figure 69 - Mass balance of magnesium in leaching under conditions of 1.2mol.L^{-1} at 50°C and 35min.

In Figure 70, a flowsheet of the mass balance of the elements present in the tailing was carried out, with a material input equal to 100ton. The steps were from the Zn tailing characterization, physical processing conditions (*rougher cleaner*), and the hydrometallurgical route (leaching and cementation). Finally, the values of the products obtained at the end of each mass process of $CaSO_4$ and $MgSO_4 \cdot 7H_2O$. The mass balance was related to each step's characterization, and after leaching to the leach liquor and the non-leached fraction.

The $MgSO_4 \cdot 7H_2O$ product was calculated based on the possible crystallization of leach liquor, considering that, according to the literature, which $MgSO_4.7H_2O$ is crystallized in 5h at a temperature of 230°C and pH 5.7, obtaining an Mg crystallization

of 81% (Wanderley et al., 2020). Therefore, with the theoretical calculation of Mg leached and characterized in the liquor in which 81% of the material was crystallized as $MgSO_4 \cdot 7H_2O$, and the Cd would be crystallized in 100% as $CdSO_4 \cdot H_2O$ to obtain a theoretical value of the Cd present in the final material after the cementation according to the allowed limits.

Therefore, the mass of Mg after leaching (7.38ton) shown in Figure 70 was considered as hypothetical obtaining of crystallized $MgSO_4 \cdot 7H_2O$ equals to 60,6ton was calculated as a product. In the same product of $MgSO_4 \cdot 7H_2O$, the Cd removal was 92.3%. On the other hand, $CaSO_4$ obtained was 64ton with the presence of Pb equals to 0.21ton. Even with Pb in the $CaSO_4$ product, there is a possibility of being used in agriculture as a soil conditioner in lower concentrations.

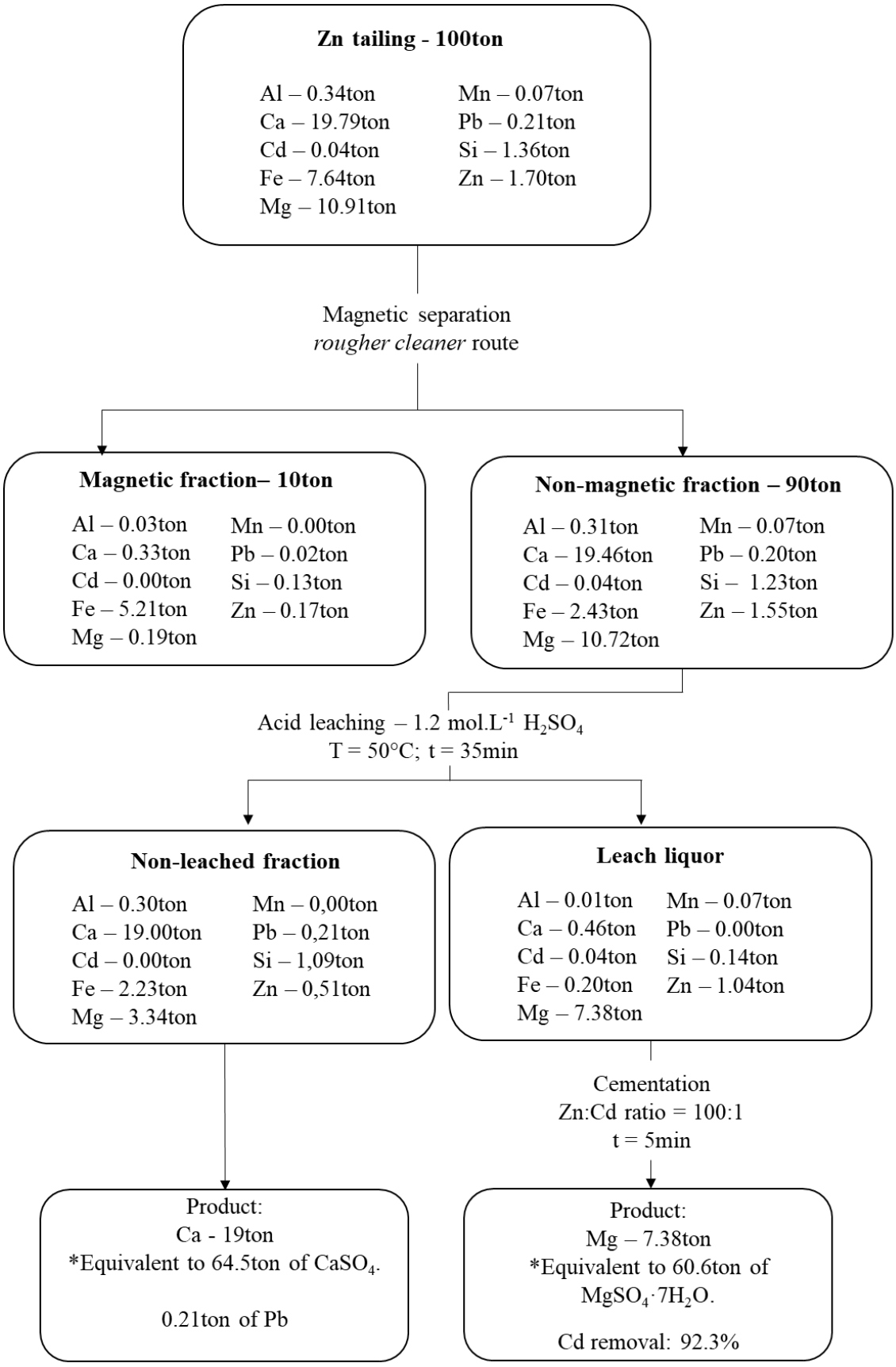

Figure 70 - Mass balance with 100ton of initial Zn tailing flotation characterized, physical processing steps, hydrometallurgical route (leaching and purification), and the byproducts obtained.

6 CONCLUSIONS

The results from the characterization of zinc ore flotation tailing showed a content of 81.7wt.% $CaMg(CO_3)_2$. In the physical processing, the magnetic separation with the *rougher cleaner* route was able to concentrate dolomite in the non-magnetic fraction up to a content of 90.3wt.% $CaMg(CO_3)_2$ obtained in the non-magnetic fraction (90%wt).

The non-magnetic fraction was submitted to a hydrometallurgical route. However, first, leaching simulations were performed to thermodynamic simulations, which indicated that the optimal parameters for Mg leaching was 1.2mol.L^{-1} H_2SO_4 and S:L ratio of 1:10 with no effect of the temperature. In thermodynamic simulations, a 100% Mg extraction was achieved.

Experimental leaching tests achieved up to 72% ± 5% Mg extraction and 2% Ca extraction using the following parameters: 1.2mol.L^{-1} H_2SO_4 and S:L of 1:10, 50°C and 35min. Such divergences are probably due to time-based (kinetics aspects) studies on leaching that were not evaluated in the thermodynamic simulations. Nevertheless, simulations showed to be a reliable basis for planning exploratory essays.

The different solubilities of $MgSO_4$ and $CaSO_4$ allowed the obtention of a soluble Mg-rich (9.6g.L^{-1}) liquor and a non-leached fraction with insoluble calcium sulfate dehydrate – gypsum. Both are potential candidates as byproducts, $MgSO_4$ as a secondary macronutrient for fertilizers and, $CaSO_4$ as gypsum for soil conditioner.

Lastly, the cementation step with zinc powder was able to remove 92% of the Cd that was found in the real leaching liquor, using a Zn:Cd ratio of 100:1 in 5min at 25°C. Thus, to respect the limits imposed by CONAMA (RESOLUTION N°. 420, OF DECEMBER 28, 2009) in Annex II, the byproduct of $MgSO_4 \cdot 7H_2O$ must be used in 40% which allows the limits of Cd as a secondary macronutrient for fertilizers, after crystallized, and the $CaSO_4$ must be used in 7.5% for each 1kg of total gypsum, which allows the limits of Pb, according to Annex V.

A mass balance was carried out, and after leaching two products were obtained – leach liquor and non-leached fraction. In the leach liquor, after cementation to eliminate Cd, the final product acquired was equivalent to 61ton of $MgSO_4 \cdot 7H_2O$. In the non-leached fraction, the final product as $CaSO_4$ achieved 64,5ton with the presence of Pb. The alternatives of the generated byproducts can be used in lower concentrations for agriculture.

REFERENCES

Abali, Y., Çopur, M., Yavuz, M., 2006. Determination of the optimum conditions for dissolution of magnesite with H2SO4 solutions. Indian J. Chem. Techonology 13, 391–397.

Abkhoshk, E., Jorjani, E., Al-Harahsheh, M.S., Rashchi, F., Naazeri, M., 2014. Review of the hydrometallurgical processing of non-sulfide zinc ores. Hydrometallurgy 149, 153–167. https://doi.org/10.1016/j.hydromet.2014.08.001

ABNT, 2018. NBR 16697, Portland cement - Requirements 12.

ABNT - Associação Brasileira de Normas Técnicas, 2008. Abnt Nbr 15900-1:2009. Água para amassamento do concreto Parte 1 Requisitos 237.

Andreas, F., 2012. Zinc from India – The protector of iron Historic steam boiler explosions 2012.

Apelblat, A., Korin, E., 2007. The vapour pressures over saturated aqueous solutions of cadmium chloride, cadmium bromide, cadmium iodide, cadmium nitrate, and cadmium sulphate. J. Chem. Thermodyn. 39, 1065–1070. https://doi.org/10.1016/j.jct.2006.12.010

Asadi, T., Azizi, A., Lee, J.C., Jahani, M., 2017. Leaching of zinc from a lead-zinc flotation tailing sample using ferric sulphate and sulfuric acid media. J. Environ. Chem. Eng. 5, 4769–4775. https://doi.org/10.1016/j.jece.2017.09.005

Aurivillius, K., 1980. A reinvestigation of the crystal structures of HgS04 and CdS04 129, 121–129.

Ayres, R.U., 1997. Metals recycling : economic and environmental implications. Resour. Conserv. Recycl. 21, 145–173. https://doi.org/10.1016/S0921-3449(97)00033-5

Bale, C.W., Bélisle, E., Chartrand, P., Decterov, S.A., Eriksson, G., Gheribi, A.E., Hack, K., Jung, I., Kang, Y., Melançon, J., Pelton, A.D., Petersen, S., Robelin, C., Sangster, J., Spencer, P., Ende, M. Van, 2016. CALPHAD : Computer Coupling of Phase Diagrams and Thermochemistry FactSage thermochemical software and databases , 2010 – 2016. Calphad 54, 35–53. https://doi.org/10.1016/j.calphad.2016.05.002

Bale, C.W., Bélisle, E., Chartrand, P., Decterov, S.A., Eriksson, G., Hack, K., Jung, I., Kang, Y., 2009. CALPHAD : Computer Coupling of Phase Diagrams and Thermochemistry FactSage thermochemical software and databases — recent developments. CALPHAD Comput. Coupling Phase Diagrams\penalty \z@ \protect \futurelet \@let@token Thermochem. 33, 295–311. https://doi.org/10.1016/j.calphad.2008.09.009

Bechir, J.L.C., 2019. Avaliação do impacto da granulometria e da liberação na flotação do minério de zinco da mina de Vazante. Dissertação (Mestrado em Engenharia de Minas) - Escola Politécnica, Universidade de São Paulo, São Paulo, 2019.

Bechir, J.L.C., Baptista, J.R., Souza, A.D. de;, Martins, E., 2019. Determination of maximum zinc recovery of Vazante mine ore by flotation process. REM - Int. Eng. J. 72, 315–320. https://doi.org/10.1590/0370-44672018720069

Beckhoff, B., Kanngießer, B., Langhoff, N., Wedell, R., Wolff, H., 2006. Handbook of Practical X-Ray Fluorescence Analysis. Springer Berlin Heidelberg. https://doi.org/10.1007/978-3-540-36722-2

Boni, M., Rudolf, P., Rudolph, J., Wet, D., Daniel, J., Balassone, G., Mondillo, N., 2009. Mineralogical signature of nonsulfide zinc ores at Accha (Peru): A key for recovery. Int. J. Miner. Process. 93, 267–277. https://doi.org/10.1016/j.minpro.2009.10.003

Bulatovic, S.M., 2007. Handbook of Flotation Reagents: Chemistry, Theory and Practice Flotation of Sulfide Ores, Handbook of Flotation Reagents: Chemistry, Theory and Practice Flotation of Sulfide Ores. https://doi.org/10.1016/B978-0-444-53029-5.X5009-6

Carpio, R.C., 2005. Otimização no Co-processamento de Resíduos na Indústria do Cimento Envolvendo Custos, Qualidade e Impacto Ambiental. Tese (Doutorado em Engenharia Mecânica) - Instituto de Engenharia Mecânica, Universidade Federal de Itajubá, Itajubá, 2005.

CHAVES, A. P. Teoria e Prática do Tratamento de Minérios, 3ª Edição. A Flotação no Brasil, São Paulo, v. 4, 2013. p. 10-12.

Cesareo, R., 2010. X-Ray Fluorescence Spectrometry. Ullmann's Encycl. Ind. Chem. https://doi.org/10.1002/14356007.b05 675

CETESB, C.A. do E. de S.P., 2016. Valores Orientadores para solo e água subterrânea no Estado de São Paulo 2016. Decisão Dir. Nº 256/2016/E, 22 Novembro 2016 1–3.

Chen, T., Yan, Z.A., Xu, D., Wang, M., Huang, J., Yan, B., Xiao, X., Ning, X., 2020. Current situation and forecast of environmental risks of a typical lead-zinc sulfide tailings impoundment based on its geochemical characteristics. J. Environ. Sci. (China) 93, 120–128. https://doi.org/10.1016/j.jes.2020.03.010

Chojnacka, K., Gorazda, K., Witek-Krowiak, A., Moustakas, K., 2019. Recovery of fertilizer nutrients from materials - Contradictions, mistakes and future trends. Renew. Sustain. Energy Rev. 110, 485–498. https://doi.org/10.1016/j.rser.2019.04.063

Comission, E., 2017. Study on the review of the list of Critical Raw Materials: Executive Sumary. Eur. Com.

CONAMA, 2013. Resolução nº 460, de 30 de dezembro de 2013 2009, 2013.

CONAMA, 2009. Resolução Nº 420, De 28 De Dezembro De 2009. Diário Of. da União nº 249 2013, 81–84. https://doi.org/10.1017/CBO9781107415324.004

Craddock, P.T., 2000. The Early History of zinc 183–191. https://doi.org/10.1016/0160-9327(87)90282-1

Czerwinski, F., 2011. Magnesium Alloys - Design, Processing and Properties. https://doi.org/10.5772/560

Dalas, E., Kallitsis, J., Sakkopoulos, S., Vitoratos, E., Koutsoukos, P.G., 1991. Cadmium sulfide precipitation in aqueous media: Spontaneous precipitation and controlled overgrowth on polyaniline. J. Colloid Interface Sci. 141, 137–145.

https://doi.org/10.1016/0021-9797(91)90309-V

D'Ans, J., 1933. Aqueous salt systems of phase theoretical interest. Am. Chem. Soc. 491-493.

Darmanto, P.S., Amalia, A., 2020. Analysis of high clinker ratio of Portland Composite Cement (PCC). South African J. Chem. Eng. 34, 116–126. https://doi.org/10.1016/j.sajce.2020.07.010

Davris, P., Balomenos, E., Panias, D., Paspaliaris, I., 2016. Selective leaching of rare earth elements from bauxite residue (red mud), using a functionalized hydrophobic ionic liquid. Hydrometallurgy 164, 125–135. https://doi.org/10.1016/j.hydromet.2016.06.012

DOU, 2016. Diário Oficial da União. Diário Of. da União nº 82 Seção 1, 2018.

Driessche, A.E.S. Van, Stawski, T.M., Kellermeier, M., 2019. Calcium sulfate precipitation pathways in natural and engineered environments. Chem. Geol. 530, 119274. https://doi.org/10.1016/j.chemgeo.2019.119274

Duarte, H., 2019. Ferro – Um Elemento Químico Estratégico Que Permeia História, Economia E Sociedade. Quim. Nova 42, 1146–1153. https://doi.org/10.21577/0100-4042.20170443

Dubiński, J., 2013. Sustainable Development of Mining Mineral Resources. J. Sustain. Min. 12, 1–6. https://doi.org/10.7424/jsm130102

Dudka, S., Adriano, D.C., 1997. Environmental Impacts of Metal Ore Mining and Processing: A Review. J. Environ. Qual. 26, 590. https://doi.org/10.2134/jeq1997.00472425002600030003x

Dutrizac, J.E., 2002. Calcium sulphate solubilities in simulated zinc processing solutions. Hydrometallurgy 65, 109–135. https://doi.org/10.1016/S0304-386X(02)00082-8

Edraki, M., Baumgartl, T., Manlapig, E., Bradshaw, D., Franks, D.M., Moran, C.J., 2014. Designing mine tailings for better environmental , social and economic outcomes : a review of alternative approaches. J. Clean. Prod. 84, 411–420. https://doi.org/10.1016/j.jclepro.2014.04.079

Ejtemaei, M., Gharabaghi, M., Irannajad, M., 2014. A review of zinc oxide mineral beneficiation using flotation method. Adv. Colloid Interface Sci. 206, 68–78. https://doi.org/10.1016/j.cis.2013.02.003

Ennaassia, E., El Kacemi, K., Kossir, A., Cote, G., 2002. Study of the removal of Cd(II) from phosphoric acid solutions by precipitation of CdS with Na2S. Hydrometallurgy 64, 101–109. https://doi.org/10.1016/S0304-386X(02)00009-9

Erdem, M., Özverdi, A., 2011. Environmental risk assessment and stabilization/solidification of zinc extraction residue: II. Stabilization/solidification. Hydrometallurgy 105, 270–276. https://doi.org/10.1016/j.hydromet.2010.10.014

European Commision, 2014. Critical Raw Materials for the EU: Report of the Ad Hoc Working Group on Defining Critical Raw Materials. European Commission: Enterprise and Industry.

Faure, A., Coudray, C., Anger, B., Moulin, I., Colina, H., Izoret, L., Théry, F., Smith,

A., 2019. Beneficial reuse of dam fine sediments as clinker raw material. Constr. Build. Mater. 218, 365–384. https://doi.org/10.1016/j.conbuildmat.2019.05.047

Freyer, D., Voigt, W., 2003. Crystallization and Phase Stability of CaSO4 and CaSO 4 - Based Salts. Monatshefte fur Chemie 134, 693–719. https://doi.org/10.1007/s00706-003-0590-3

Friedrich, H.E., Mordike, B.L., 2006. Magnesium technology: Metallurgy, design data, applications, Magnesium Technology: Metallurgy, Design Data, Applications. https://doi.org/10.1007/3-540-30812-1

Gesoglu, M., Güneyisi, E., Nahhab, A.H., Yazıcı, H., 2016. The effect of aggregates with high gypsum content on the performance of ultra-high strength concretes and Portland cement mortars. Constr. Build. Mater. 110, 346–354. https://doi.org/10.1016/j.conbuildmat.2016.02.045

Guedes, O.A., Couto, G.S., Costa, M.V.C., Oliveira, H.F., Silva, J.A., Decurcio, D.A., Borges, Á.H., 2014. Análise da presença de metais pesados nos cimentos Portland e à base de MTA por meio da espectroscopia de dispersão de raios-X Analysis of heavy metals contents in Portland and MTA-based cements using energy-dispersive X-ray analyses. Robrac 23, 176–180.

Gupta, C.K., 2003. Chemical Metallurgy: Principles and Practice. Wiley-VCH; 1° ed. 831p. doi:10.1002/3527602003

Halikia, I., Voudouris, N., 2005. Investigation of zinc dissolution and cadmium precipitation rates in a Cd2+/Zn cementation system. Trans. Institutions Min. Metall. Sect. C Miner. Process. Extr. Metall. 114, 95–108. https://doi.org/10.1179/037195505X49732

Hansen, H.K., Yianatos, J.B., Ottosen, L.M., 2005. Speciation and leachability of copper in mine tailings from porphyry copper mining : Influence of particle size 60, 1497–1503. https://doi.org/10.1016/j.chemosphere.2005.01.086

Hansen, S., Sadeghian, P., 2020. Recycled gypsum powder from waste drywalls combined with fl y ash for partial cement replacement in concrete. J. Clean. Prod. 274, 122785. https://doi.org/10.1016/j.jclepro.2020.122785

Härdter, R., Rex, M., Orlovius, K., 2004. Effects of different Mg fertilizer sources on the magnesium availability in soils 249–259.

Havlik, T., 2001. Hydrometallurgy, Hydrometallurgy. https://doi.org/10.1016/S0304-386X(01)00178-5

Horst, Friedrich E.; Mordike, B.L., 2006. Magnesium Technology - Metallurgy, Design Data,Applications.

Inácio, L., Antonio, L., Elias, R., 2010. Tratamento de Minérios, 5ª Edição. ed. Centro de Tecnologia Mineral (CETEM). Rio de Janeiro.

Jackson, E., 1986. Hydrometallurgical Extraction And Reclamation. 266p.

Jha, M.K., Kumar, V., Singh, R.J., 2001. Review of hydrometallurgical recovery of zinc from industrial wastes. Resour. Conserv. Recycl. 33, 1–22. https://doi.org/10.1016/S0921-3449(00)00095-1

Jones, J.B.J., 2012. Plant Nutrition and soil fertility manual. CRC Press, 2ª ed. 306p.

Junca, E., 2009. Estudo da separação e aproveitamento da parte metálica e dos óxidos presentes no resíduo gerado no corte de rochas ornamentais 88. Dissertação (Mestrado em Engenharia Metalúrgica e de Materiais) - Escola Politécnica, Universidade de São Paulo, São Paulo, 2009.

Karidakis, T., 2005. Removal of magnesium from nickel laterite leach liquors by chemical precipitation using calcium hydroxide and the potential use of the precipitate as a filler material 76, 105–114. https://doi.org/10.1016/j.hydromet.2004.09.007

Kay, H., 1969. Treatment of Nickelliferous Oxidic Materials for the Recovery of Nickel Values.

Klein, C., Mizusaki, A.M.P., 2007. Cimentação Carbonática em Reservatórios Siliciclásticos - O Papel da Dolomita -. Pesqui. em Geociências 34, 91. https://doi.org/10.22456/1807-9806.19465

Ku, Y., Wu, M.H., Shen, Y.S., 2002. A study on the cadmium removal from aqueous solutions by zinc cementation. Sep. Sci. Technol. 37, 571–590. https://doi.org/10.1081/SS-120001448

Kukurugya, F., Rahfeld, A., Möckel, R., Nielsen, P., Horckmans, L., Spooren, J., Broos, K., 2018. Recovery of iron and lead from a secondary lead smelter matte by magnetic separation. Miner. Eng. 122, 17–25. https://doi.org/10.1016/j.mineng.2018.03.030

Lei, C., Yan, B., Chen, T., Quan, S.X., Xiao, X.M., 2015. Comprehensive utilization of lead-zinc tailings, part 1: Pollution characteristics and resource recovery of sulfur. J. Environ. Chem. Eng. 3, 862–869. https://doi.org/10.1016/j.jece.2015.03.015

Lew, K., 2008. Understanding the elements of the periodic table: Zinc. Rosen Central, 48p.

Lewis, A.E., 2010. Review of metal sulphide precipitation. Hydrometallurgy 104, 222–234. https://doi.org/10.1016/j.hydromet.2010.06.010

Li, C., Wen, Q., Hong, M., Liang, Z., Zhuang, Z., Yu, Y., 2017. Heavy metals leaching in bricks made from lead and zinc mine tailings with varied chemical components. Constr. Build. Mater. 134, 443–451. https://doi.org/10.1016/j.conbuildmat.2016.12.076

Lide, D.R., 1996. CRC Handbook of Chemistry and Physics, 76th edition. Occup. Environ. Med. 53, 504–504. https://doi.org/10.1136/oem.53.7.504

Liu, T., Tang, Y., Han, L., Song, J., Luo, Z., Lu, A., 2017. Recycling of harmful waste lead-zinc mine tailings and fly ash for preparation of inorganic porous ceramics. Ceram. Int. 43, 4910–4918. https://doi.org/10.1016/j.ceramint.2016.12.142

Lopes, A.S., 1998. Manual Internacional de Fertilidade do Solo. Associação Brasileira para Pesquisa da Potassa e do Fosfato.

Lottermoser, B.G., 2007. Mine Wastes - Characterization, Treatment, Environmental Impacts. https://doi.org/10.1007/978-3-642-12419-8

Luo, Z., Yang, J., Ma, H., Liu, M., Ma, X., 2015. Recovery of magnesium and

potassium from biotite by sulfuric acid leaching and alkali precipitation with ammonia. Hydrometallurgy 157, 188–193. https://doi.org/10.1016/j.hydromet.2015.08.018

M.J., M., Rosemary, F., Carl, B., Samson Oluwasey, B., 2016. Statistical analysis and concentration of iron ore using Longi LGS 500 WHIMS. Int. J. Min. Sci. Technol. https://doi.org/10.1016/j.ijmst.2016.05.052

Magalhães Baltar, C.A., 1980. Flotação de minérios oxidados de zinco - Uma revisão da literatura. Ministério das Minas e Energ. - Cent. Tecnol. Miner. - CETEM 1–27.

Mantus, E. K., (1992). All Fired Up – Burning Hazardous Waste in Cement Kilns. Environmental Toxicology International, Washington, USA.

Marabini, A.M., Plescia, P., Maccari, D., Burragato, F., Pelino, M., 1998. New materials from industrial and mining wastes : glass-ceramics and glass- and rock-wool fibre 53, 121–134.

Mathieux, F. (European C., Nuss, P. (Federal E.A.G., Bobba, S. (Politecnico di T., 2017. Critical raw materials and the circular economy. https://doi.org/10.2760/378123

Meurer, A.P., Amorim, R.A., Quintanilha, L.C., Parente, D.C., 2019. Effluent reuse in the manufacture of concrete blocks for sealing masonry. ALCONPAT 9, 215–227. https://doi.org/doi.org/10.21041/ra.v9i2.278

Mineral Resources Program, 2011. Zinc — The Key to Preventing Corrosion. U.S. Geological Survey, 2p.

Monteiro, N.B.R., da Silva, E.A., Moita Neto, J.M., 2019. Sustainable development goals in mining. J. Clean. Prod. 228, 509–520. https://doi.org/10.1016/j.jclepro.2019.04.332

Moradi, S, Monhemius, A.J., 2011. Mixed sulphide – oxide lead and zinc ores : Problems and solutions. Miner. Eng. 24, 1062–1076. https://doi.org/10.1016/j.mineng.2011.05.014

Moradi, S., Monhemius, A.J., 2011. Mixed sulphide-oxide lead and zinc ores: Problems and solutions. Miner. Eng. 24, 1062–1076. https://doi.org/10.1016/j.mineng.2011.05.014

Mordike, B.L., Ebert, T., 2001. Magnesium Properties - applications - potential. Mater. Sci. Eng. A 302, 37–45. https://doi.org/10.1016/S0921-5093(00)01351-4

Nouairi, J., Hajjaji, W., Costa, C.S., Senff, L., Patinha, C., Ferreira da Silva, E., Labrincha, J.A., Rocha, F., Medhioub, M., 2018. Study of Zn-Pb ore tailings and their potential in cement technology. J. African Earth Sci. 139, 165–172. https://doi.org/10.1016/j.jafrearsci.2017.11.004

Önal, G., Bulut, G., Gül, A., Kangal, O., Perek, K.T., Arslan, F., 2005. Flotation of Aladağ oxide lead-zinc ores. Miner. Eng. 18, 279–282. https://doi.org/10.1016/j.mineng.2004.10.018

Özdemir, M., Çak, D., K, İ., 2009. Magnesium recovery from magnesite tailings by acid leaching and production of magnesium chloride hexahydrate from leaching solution by evaporation. Int. J. Miner. Process. 93, 209–212.

https://doi.org/10.1016/j.minpro.2009.08.001

Paliwal, M., Jung, I., 2019. Calphad Precipitation kinetic model and its applications to Mg alloys. Calphad 64, 196–204. https://doi.org/10.1016/j.calphad.2018.12.006

Peiró, L.T., Nuss, P., Blengini, G.A., 2018. Towards Recycling Indicators based on EU flows and Raw Materials System Analysis data policies through RMIS. https://doi.org/10.2760/092885

Perez, J.P.H., Folens, K., Leus, K., Vanhaecke, F., Van Der Voort, P., Du Laing, G., 2019. Progress in hydrometallurgical technologies to recover critical raw materials and precious metals from low-concentrated streams. Resour. Conserv. Recycl. 142, 177–188. https://doi.org/10.1016/j.resconrec.2018.11.029

Podder, J., Kalkura, N., 2001. Crystallization and characterization of orthorhombic MgSO4.7H2O. Cryst. Res. Technol. 36, 1357e1364. https://doi.org/10.1002/1521-4079(200112)36:12<1357::AID-CRAT1357>3.0.CO;2-7

Pourbaix, M. Atlas of electrochemical equilibria in aqueous solutions. Brussels: CEBELCOR, 1974. 644 p.

Psomopoulos, C.S., Themelis, N.J., 2016. Use of waste derived fuels in cement industry - a review. Manag. Environ. Qual. An Int. Journa. https://doi.org/10.1108/MEQ-01-2015-0012

Puthiya, S., Mucci, A., Arakaki, T., 2017. Dolomite dissolution in aqueous solutions in the presence of nucleotides and their structural components at 25 ° C and pCO 2 ~ 1 atm Dolomite dissolution in aqueous solutions in the presence of nucleotides and their structural components at 25 ° C and pCO. Chem. Geol. 465, 64–74. https://doi.org/10.1016/j.chemgeo.2017.05.022

Putnis, A. 1995. Introduction to mineral sciences. Cambridge, Cambridge University. https://doi.org/10.1017/CBO9781139170383

Ramalingom, S., Podder, J., Narayana Kalkura, S., 2001. Crystallization and characterization of orthorhombic β-MgSO4·7H2O. Cryst. Res. Technol. 36, 1357–1364. https://doi.org/10.1002/1521-4079(200112)36:12<1357::AID-CRAT1357>3.0.CO;2-7

Renard, F., Røyne, A., Putnis, C. V, 2019. Timescales of interface-coupled dissolution-precipitation reactions on carbonates. Geosci. Front. 10, 17–27. https://doi.org/10.1016/j.gsf.2018.02.013

Reuter, M., 2013. Metal Recycling: Opportunities, Limits, Infrastructure. UNEP, International Resource Panel.

Robson, H.L., 1927. The system MgSO4-H2O from 68 to 240°C. J. Am. Chem. Soc. 49, 2772e2783. https://doi.org/10.1021/ja01410a016.

Rosenqvist, T., 2004. Principles of extractive metallurgy. Akademika Pub; 2ª ed, 528p.

Sadegh Safarzadeh, M., Bafghi, M.S., Moradkhani, D., Ojaghi Ilkhchi, M., 2007. A review on hydrometallurgical extraction and recovery of cadmium from various resources. Miner. Eng. 20, 211–220. https://doi.org/10.1016/j.mineng.2006.07.001

Sadik, C., Moudden, O., El Bouari, A., El Amrani, I.E., 2016. Review on the elaboration and characterization of ceramics refractories based on magnesite and

dolomite. J. Asian Ceram. Soc. 4, 219–233. https://doi.org/10.1016/j.jascer.2016.06.006

Sampaio, J.A., França, S.C.A., Braga, P.F.A., 2007. Tratamento de Minérios: práticas laboratoriais, CETEM-MCT Centro de Tecnologia Mineral - Ministério da Ciência e Tecnologia.

Santos, J.F. dos, 2009. Secretaria de geologia, mineração e transformação mineral - Ministério de Minas e Energia - MME.

Schulze, R., Guinée, J., van Oers, L., Alvarenga, R., Dewulf, J., Drielsma, J., 2020. Abiotic resource use in life cycle impact assessment—Part I- towards a common perspective. Resour. Conserv. Recycl. 154, 104596. https://doi.org/10.1016/j.resconrec.2019.104596

SDA, 2016. INSTRUÇÃO NORMATIVA SDA Nº 27, 05 DE JUNHO DE 2006 (Alterada pela IN SDA nº 7, de 12/04/2016, republicada em 02/05/2016).

Sędzimir, J.A., 2002. Precipitation of metals by metals (cementation) - Kinetics, equilibria. Hydrometallurgy 64, 161–167. https://doi.org/10.1016/S0304-386X(02)00033-6

Shen, L., Sippola, H., Li, X., Lindberg, D., Taskinen, P., 2019. Thermodynamic Modeling of Calcium Sulfate Hydrates in the CaSO4-H2O System from 273.15 to 473.15 K with Extension to 548.15 K. J. Chem. Eng. Data 64, 2697–2709. https://doi.org/10.1021/acs.jced.9b00112

Shi-bao, C., Meng, W., Shan-shan, L.I., Zhong-qiu, Z., 2018. Overview on current criteria for heavy metals and its hint for the revision of soil environmental quality standards in China. J. Integr. Agric. 17, 765–774. https://doi.org/10.1016/S2095-3119(17)61892-6

Sierra, C., Martínez, J., Menéndez-aguado, J.M., Afif, E., Gallego, J.R., 2013. High intensity magnetic separation for the clean-up of a site polluted by lead metallurgy. J. Hazard. Mater. 248–249, 194–201. https://doi.org/10.1016/j.jhazmat.2013.01.011

Sinclair, R.J.., 2005. The Extractive Metallurgy of Zinc. https://doi.org/10.1007/978-1-4684-8425-0

Singh, S.K., Singh, A., Singh, B., Vashistha, P., 2020. Application of thermo-chemically activated lime sludge in production of sustainable low clinker cementitious binders. J. Clean. Prod. 264, 121570. https://doi.org/10.1016/j.jclepro.2020.121570

Solihin, Indriani, Mubarok, M.Z., 2018. Dissolution Profile of Dolomite in Chloric Acid Solution: The Effect of Chloric Acid Concentration and Pulp Density. AIP Conf. Proc. 1964, 1–7. https://doi.org/10.1063/1.5038304

Song, Y., Wilson, M.J., Moon, H., Bacon, J.R., Bain, D.C., 1999. Chemical and mineralogical forms of lead , zinc and cadmium in particle size fractions of some wastes , sediments and soils in Korea. Appl. Geochemistry 14, 621–633.

Souza, A.D., Pina, P.S., Lima, E.V.O., Silva, C.A., Leão, V.A., 2007. Kinetics of sulphuric acid leaching of a zinc silicate calcine 89, 337–345. https://doi.org/10.1016/j.hydromet.2007.08.005

Souza, A.D., Pina, P.S., Santos, F.M.F., Silva, C.A., Leão, V.A., 2009. Hydrometallurgy Effect of iron in zinc silicate concentrate on leaching with sulphuric acid. Hydrometallurgy 95, 207–214. https://doi.org/10.1016/j.hydromet.2008.05.049

Sun, H., Qian, J., Yang, Y., Fan, C., Yue, Y., 2020. Optimization of gypsum and slag contents in blended cement containing slag. Cem. Concr. Compos. 112, 103674. https://doi.org/10.1016/j.cemconcomp.2020.103674

Tanna, B., Schipholt, B., (2003). Waste-derived Fuel use in Cement Kilns. Available in: http://www.eratech.com/papers/wdf.html.

Tolonen, E.T., Rämö, J., Lassi, U., 2015. The effect of magnesium on partial sulphate removal from mine water as gypsum. J. Environ. Manage. 159, 143–146. https://doi.org/10.1016/j.jenvman.2015.05.009

U.S. Geological Survey, 2020. Mineral Commodity Summaries, United States Geological Survey.

UN. General Assembly (42nd sess. : 1987-1988), 1987. Report of the World Commission on Environment and Development : resolution / adopted by the General Assembly. Resolut. Decis. Adopt. by Gen. Assem. Dur. its 42nd Sess. 154–156.

USGS, 2020. Zinc. U.S. Geol. Surv. Miner. Commod. Summ. 190–191.

Utimura, S.K., 2014. Reciclagem de resíduos de equipamentos eletroeletrônicos: separação de ABS e HIPS por flotação. Dissertação (Mestrado em Engenharia Química) - Escola Politécnica, Universidade de São Paulo, São Paulo, 2009.

Vaillant, J.M.M., 2013. Avaliação dos parâmetros de lixiviação de metais pesados em matriz de cimento portland por meio da condutividade elétrica. Tese (Doutorado em Engenharia Civil) - Engenharia Civil, Universidade Federal de Santa Catarina, Florianópolis, 2013. 246p.

Walle, A. Van De, Nataraj, C., Liu, Z., 2018. Calphad The Thermodynamic Database Database. Calphad 61, 173–178. https://doi.org/10.1016/j.calphad.2018.04.003

Wanderley, K.B., Junior, A.B.B., Espinosa, D.C.R., Tenório, J.A.S., 2020. Kinetic and thermodynamic study of magnesium obtaining as sulfate monohydrate from nickel laterite leach waste by crystallization. J. Clean. Prod. 122735. https://doi.org/10.1016/j.jclepro.2020.122735

Wang, X., Yu, R., Shui, Z., Zhao, Z., Song, Q., Yang, B., Fan, D., 2018. Development of a novel cleaner construction product: Ultra-high performance concrete incorporating lead-zinc tailings. J. Clean. Prod. 196, 172–182. https://doi.org/10.1016/J.JCLEPRO.2018.06.058

Wang, Yanliang, Zhou, H., Wang, Yabing, Li, F., Sun, X., 2017. Separation of high-purity yttrium from ion-absorbed rare earth concentrate using (2,6-dimethylheptyl) phenoxy acetic/propanoic acid. Sep. Purif. Technol. 184, 280–287. https://doi.org/10.1016/j.seppur.2017.04.049

Whalen, J.K., 2012. Soil fertility improvement and integrated nutrient management – A global perspective. Rijeka, Croatia.

Williams, M.L., 1996. CRC Handbook of Chemistry and Physics, 76th edition. Occup. Environ. Med. 53, 504–504. https://doi.org/10.1136/oem.53.7.504

Wills, B. G.; Finch, J. A.; Mineral Processing Technology, 8th Edition. Canada, 2015. p. 265-321.

Xiong, Y., Wu, B., Zhu, J., Fan, X., Cai, P., Wen, J., Liu, X., 2014. Preparation of magnesium hydroxide from leachate of dolomitic phosphate ore with dilute waste acid from titanium dioxide production. Hydrometallurgy 142, 137–144. https://doi.org/10.1016/j.hydromet.2013.11.013

Xu, H., Wei, C., Li, C., Fan, G., Deng, Z., Li, M., Li, X., 2010. Sulfuric acid leaching of zinc silicate ore under pressure. Hydrometallurgy 105, 186–190. https://doi.org/10.1016/j.hydromet.2010.07.014

Xu, H., Wei, C., Li, C., Fan, G., Deng, Z., Zhou, X., Qiu, S., 2012. Leaching of a complex sulfidic, silicate-containing zinc ore in sulfuric acid solution under oxygen pressure. Sep. Purif. Technol. 85, 206–212. https://doi.org/10.1016/j.seppur.2011.10.012

Younesi, S.R., Alimadadi, H., Alamdari, E.K., Marashi, S.P.H., 2006. Kinetic mechanisms of cementation of cadmium ions by zinc powder from sulphate solutions. Hydrometallurgy 84, 155–164. https://doi.org/10.1016/j.hydromet.2006.05.005

APPENDIX 1

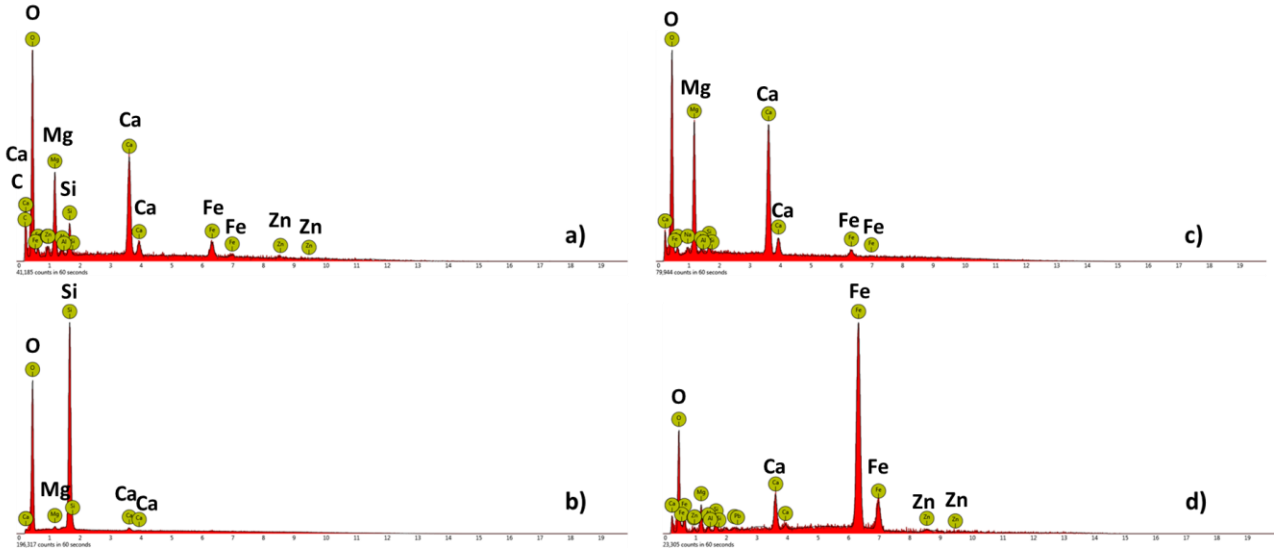

APPENDIX 2

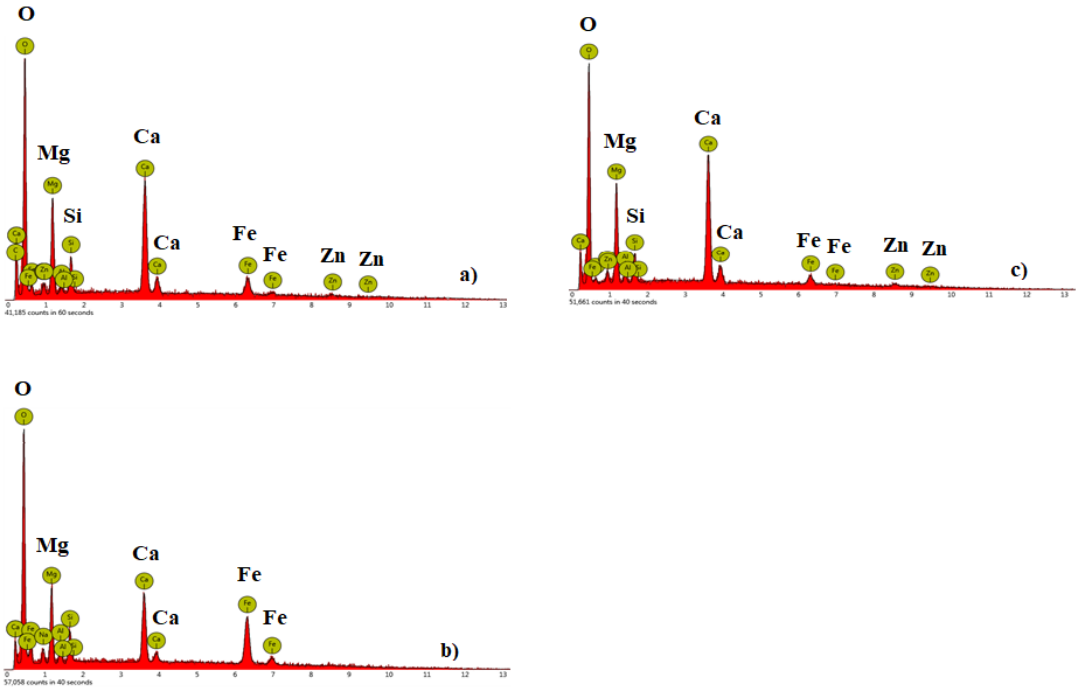

APPENDIX 3

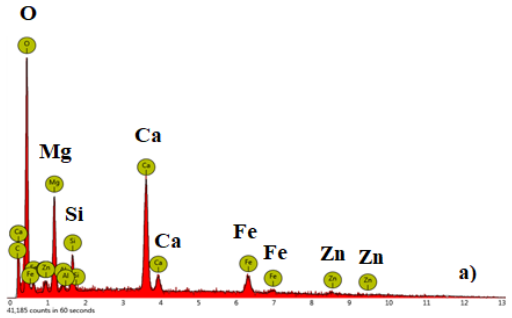

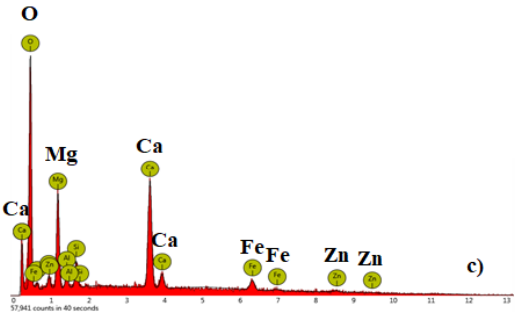

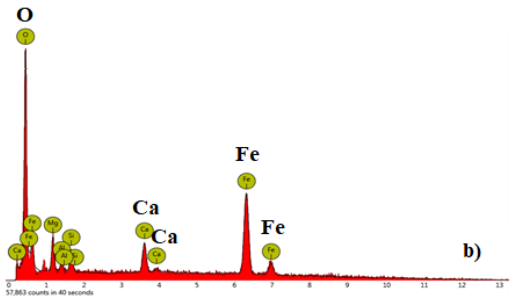

APPENDIX 4

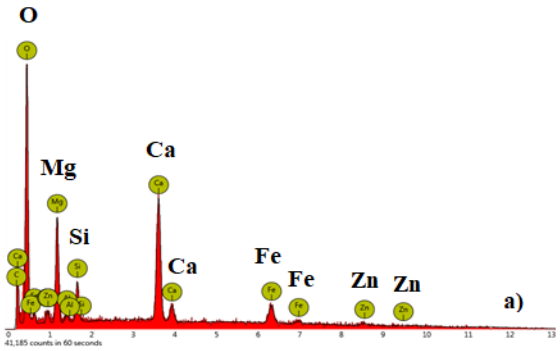

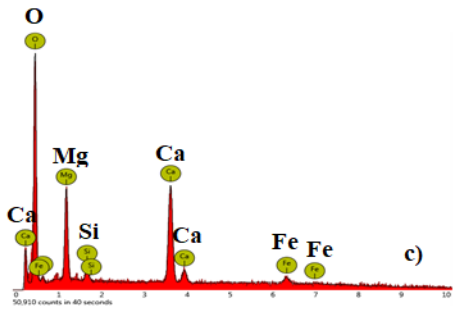

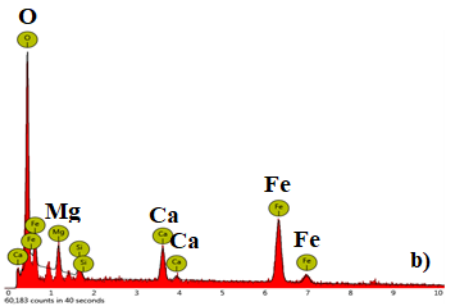

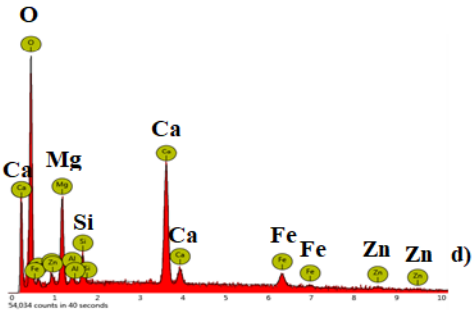

APPENDIX 5

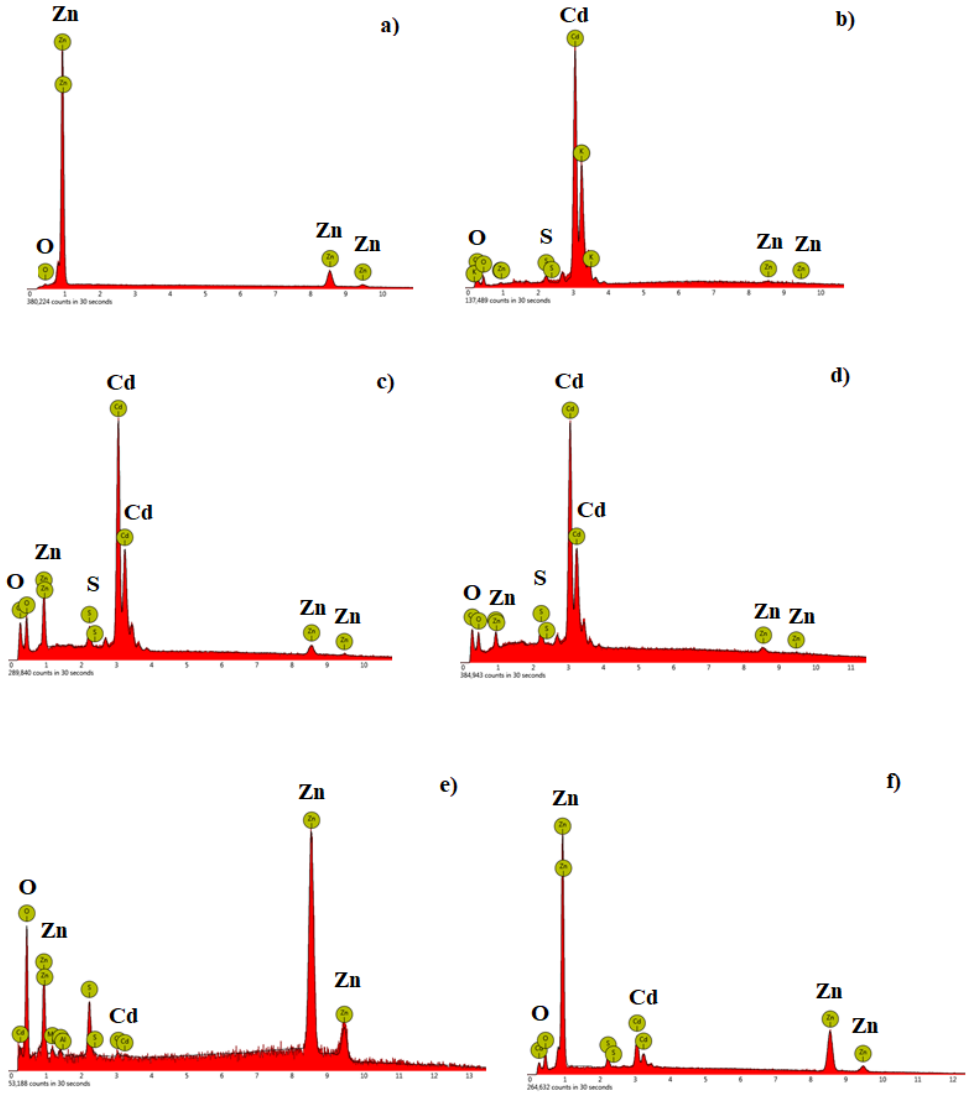
a)
Zn
O
Zn
Zn
b)
Cd
O
S
Zn
Zn
c)
Cd
Cd
Zn
O
S
Zn
Zn
d)
Cd
Cd
O
Zn
S
Zn
Zn
e)
Zn
O
Zn
Zn
Cd
f)
Zn
O
Cd
Zn
Zn